The Geologic History of Lake of the Woods, Minnesota, Reconstructed Using Seismic-Reflection Imaging and Sediment Core Analysis

A THESIS
SUBMITTED TO THE FACULTY OF THE GRADUATE SCHOOL OF
THE UNIVERSITY OF MINNESOTA
BY

Devin D. Hougardy

IN PARTIAL FULFILLMENT OF THE REQUIREMENTS
FOR THE DEGREE OF
MASTER OF SCIENCE

Dr. Steve M. Colman and Dr. Nigel J. Wattrus

July 2014

Acknowledgements

I would like to thank my advisors, Dr. Steve Colman and Dr. Nigel Wattrus, for their guidance and continuous support throughout this thesis. I am sincerely grateful for the invaluable opportunities that were offered to me during my time at the Large Lakes Observatory (LLO) and University of Minnesota-Duluth (UMD). I would also like to thank my committee members Dr. Mark Edlund and Dr. Andrew Breckenridge for their insight, comments, and inspiration.

A special thank you to Captain Randy Beebe of the *R/V Arctic Fox* for enduring eight long days through turbulent weather, hatching chironomids, and biting flies on Lake of the Woods. Without your dedication this project would not have been possible. Thank you to the three Aaron's (Aaron Slonecker, Aaron "Wally" Lingwall, and Aaron DeRusha) for their support in coring Lake of the Woods during the March weather and assisting with seismic acquisition, to my colleagues at the LLO and UMD, and to family and friends.

Funding was made possible largely through the Lake of the Woods Water Sustainability Foundation and from various block grants through the Department of Geological Sciences at UMD.

Abstract

The history of glacial Lake Agassiz is complex and has intrigued researchers for over a century. Over the course of its ~5,000 year existence, the size, shape, and location of Lake Agassiz changed dramatically depending on the location of the southern margin of the Laurentide Ice Sheet (LIS), the location and elevation of outflow channels, and differential isostatic rebound. Some of the best-preserved sequences of Lake Agassiz sediments are found in remnant lake basins where erosional processes are less pronounced than in adjacent higher-elevation regions. Lake of the Woods (LOTW), Minnesota, is among the largest of the Lake Agassiz remnant lakes and is an ideal location for Lake Agassiz sediment accumulation.

High-resolution seismic-reflection (CHIRP) data collected from the southern basin of LOTW reveal up to 28 m of stratified lacustrine sediment deposited on top of glacial diamicton and bedrock. Five seismic units (SU A-E) were identified and described based on their reflection character, reflection configuration, and external geometries. Three prominent erosional unconformities (UNCF 1-3) underlie the upper three seismic units and indicate that deposition at LOTW was interrupted by a series of relatively large fluctuations in lake level. The lowermost unconformity (UNCF-1) truncates uniformly draped reflections within SU-B at the margins of the basin, where as much as four meters of sediment were eroded. The drop in lake level is interpreted to be contemporaneous with the onset of the low-stand Moorhead phase of Lake Agassiz identified from subaerial deposits in the Red River Valley, Rainy River basin, and Lake Winnipeg.

A rise in lake level, indicated by onlapping reflections within SU-C onto UNCF-1, shifted the wave base outwards and as much as 11 m of sediment were deposited (SU-C) in the middle of the basin before a second drop, and subsequent rise, in lake level resulted in the formation of UNCF-2. Reflections in the lower part of SU-D onlap onto UNCF-2 only near the margins of the basin, suggesting that water occupied much of the middle of the southern basin after lake level drawdown. The reflection character and configuration of SU-C and SU-D are genetically different indicating that the depositional environment had changed following the formation

of UNCF-2. Piston-type sediment cores collected from the southern basin of LOTW at depths that correspond to the middle of SU-D contain high amounts of organic material and charcoal fragments and sediment that are probably not related to Lake Agassiz. Instead, they were likely deposited during a transitional phase between when Lake Agassiz left the LOTW basin (UNCF-2) and inundation of LOTW from the northern basin due to differential isostatic rebound (UNCF-3).

All sediment cores collected from the southern basin of LOTW record the uppermost unconformity, analogous in depth to UNCF-3 in the seismic images, which separates modern sediments from mid to late-Holocene sediments. The lithology of sediments below this unconformity varies across the basin from gray clay to laminated silt and clay. Radiocarbon ages from two peat layers immediately below the unconformity indicate that subaerial conditions had existed prior to the formation of UNCF-1, at about 7.75 ka cal BP. The timing correlates well with other lakes in the upper Midwest that record a prolonged dry climate during the mid-Holocene. UNCF-3 is planar and erosional across the entire survey area but erosion is greatest in the northern part of the basin as the result of a southward transgressing wave base driven by differential isostatic rebound.

Deposition in the southern basin probably resumed around 3.3 ka cal BP, though no radiocarbon dates were collected directly above UNCF-3. The lithology of sediment above UNCF-3 is highly uniform across the basin and represents modern sedimentation. Late-Holocene sedimentation rates were calculated at about 0.9 mm $year^{-1}$ and are roughly double the sedimentation rates in the NW Angle basin, suggesting that erosion of the southern shoreline contributes significantly to deposition in the southern basin.

Table of Contents

List of Tables

List of Figures

Chapter 1: Introduction

Instrumental measurements and temperature reconstructions from multi-proxy records indicate that global temperatures are rising dramatically as the result of increased concentrations of CO_2 in the atmosphere (Mann and Bradley, 1999; Mann and Jones, 2003; Marcott et al., 2013). In the high northern latitudes where strong positive feedbacks amplify global trends (Miller et al., 2010), increased land surface and ocean temperatures have led to a substantial reduction in glacier and ice cap volume. As a result, freshwater previously stored as ice is now entering the oceans. In order to predict how the planet's climate will respond, researchers have studied the geologic record for evidence of prior events in which large amounts of freshwater have entered the oceans. Drainage from glacial Lake Agassiz, the largest of the North American glacial lakes formed during the last deglaciation, into the North Atlantic Ocean has been suggested as the mechanism for multiple global cooling events, including the start of the Younger Dryas (Broecker et al., 1989) at 12.9 ka cal BP (thousand calendar years before present) and the "8.2 ka cal BP" cooling event (Barber et al., 1999). These findings have stimulated a series of investigations aimed at building upon a century's worth of research to better understand the history of Lake Agassiz. Many questions still remain regarding the chronology and location of drainage events. However, as technological advances open up new avenues of research, the story has become more robust. Among these advances are seismic-reflection surveys from lakes whose basins were once occupied by Lake Agassiz.

In this thesis, I present and describe the results of the first high-resolution seismic-reflection survey of Lake of the Woods (LOTW), Minnesota, USA (Figure 1). LOTW is a large remnant lake of glacial Lake Agassiz located on the international border of Canada and the United States. Surprisingly little research has been focused on the formation and evolution of LOTW. Yang and Teller (2005) modeled the extent and depth of water over the LOTW basin at various time intervals by calculating the amount of postglacial isostatic rebound at specific isobases across the LOTW basin (see section 2.3.2). They concluded that Lake Agassiz occupied the

southern basin of LOTW until ~10.0 cal ka BP, leaving behind an isolated LOTW in the northern basin.

Yang and Teller's paleotopographic reconstructions suggest that after ~10.0 cal ka BP the southern basin lay unoccupied until differential isostatic rebound caused LOTW to transgress southward into the southern basin until just prior to ~7.0 cal ka BP. Continued differential isostatic rebound, following the inundation of the southern basin, resulted in a rising lake level that eventually reached its modern day height. This interpretation is contradicted by Mellors (2010), who in a comprehensive multi-proxy study on several sediment cores taken from multiple locations across LOTW, determined that lacustrine sediments *were* deposited in the southern basin between 10.0-7.0 cal ka BP and speculated that they might be of Lake Agassiz origin. Inconsistencies in the two interpretations demonstrate the need for further investigation.

High-resolution seismic-reflection (CHIRP) data were collected from LOTW as a part of an ongoing multi-proxy investigation, funded by the Lake of the Woods Water Sustainability Foundation (LOTW-WSF), aimed at understanding the temporal relationships between sedimentation, nutrient dynamics, and biological communities in the southern basin of the lake. The original intent of the seismic survey was to define the depositional basins as a means to better understand the sedimentation patterns in LOTW. A preliminary survey was conducted in October 2011 to assess the character of sediment. This survey revealed, among other things, a complex arrangement of lacustrine sediments overlying a laterally variable acoustic basement. It became clear that the seismic equipment used for the survey was capable of producing high-resolution images of LOTW sediment and further investigation into the character and configuration of the sediment would be fruitful.

The goals of this thesis are to (1) reconstruct the late-Quaternary geologic history of LOTW using high-resolution seismic-reflection images and sediment core analysis. Our intent is to look for indicators of lake level fluctuations related to Lake Agassiz, at LOTW, that can help constrain the position of Lake Agassiz at different points in time. In addition to the seismic survey, four sediment cores were collected from the southern basin in order to "ground truth" the seismic images and obtain

material for radiocarbon dating. I also seek to clarify whether a lacustrine environment existed in the southern basin of LOTW following the abandonment of the region by Lake Agassiz as Mellors (2010) suggested. If so, did lacustrine environments exist until differential isostatic rebound resulted in coalescence of the northern and southern basins? The second (2) goal of this thesis is to define the depositional basins of LOTW as a means to understand the sedimentation patterns of the lake. To do this, sediment thickness maps of the southern basin were created from the seismic-reflection data using the methods outlined in Chapter 3.

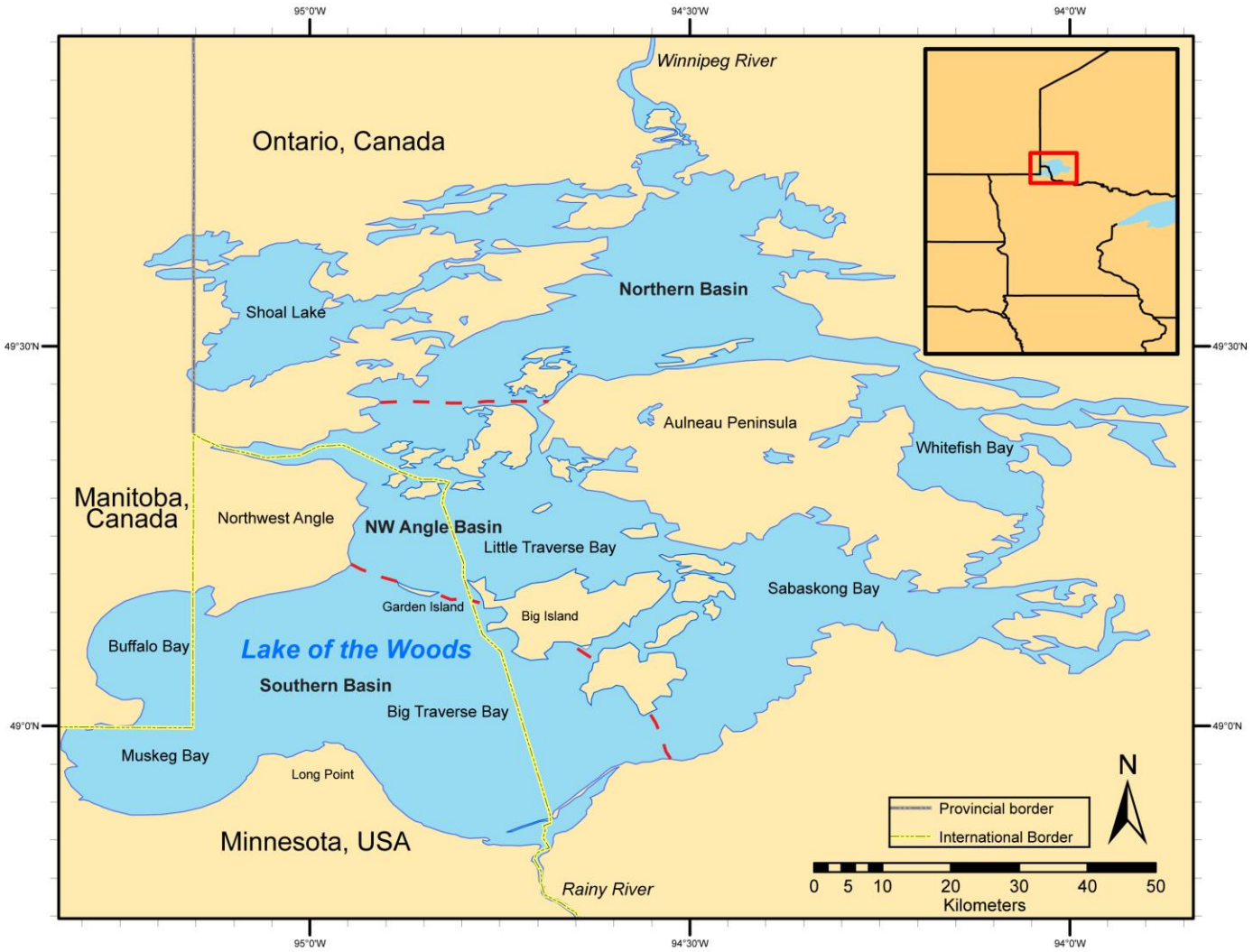

Figure 1 Map of Lake of the Woods. Map of modern-day Lake of the Woods (LOTW) located on the international border of Canada and the United States (inset). Dashed red lines separate sub-basins from the now hydrologically connected lake.

Chapter 2: Background

2.1 Laurentide Ice Sheet

The Laurentide Ice Sheet (LIS) was the largest of the North American ice sheets covering much of North America during the Wisconsin Glaciation (80-11 ka BP; thousand years before present). During the Last Glacial Maximum (~21 ka cal BP), when the ice sheet was at its greatest extent (Figure 2), the southern margin extended from the Rocky Mountain piedmont to the Atlantic seaboard and reached as far south as Des Moines, Iowa (Dyke and Prest, 1987). Due to its immense size, the LIS had a profound influence on climate (Hays et al., 1976; Manabe and Broccoli, 1985; Clark, 1994), oceanic circulation (Ruddiman and McIntyre, 1981), isostatic deformation (Clark et al., 1994), glacial lake development (Upham, 1895; Clayton and Moran, 1982; Teller, 1987), and geomorphology (Wright, 1971; Clayton and Moran, 1982; Hughes et al., 1985) during and after its existence. Many of these topics were brought to light in reviews by Wright (1971), Dyke and Prest (1987), Fulton and Prest (1987), and Mickelson and Colgan (2003) but are beyond the scope of this project and will not be addressed in detail here. However, a few important concepts need to be reviewed in order to understand the impact of the LIS in the LOTW region.

Although a variety of ice sheet reconstructions have been made, in general, they tend to show that ice thickness was greatest over Hudson Bay, Canada and thinned radially towards its margins. Crustal depression caused by the weight of the ice resulted in viscous deformation of the mantle, the production of a forebulge near the southern ice margin, and isostatic rebound after the ice was removed (Clark et al., 1994). Retreat of the southern margin towards Hudson Bay was not continuous, but was interrupted by several phases of ice readvance (Clayton and Moran, 1982).

The timing of ice retreat from LOTW has been difficult to pinpoint due to the lack of datable material from glacial tills and lake sediments in the region. Deglaciation of the Rainy River basin, ~100 km to the east of LOTW, occurred when Lake Agassiz water levels stood at the Herman level (Johnston, 1946). Deglaciation of the southern basin of LOTW probably occurred at about the same time, or shortly

after ice retreated north of the Rainy River basin. Therefore the age of the Herman shoreline, and initiation of Lake Agassiz into LOTW, can be used as a maximum age for deglaciation of the southern basin of LOTW (see section 2.2.1). Ice retreat from the more northerly basins of LOTW would have occurred sometime after the southern basin.

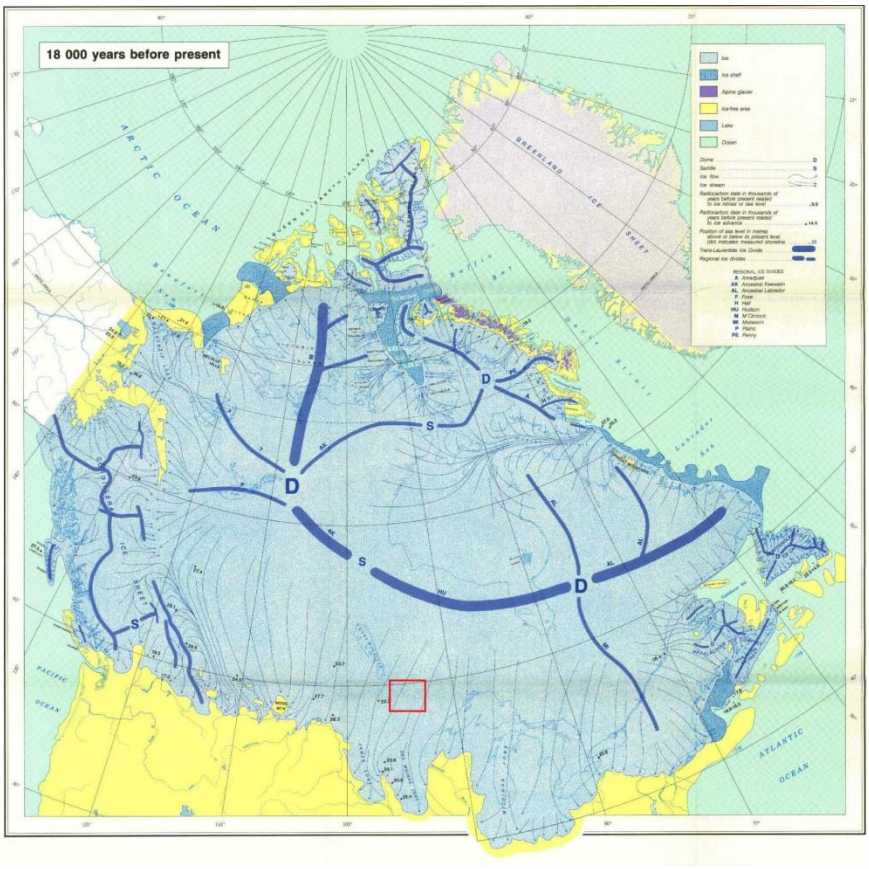

Figure 2 Laurentide Ice Sheet at ~21 ka cal BP. Area covered by the Laurentide Ice Sheet when it stood at or near the late-Wisconsinian limit at ~21 ka cal BP. Red box indicates the location of LOTW (modified from Dyke and Prest, 1987).

2.2 Lake Agassiz

2.2.1 Formation and Lake Phases

The history and evolution of Lake Agassiz is complex and has been studied by researchers for more than a century (e.g., Upham (1895); Clayton and Moran (1982); Teller (1995); Thorleifson (1996); Fisher (2005)). Technological advances over the past 50 years have opened up new avenues of research, such as seismic-reflection surveys in lake basins (Colman et al., 1994; Voytek et al., 2011), GIS based

paleotopographic modeling (Leverington et al., 2002; Leverington and Teller, 2003; Teller et al., 2005), and the application of new dating methods (Lowell et al., 2009; Lepper et al., 2013). These new developments have furthered our understanding of the behavior of Lake Agassiz as well as raised questions of the certainty of previous research. Specifically, the growing archive of radiocarbon and optically stimulated luminescence (OSL) dates has helped constrain the timing of lake phases and drainage events (Lowell et al., 2009; Lepper et al., 2007; Lepper et al., 2013).

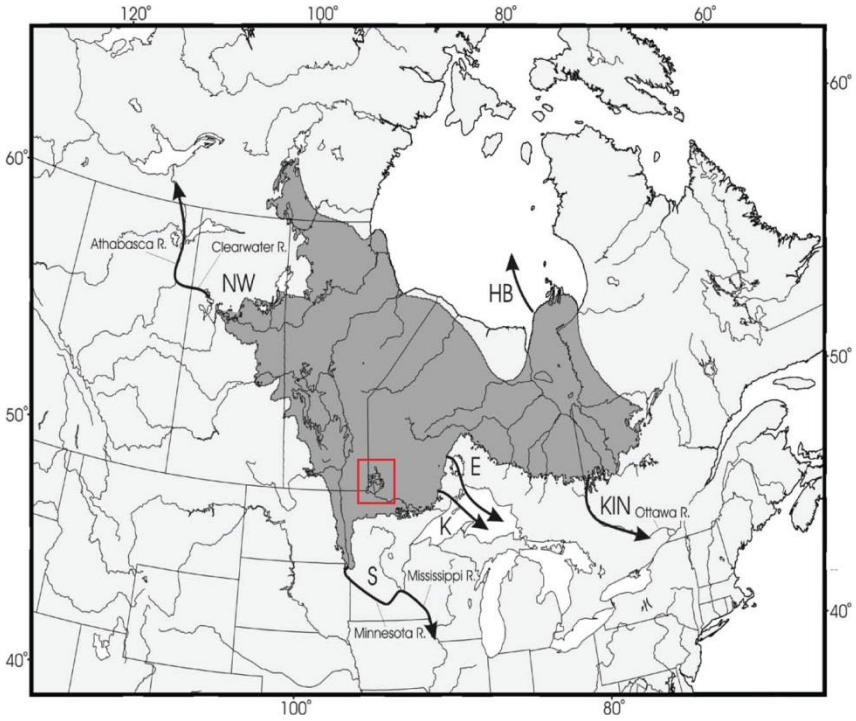

Figure 3 Total extent of Lake Agassiz. Total extent of Lake Agassiz during its existence and main drainage routes. Outlets indicated are NW=northwestern outlet, S=southern outlet, K=eastern outlets through Thunder Bay area, E=eastern outlets through Nipigon basin, KIN=Kinojevis outlet, HB=Hudson Bay outlet. Note: Lake Agassiz never occupied the entire gray shaded area at any one time. Red box indicates the location of LOTW (modified from Teller et al., 2005).

During the early stages of deglaciation (21-14 ka BP) meltwater from the Laurentide Ice Sheet drained south through the Minnesota and Mississippi Rivers into the Gulf of Mexico. Once the southern ice margin retreated north of the continental drainage divide, meltwater and surface runoff from a 2 x 10^6 km^2 watershed was impounded in front of the southward sloping ice margin leading to

the formation of several large proglacial lakes (Fenton et al., 1983; Teller, 1995; Thorleifson, 1996). Of these, Lake Agassiz was the largest (Figure 3). Over the course of its ~5,000 year existence, the size, shape, and location of Lake Agassiz changed dramatically. These parameters were controlled by the location of the LIS ice margin, the elevation and location of outflow channels, and differential isostatic rebound (Teller, 2004).

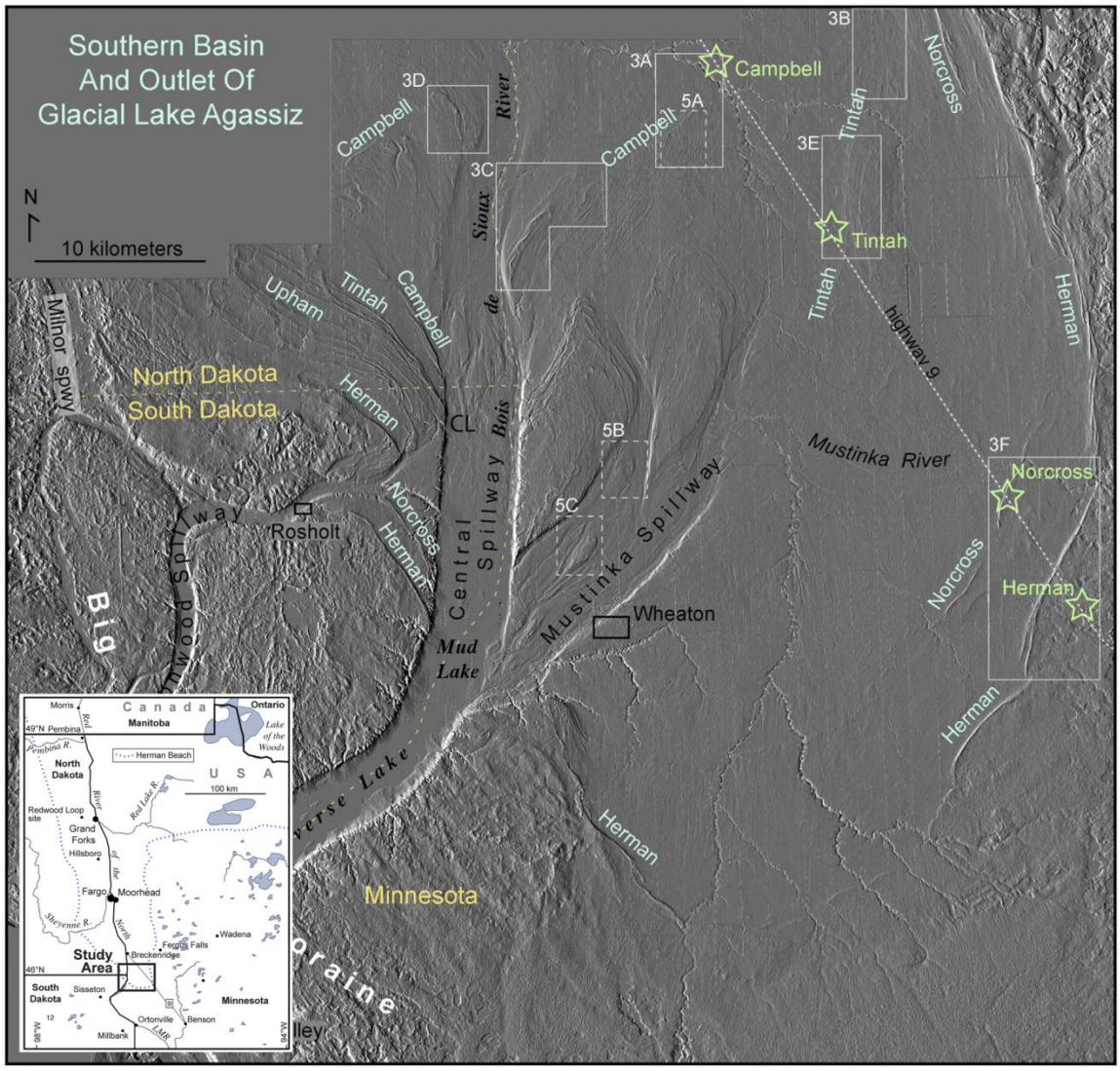

Figure 4 LiDAR image of Lake Agassiz shorelines. Locations of Lake Agassiz shorelines in west central Minnesota (inset) named by Upham after towns along Minnesota Highway 9 (dashed line). They are, in descending order from Big Stone Moraine (southwest), the Herman, Norcross, Tintah, and Campbell shorelines. Note: an additional shoreline (Upham) is indicated here though it is not discussed in the text (modified from Lepper et al., 2013).

The formation of Lake Agassiz began after the Red River lobe of the LIS retreated north of the continental drainage divide from the Big Stone Moraine located in west-central Minnesota. Just north of the Big Stone Moraine, a series of ancient shorelines record the surface elevation of Lake Agassiz at different periods of its existence (Figure 4). First named by Upham (1895) for towns along Highway 9 in Minnesota, they are in descending order, the Herman, Norcross, Tintah, and Campbell shorelines. Because shorelines represent static water planes, their extension around the lake margin establishes synchronous lake levels. Transitions between shoreline positions represent significant water-level fluctuations (Lepper et al., 2013).

Organic material is rare in Lake Agassiz beaches, so their ages have traditionally been based on the chronologies of glacial events either within or outside of the Agassiz basin (Teller and Leverington, 2004). This has led to several different interpretations regarding the timing of lake phases and associated fluctuations in lake level between them (Thorleifson, 1996; Teller et al., 2000, Teller and Leverington, 2004; Fisher, 2005; Lepper et al., 2007; Lepper et al., 2013). Recently, the application of OSL dating methods has made it possible to date Lake Agassiz beaches where previous attempts using radiocarbon dating have been limited by the paucity of organic material in the beaches. Three studies (Lepper et al., 2007; Lepper et al., 2011; Lepper et al., 2013) using OSL dating of Lake Agassiz beaches have shown the method to be reliable by producing ages that correlate well with the few radiocarbon dates available.

In general, the history of Lake Agassiz has been sub-divided into lake phases that correspond to the lake's outlet history. The first phase (Lockhart phase) began immediately following the retreat of the Red River lobe north of Big Stone Moraine. During the Lockhart phase, meltwater and runoff from the LIS were impounded between the front of the ice margin and the continental drainage divide (Big Stone Moraine). Overflow spilled through the southern outlet, carried by Glacial River Warren, carving a massive channel now occupied by the Minnesota and Upper Mississippi Rivers (Figure 3). As the ice margin continued its northward retreat up the Red River Valley, the surface area and volume of Lake Agassiz increased.

The Lockhart Phase is marked by the Brenna Formation (lacustrine clays) in the Red River Valley of North Dakota and Minnesota where water depths were at least a few tens of meters (Thorleifson, 1996) but less than 100 m (Bajc et al., 2000) in the Rainy River lowland. OSL dates from Lepper et al. (2013) indicate that the Herman and Norcross shorelines formed during the Lockhart at 14.1±0.3 and 13.6±0.2 ka cal BP, respectively (Figure 5). Lepper et al. (2013) also place the Tintah shoreline during the Lockhart phase despite obtaining two significantly younger OSL dates of 8.6±0.2 and 11.5±0.2 ka cal BP, respectively. They argue that the Tintah shoreline deposits contain different stratigraphic and sedimentological characteristics than the other shoreline deposits, reflecting a more complex formation history, and more work is needed to better constrain the age of the Tintah shoreline. Fisher (2005) proposed that episodic incision of the southern spillway channel resulted in rapid lake level drawdown and the abandonment of higher elevation shorelines. Because the elevation of the Tintah shoreline is ~10 m higher than the elevation of the southern sill, they suggest that it wasn't until after the abandonment of the Tintah that the surface of Lake Agassiz dropped below the southern sill.

The Lockhart phase ended when a new lower elevation outlet opened resulting in the abandonment of the southern outlet, regression of Lake Agassiz, and initiation of the low-water Moorhead phase. Many researchers have suggested the new outlet was located to the east near Thunder Bay, Ontario (Figure 3) (Teller et al., 2005), although no clear spillway has been identified in western Ontario (Lowell et al., 2009). The southern basin of Lake Agassiz was subaerially exposed during Moorhead phase, as indicated by deposition of the fluvial Poplar River Formation, forest and wetland remains in the Fargo, North Dakota region (Yansa et al., 2002; Yansa and Ashworth, 2005), and subaerially exposed organic material in the Red River Valley, Lake Manitoba, Rainy River basin, and Lake of the Woods regions (Teller and Thorleifson, 1983; Thorleifson, 1996; Bajc et al., 2000).

During the late Moorhead phase, Lake Agassiz transgressed southward, towards the southern outlet, driven by differential isostatic rebound. This transgression is recorded by the burial of a delta at Fargo, North Dakota (Yansa et

al., 2002; Yansa and Ashworth, 2005). It is unclear whether Lake Agassiz reached the southern outlet before a new outlet opened in the northwest (Fisher, 2005) through the Clearwater and Athabasca River Valleys and into the Arctic Ocean (Figure 3).

The timing of the beginning and ending of the subsequent Emerson phase remains uncertain. Teller (2001) suggested that after the eastern outlet was abandoned, the new outlet alternated from the northwestern location, when retreat of the LIS opened the Clearwater drainage route (at ~11.7-11.3 ka cal BP and ~11.2-10.6 ka cal BP), to the southern location, when advancement of the LIS closed the Clearwater route (at ~11.9-11.7 and ~11.3-11.2 ka cal BP). This resulted in a series of regressions and transgressions which, ultimately, led to the formation of the Norcross, Tintah, and Upper Campbell shorelines. Thorleifson (1996) suggested that the northwestern location opened at ~11.9 ka cal BP, followed by the opening of the southern outlet at ~11.2 ka cal BP. This option also requires the Norcross, Tintah, and Campbell shorelines to have formed after the Moorhead phase. Smith and Fisher (1993) and Fisher et al. (2002) suggested that the Moorhead phase did not end until the northwest outlet opened at ~11.3 ka cal BP. Furthermore, Fisher (2005) argued there is insufficient stratigraphic and sedimentological evidence of multiple transgressions in the Agassiz basin to support the scenarios suggested by Teller (2001) and Thorleifson (1996). Ages from Lepper et al., (2013), specifically from the Herman and Norcross shorelines, support Fisher's (2005) claims that these shorelines formed prior to the Moorhead phase, putting into question whether multiple transgressions actually occurred.

However, at least one transgression did occur, resulting in the formation of the Campbell shoreline. The Campbell shoreline is the most extensive and best developed shoreline in the Agassiz basin. Teller (2001) states that "a transgressive shoreline stranded during its upslope migration provides the mechanism for forming such a beach". The Campbell shoreline remains the only beach to have been successfully dated using radiocarbon methods. Ages of ~10.5 ka cal BP (Mann et al., 1997) and ~10.6 ka cal BP (Risberg et al., 1995) agree well with an average OSL age of 10.5±0.3 ka cal BP from Lepper et al. (2013). These dates coincide with

abandonment of the northwestern outlet at ~10.6 ka cal BP (Fisher, 2007) and suggest the southern outlet was reoccupied at this time.

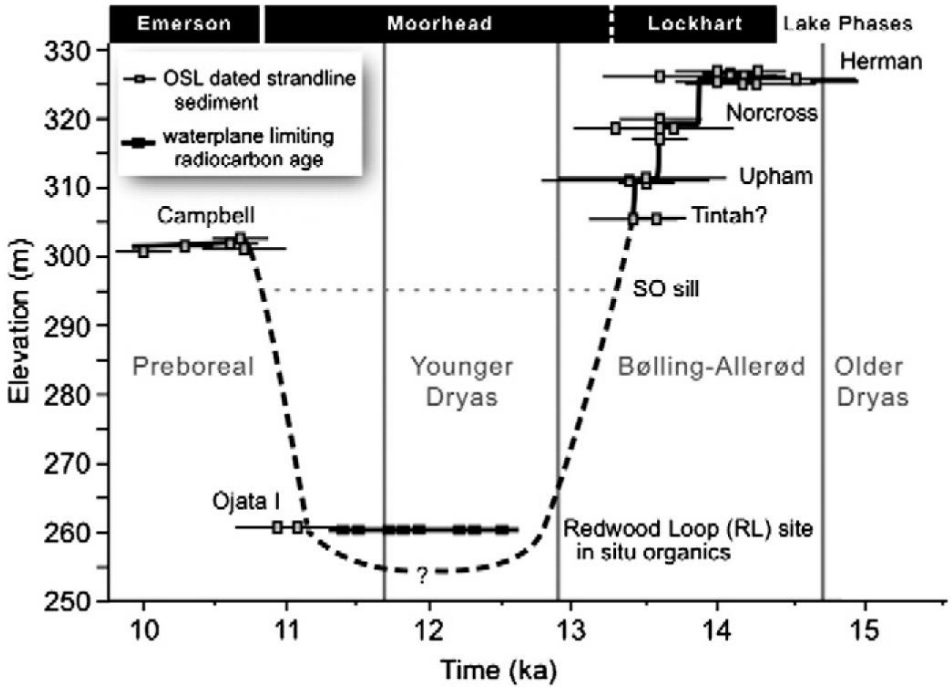

Figure 5 Timing of Lake Agassiz lake phases. Schematic of Lake Agassiz lake-level fluctuations as a function of time along with notable climate intervals. The Herman, Norcross and possibly Tintah shorelines formed during the Lockhart phase and prior to at least a 45 m drop in lake-level. Lake-level remained low throughout the majority of the Moorhead (during the Younger Dryas) before eventually rising to an elevation of ~300 m, the height at which the Campbell shoreline was formed. The formation of the Campbell shoreline corresponds to an shift in outlet location and the beginning of the Emerson phase (from Lepper et al., 2013).

The lithology of Lake Agassiz sediments during the Emerson phase reflects dynamic conditions at the time of deposition. In the Red River Valley, the Sherack Formation (laminated silty clay lacustrine sediments) overlies subaerial organic material and Brenna Formation sediments. In northwestern Ontario, Johnston (1946) notes "fossiliferous lacustrine and fluvial sands, organic-rich sediment, and an erosional unconformity are overlain by clay and silt" that are comparable in age to the Sherack Formation (Teller and Thorleifson, 1983).

The southern outlet was abandoned sometime between 10.6-10.2 ka cal BP (Fisher 2003; Fisher 2005). By 10.2 ka cal BP deglaciation in the Superior Basin was well underway, allowing for drainage through the eastern outlet into the Laurentian Great Lakes and into the Atlantic Ocean. For the next 1,800 years, Lake Agassiz followed the receding LIS ice-margin north, draining east through progressively lower and more northerly outlets. Finally, the remaining ice was breached, causing Lake Agassiz to catastrophically drain into Hudson Bay (Leverington and Teller, 2003 and references therein). The final drainage was closely dated to about 8.4 cal ka BP and implicated as the cause of the widespread "8.2 ka cal BP" climate cooling event (Barber et al., 1999).

2.2.2 Climatic Impacts of Lake Agassiz Drainage

Large amounts of freshwater discharged into the North Atlantic Ocean as a result of shifts in the drainage route of Lake Agassiz has been suggested as a mechanism for triggering several abrupt hemisphere-scale climate changes during deglaciation (Barber et al., 1999; Broecker et al., 1989; Clark et al., 2001; Teller et al., 2002; Teller et al., 2005). Numerical modeling has revealed that increased freshwater input into the northern Atlantic is capable of suppressing the formation of the North Atlantic Deep Water (NADW), limiting the supply of heat to the northern hemisphere (Clark et al., 2001; Zhang and Delworth, 2005). Impounded meltwater (Lake Agassiz) released to the east through Thunder Bay and into the Atlantic Ocean via the St. Lawrence River (initiating the low-water Moorhead Phase) has historically been viewed as the source of one of these freshwater inputs, driving the start of the Younger Dryas at about 12.9 ka cal BP (Teller et al., 2002, 2005).

This hypothesis has since come into scrutiny from Lowell et al. (2009) who argue that ice blocked this eastward drainage route until after the start of the Younger Dryas. Furthermore, Voytek et al. (2012) argue that there is insufficient evidence of channel scouring or fan deposits in the Thunder Bay region required for such a massive discharge, analogous to features that formed later and farther east (Gary et al., 2012). Nevertheless, eastward drainage of Lake Agassiz, perhaps non-

catastrophically, is still argued as the route of discharge during the Younger Dryas (Carlson et al., 2007; Carlson and Clark, 2012).

2.2.3 Shorelines and Differential Isostatic Rebound

Depression of the Earth's crust caused by the weight of the Laurentide Ice Sheet was greatest near Hudson Bay, where the ice was thickest, and least near the ice margins. As the amount of ice was reduced during and following deglaciation, the depressed crust began to rise from the center of maximum depression through the process of glacio-isostatic rebound (Walcott, 1972; Clark et al., 1994; Leverington et al., 2002). Using modern elevation data from ancient Lake Agassiz shorelines, Teller and Thorleifson (1983) demonstrated that isostatic rebound occurred differentially between the southern outlet and the northeastern limits of the lake. This can be seen in Figure 6 by the modern elevation difference in shorelines from north to south (each shoreline *formed* at a single elevation). When combined, these shorelines can be used to create isobases, lines of equal post-glacial uplift, for the region occupied by Lake Agassiz (Figure 7). Today, the deglaciated landscape, including Lake of the Woods, continues to rise, tilting toward the southwest because of differential rebound (Teller, 2001). The rate of rebound decreases with time (Clark et al., 1994), in a way that is commonly described as exponential decay (Lewis et al., 2005).

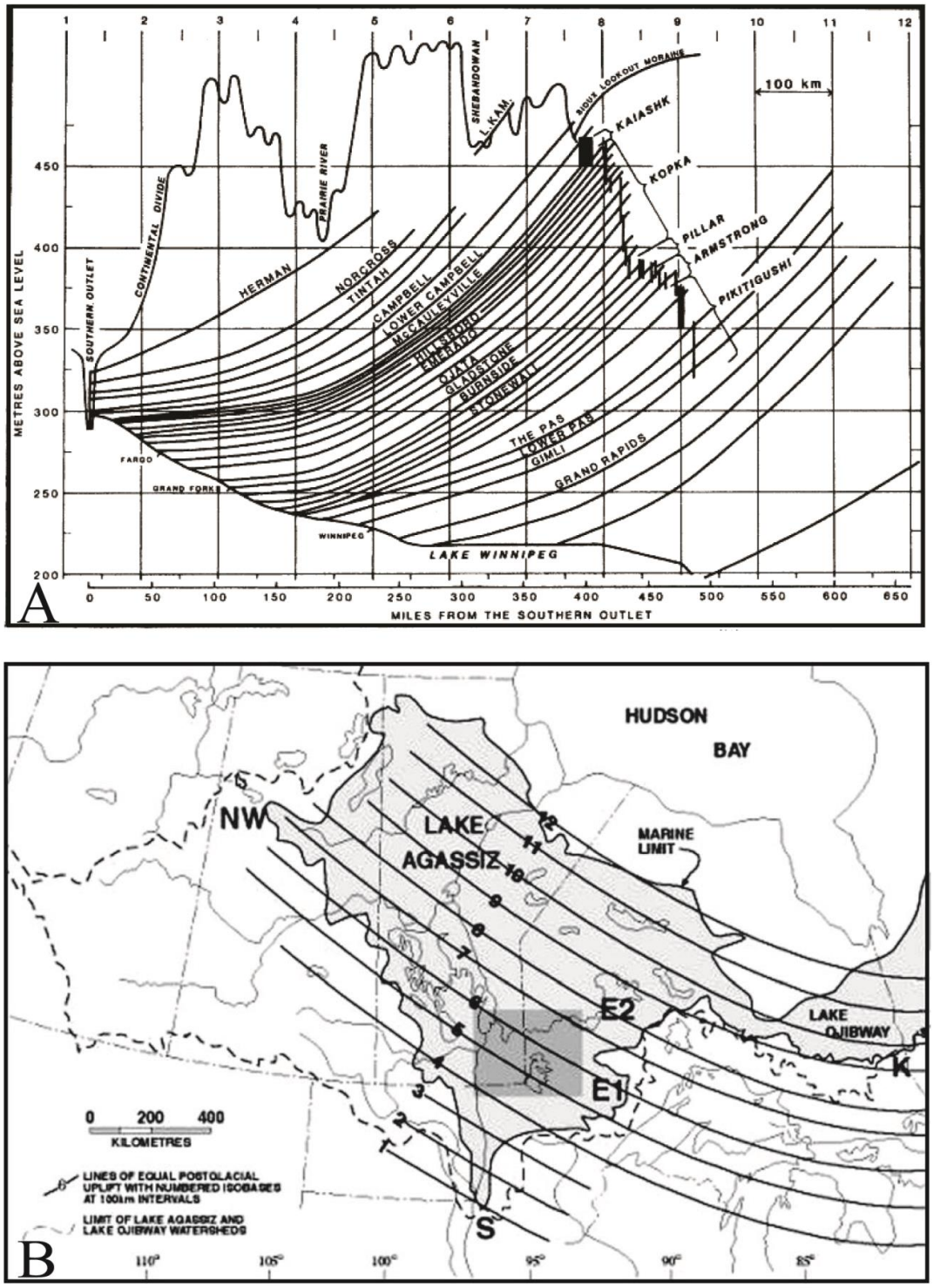

Figure 6 Lake Agassiz isobases. (A) Modern elevation of major water planes of Lake Agassiz extending from the southern outlet towards the northeast perpendicular to isobase lines, reconstructed from shorelines and beach deposits. (B) Isobase lines representing contours of equal isostatic rebound spaced at 100 km intervals from multiple shoreline data. Lake of the Woods is approximately located between isobase 4.75 to isobase 5.75 (from Teller and Thorleifson, 1983 (A) and Yang and Teller, 2005 (B)).

2.3 Lake of the Woods

2.3.1 Site Description

LOTW is a large irregularly shaped lake located on the international border between the United States and Canada (Figure 1). In its entirety the lake is 110 km long and as much as 95 km wide. The southern part of the basin is separated from the northern part by a region called the Northwest Angle, the northern-most part of the contiguous United States. Though the LOTW basin is now hydrologically connected, the lake contains several sub-basins suggesting localized regions of the lake may have operated individually until the entire lake coalesced. The focus of this project is primarily in the southern basin; however, references to other parts of the lake are made in relation to the separation between sub-basins (Figure 1). The southern basin, (shared by Minnesota, Manitoba, and Ontario) is mostly shallow open-water, with water depths averaging 9-10 m. The Rainy River, located in the southeast section of the basin, is the primary inlet accounting for ~75 percent of the total water input into the lake (Yang and Teller, 2005).

The northern basin (shared by Manitoba and Ontario) contains the majority of the lake's 14,000 islands and 40,000 km of shoreline. Hydrologically connected to LOTW is Shoal Lake, the primary source of drinking water for the city of Winnipeg, Manitoba. Two outlets, located in the northern section of the basin near the town of Kenora, Ontario, drain more than 91 percent of the total overflow from LOTW into the Winnipeg River and then into Lake Winnipeg 235 km downstream (Yang and Teller, 2005). The western and larger of the two outlets was dammed in 1887 followed by the damming of the smaller eastern outlet in 1906 to the meet power requirements of the local paper mill (LWCB, 2002). Consequently, the average water-level increased by ~1.8 m above the natural outlet levels (LWCB, 2002). The northern basin is also predominately shallow, but some areas reach depths of more than 45 m (Yang and Teller, 2005).

2.3.2 Isolation from Lake Agassiz

Sometime after ~13.5 ka cal BP, the LIS retreated north of LOTW, depositing sandy loamy till on top of the pre-existing bedrock along the way. As the ice-margin

moved north and down the regional slope, Lake Agassiz immediately began to fill the newly deglaciated landscape, submerging the LOTW basin. For the next several millennia Lake Agassiz occupied the LOTW region, its depth and extent being controlled by Agassiz outlets and differential isostatic rebound. Stratigraphic evidence from Wampum, Manitoba (40 km to the west of Lake of the Woods) captures lake-level fluctuations associated with the Lockhart, Moorhead, and Emerson phases (Teller et al., 2000). The LOTW basin probably experienced similar conditions. Paleotopographic snapshots by Yang and Teller (2005) indicate that LOTW remained part of Lake Agassiz, with water levels in that basin at times 22-65 m above present day water level, until ~10.0 cal ka BP when LOTW became isolated and completely independent (Figures 8 and 9).

At the time of its isolation, LOTW was much smaller than it is today (more than 80 percent smaller in surface area as suggested by Yang and Teller, 2005) and was located in the northern basin near its two outlets. Since then it has gradually transgressed southward to its modern day position due to differential isostatic rebound and the resulting southwestward tilting. Yang and Teller (2005) modeled the depth and extent of LOTW at different stages during its southward transgression (Figure 9) by calculating the amount of postglacial isostatic rebound at various isobases across the LOTW region (Table 1). As the lake expanded, smaller basins merged, increasing the total surface area and volume of the lake by >3,600 km^2 and 30 km^3, respectively (Table 2). Topography emerged from the northern basin, creating a complex system of interconnected waterways. Many of the islands in this region were stripped of their overlying till as they emerged through the near-surface wave zone of the lake.

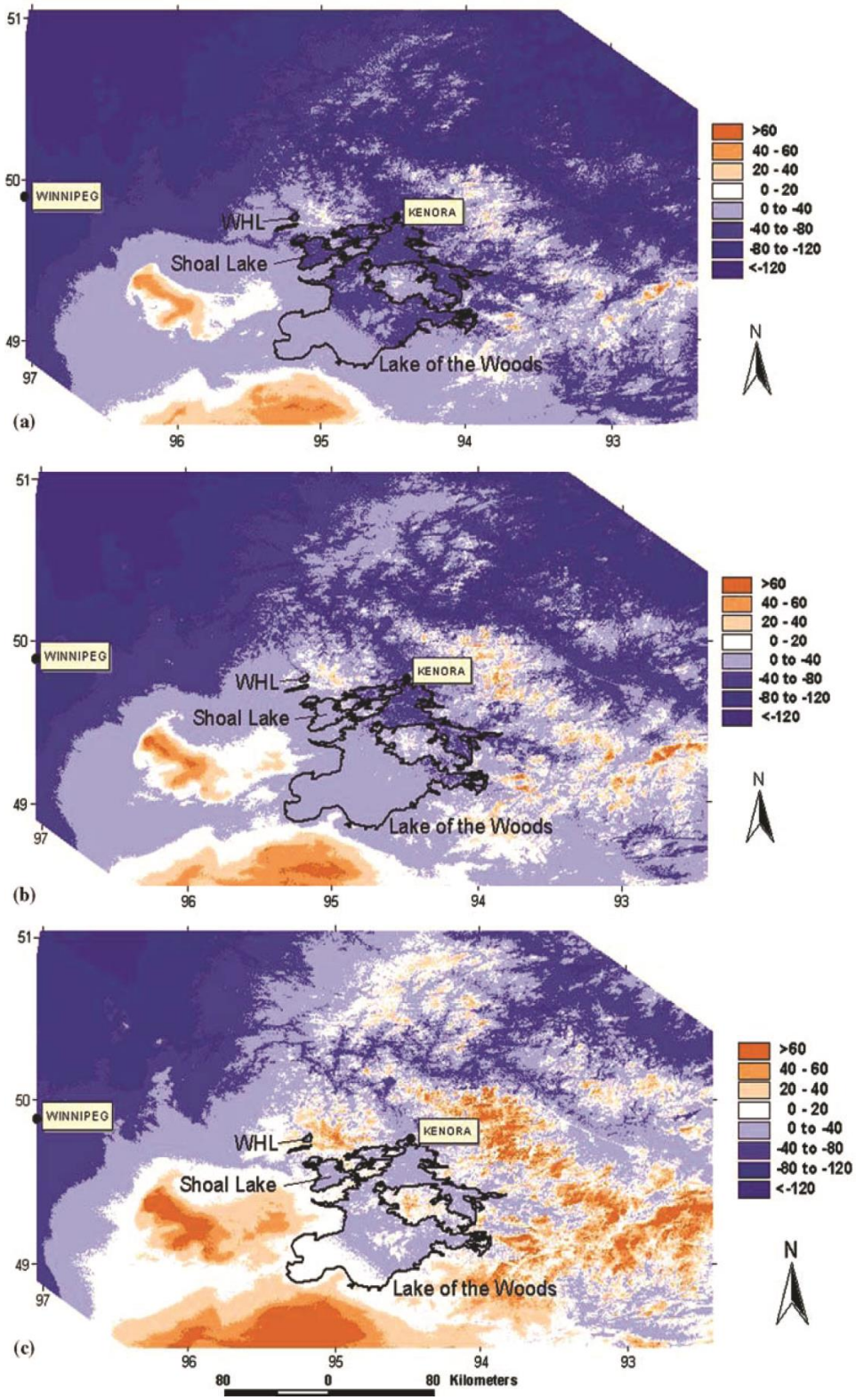

Figure 7 Snapshots of Lake Agassiz at Lake of the Woods. Extent and depth (m) of water in the Lake of the Woods region (blue shades) and elevation (m) of surrounding land above lake level (white to orange shades) at (a) 11,000, (b) 10,500, and (c) 10,000 cal years BP (from Yang and Teller, 2005).

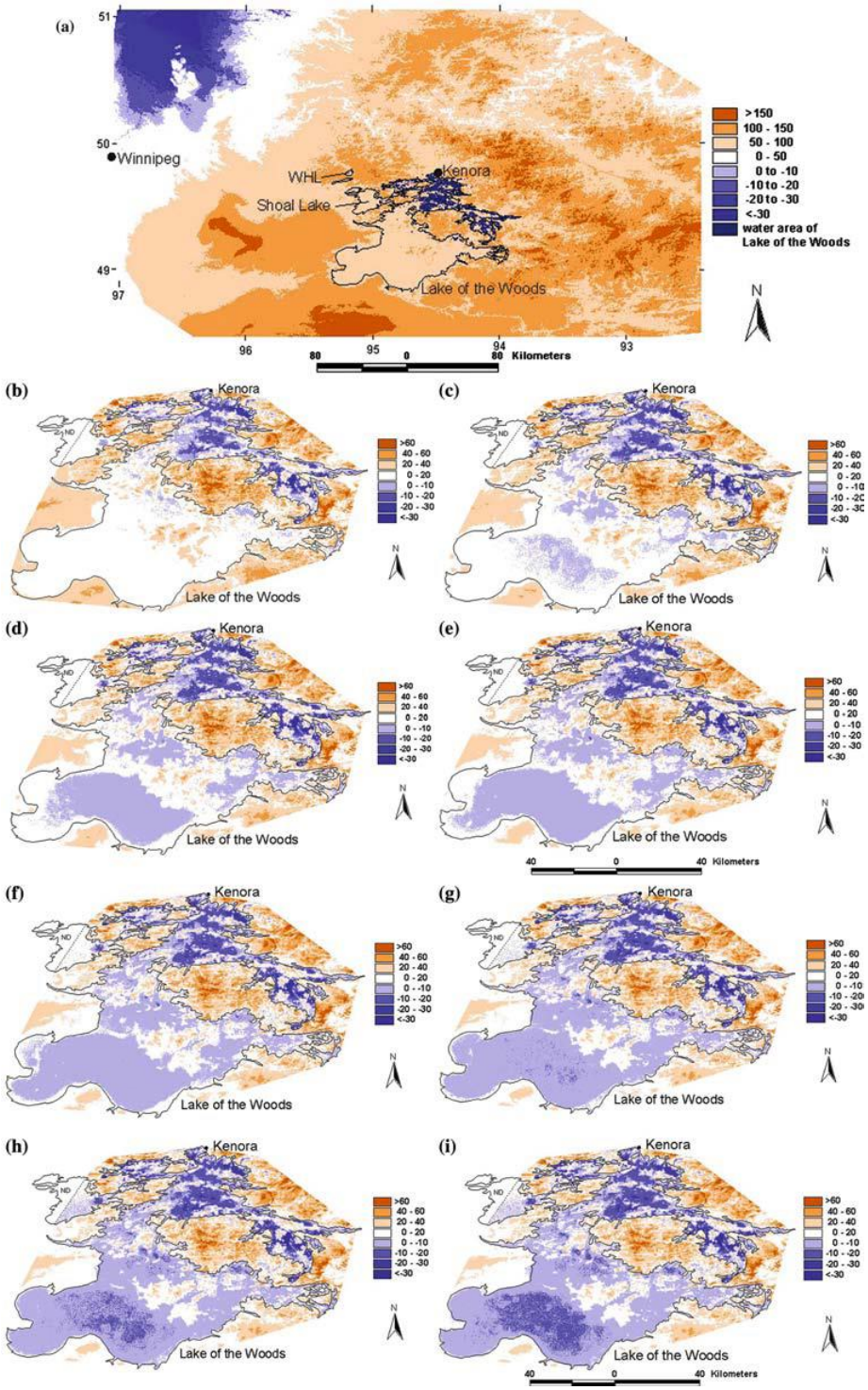

Figure 8 Snapshots of extent of Lake of the Woods. Extent and depth (m) of water in the Lake of the Woods region (blue shades) and elevation (m) of surrounding land above the lake level of Lake Agassiz (white to orange shades) at (a) 9,000 cal years BP, and above the lake level of Lake of the Woods at (b) 8,000, (c) 7,000, (d) 6,000, (e) 5,000, (f) 4,000, (g) 3,000, (h) 2,000, and (i) 1,000 cal years BP. These stages only take into consider isostatic rebound data and assume a positive hydrologic budget which may not have been the case during the Holocene (from Yang and Teller, 2005).

Table 1 Postglacial isostatic rebound values. Postglacial isostatic rebound values (m) at specific isobases (i) since specific times, beginning 11,000 cal yr B.P. to 500 years in the future. Isobase numbers refer to those shown in Figure 6B (from Yang and Teller, 2005).

Isobase (i)	3.75	4.0	4.25	4.50	4.82	5.0	5.25	5.50	5.75	6.0	6.125	6.25	6.50	6.75	7.0	7.25	7.50	7.75	8.0
ELC	314.9	318.1	322.2	324.9	332	338.1	347.5	356.1	364.3	373.2	381.1	390	399.5	414.3	425	441.1	455	468	482.5
ELCSO	288.1	288.1	288.1	288.1	288.1	288.1	288.1	288.1	288.1	288.1	288.1	288.1	288.1	288.1	288.1	288.1	288.1	288.1	288.1
RULC	26.8	30	34.1	36.8	43.9	50	59.4	68	76.2	85.1	93	101.9	111.4	126.2	136.9	153	166.9	179.9	194.4
s	3500	3500	3500	3500	3500	3500	3500	3500	3500	3500	3500	3500	3500	3500	3500	3500	3500	3500	3500
A	1.40	1.57	1.79	1.93	2.30	2.62	3.11	3.56	3.99	4.46	4.87	5.34	5.84	6.61	7.17	8.02	8.74	9.43	10.19
Cal yr	RU	RU	RU	RU	RU	RU	RU	RU	RU	RU	RU	RU	RU	RU	RU	RU	RU	RU	RU
B.P.	at i3.75	at i4.0	at i4.25	at i4.50	at i4.82	at i5.0	at i5.25	at i5.50	at i5.75	at i6.0	at i6.125	at i6.25	at i6.50	at i6.75	at i7.0	at i7.75	at i7.50	at i7.75	at i8.0
+500	0.22	0.24	0.27	0.30	0.35	0.40	0.48	0.55	0.61	0.68	0.75	0.82	0.90	1.02	1.10	1.23	1.34	1.45	1.56
+200	0.08	0.09	0.11	0.11	0.14	0.15	0.18	0.21	0.23	0.26	0.29	0.31	0.34	0.39	0.42	0.47	0.51	0.55	0.60
0	0.00	0.00	0.00	0.00	0.00	0.00	0.00	0.00	0.00	0.00	0.00	0.00	0.00	0.00	0.00	0.00	0.00	0.00	0.00
1,000	0.46	0.52	0.59	0.64	0.76	0.87	1.03	1.18	1.32	1.47	1.61	1.77	1.93	2.19	2.37	2.65	2.89	3.12	3.37
2,000	1.08	1.21	1.38	1.49	1.77	2.02	2.40	2.75	3.08	3.44	3.76	4.12	4.50	5.10	5.53	6.18	6.74	7.27	7.85
3,000	1.90	2.13	2.42	2.62	3.12	3.55	4.22	4.83	5.42	6.05	6.62	7.24	7.92	8.97	9.73	10.87	11.86	12.79	13.82
4,000	3.00	3.36	3.82	4.12	4.91	5.60	6.65	7.61	8.53	9.52	10.42	11.40	12.47	14.12	15.32	17.12	18.68	20.13	21.75
5,000	4.46	4.99	5.67	6.12	7.30	8.31	9.87	11.30	12.67	14.15	15.48	16.94	18.52	20.98	22.76	25.43	27.74	29.91	32.32
6,000	6.39	7.16	8.13	8.78	10.47	11.93	14.17	16.22	18.18	20.30	22.21	24.31	26.57	30.10	32.66	36.50	39.81	42.91	46.37
7,000	8.97	10.04	11.42	12.32	14.70	16.74	19.88	22.76	25.51	28.49	31.17	34.11	37.29	42.25	45.83	51.22	55.87	60.22	65.08
8,000	12.40	13.88	15.78	17.03	20.32	23.14	27.49	31.47	35.27	39.38	43.09	47.16	51.56	58.40	63.36	70.81	77.24	83.26	89.97
9,000	16.97	19.00	21.59	23.30	27.80	31.66	37.61	43.06	48.25	53.88	58.96	64.52	70.54	79.91	86.68	96.88	105.68	113.91	123.09
10,000	23.05	25.80	29.32	31.65	37.75	43.00	51.08	58.47	65.53	73.18	80.07	87.62	95.79	108.52	117.72	131.56	143.52	154.70	167.16
10,500	26.80	30.00	34.10	36.80	43.90	50.00	59.40	68.00	76.20	85.10	93.11	101.90	111.40	126.20	136.90	153.00	166.90	179.90	194.40
11,000	31.13	34.85	39.61	42.75	51.00	58.08	69.00	78.99	88.52	98.85	108.16	118.37	129.40	146.59	159.03	177.73	193.87	208.97	225.82

Isobase (i) number relates to distance (*100 km) from isobase 1 at southern end of Lake Agassiz.
ELC = modern elevation of Lower Campbell beach at each isobase.
ELCSO = modern elevation of Lower Campbell beach at southern outlet of Lake Agassiz (isobase 1.3).
RULC = uplift of Lower Campbell beach at each isobase, as related to southern outlet (isobase 1.3) = ELC - ELCSO.
s = relaxation time (cal yr B.P.)
A = amplitude factor at various isobases = RULC/(exp(10500/s)-1). 10500 is the age in cal yr B.P. of Lower Campbell beach.
RU = relative uplift compared to isobase 1.3 (i1.3), which extends through the southern outlet of Lake Agassiz.

Table 2 Depth and area of late Lake Agassiz and Lake of the Woods. The evolution of lake area, bathymetry, and volume of Lake of the Woods (from Yang and Teller, 2005).

Periods	Cal yr B.P.	Maximum depth (m)	Mean Depth (m)	Area (km^2)	Volume (km^3)
Lake of the Woods Period	Present	66.9	8.1	4524	37
	1,000	67.0	7.6	4415	34
	2,000	67.0	7.4	4292	32
	3,000	66.0	6.9	4052	28
	4,000	66.0	6.3	3676	23
	5,000	65.0	5.8	3227	19
	6,000	65.0	5.6	2857	16
	7,000	64.0	6.1	1822	11
	8,000	63.0	8.3	1061	9
	9,000	61.0	8.5	858	7
Lake Agassiz Period	10,000	89.0	14.7	-	-
	10,500	116.0	31.4	-	-
	11,000	132.0	43.8	-	-

While some parts of the southern basin would have been exposed early in post-Agassiz time, there likely also would have been areas of stagnant water and wetlands strewn across the basin, similar to the conditions seen today near the southern shoreline. Deeper pools may have also existed, fed by the Rainy River and other tributaries. Mellors (2010) identified cold-water ostracode remains from a core in the southern basin (WOO06-1A) until ~8.1 ka cal BP, well after Yang and Teller's (2005) paleotopographic images indicate Lake Agassiz left the basin (Figure 7c). He suggests cold water supplied by the Rainy River provided Lake Agassiz-like ecological conditions following the isolation of LOTW.

Further to the north, in the NW Angle basin (Figure 1), Mellors (2010) described several paleosols from sediment cores WOO06-4A, WOO06-5A, and WOO06-5A (Figure 9), which indicate periods when lake-levels were lower than the outlet (presumably the northern outlet of LOTW). The site of WOO06-4A appears to have been occupied by Lake Agassiz until as late 9.0 ka cal BP before becoming subaerially exposed from 8.4–7.8 ka cal BP (Figure 9). Paleosols from adjacent sites WOO06-5A and WOO06-6A indicate subaerial conditions existed at these locations later, from 7.8 ka cal BP to 5.5 and 4.9 ka cal BP, respectively. Mellors (2010) suggested that dryer than normal conditions during the mid-Holocene resulted in

subaerial conditions at sites WOO06-5A and WOO06-6A while the lower elevation site WOO06-4A became flooded.

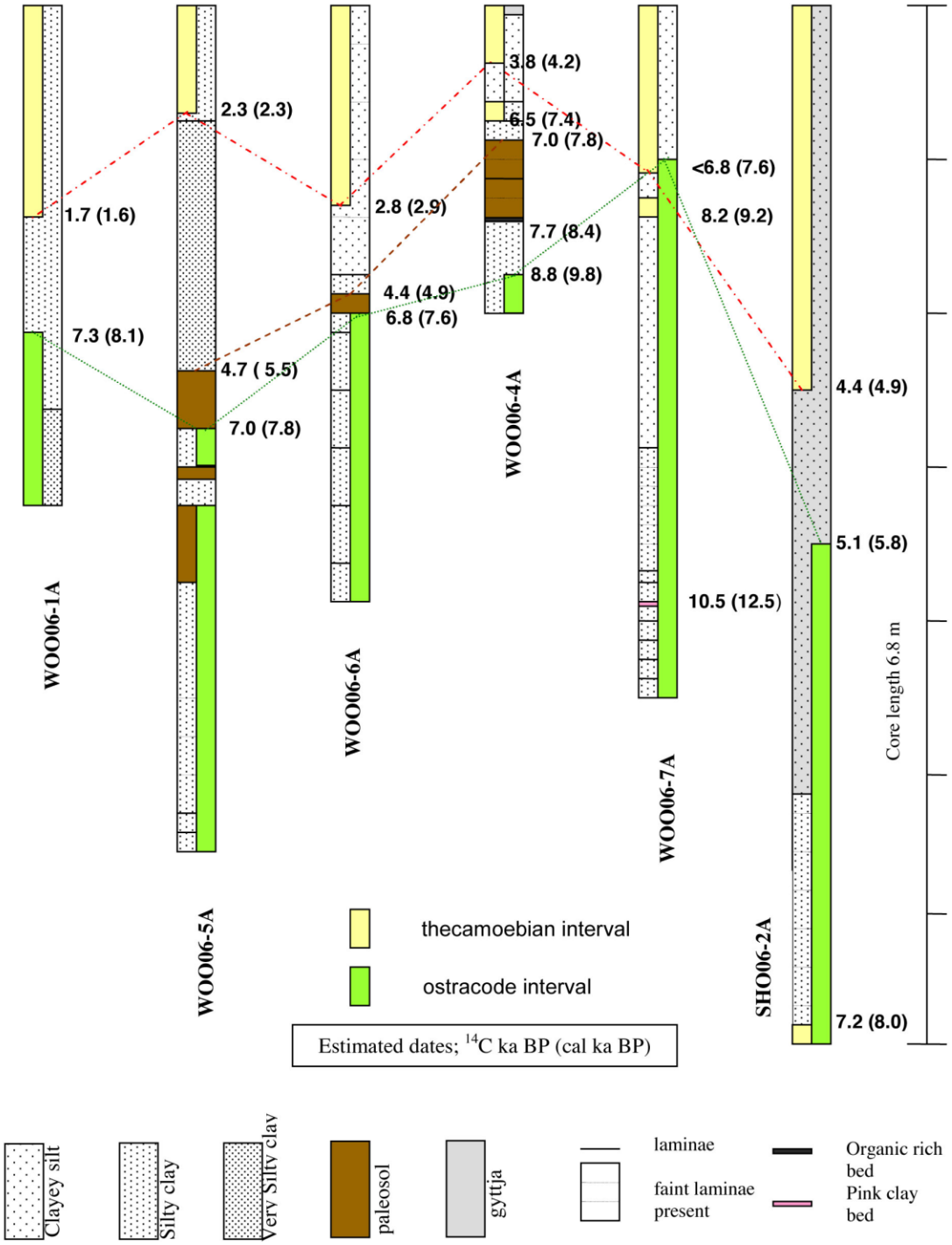

Figure 9 Stratigraphic correlations of Mellors (2010) sediment cores. Estimated correlations of sediment cores collected by Mellors (2010) from the southern basin (WOO06-1A), the NW Angle basin (WOO06-5A, WOO06-6A, and WOO06-4A), northern basin (WOO06-7A), and Shoal Lake (SHO06-2A). Locations of cores are shown in Figure 11 (from Mellors, 2010).

In the northern basin, sediment core WOO06-7A contains a diagnostic Lake Agassiz pink clay bed marker that dates to 12.9 ka cal BP. The appearance of thecamoebians, abundant plant and insect macrofossils, and abundant charcoal, none typical of Lake Agassiz sediments, implies separation of LOTW from Lake Agassiz occurred sometime about 10.0 ka cal BP, about 1,000 years before the time suggested by data from core site WOO06-4A. Mellors (2010) suggested that there may have been a connected channelway between Lake Agassiz and the NW Angle basin after the northern basin separated from Lake Agassiz.

2.3.3 Lake-Level Sensitivity During the Holocene

The paleotopographic models by Yang and Teller (2005) are only based upon the differential isostatic rebound of the lake outlet and assume a positive hydrologic budget (i.e. an over-flowing lake) throughout the Holocene. Studies of nearby lakes and lagoons (Moon Lake, Valero-Garcés et al., 1997; Wampum, Teller et al., 2000; Lake Winnipeg, Lewis et al., 2001; West Hawk Lake, Teller et al., 2008), however, indicate that, under drier conditions during the middle Holocene, the hydrologic budgets of many lakes were negative, resulting in relatively low lake levels. Once a hydrologic budget becomes negative, lake levels become extremely sensitive to climate and can fluctuate rapidly. Even groundwater-fed lakes, such as Elk Lake, Minnesota, were sensitive to Holocene dryness (Bradbury et al., 1993) and experienced large lake-level declines (Colman et al., 2012). Separating climate-induced lake-level changes from those due to differential uplift, however, is challenging because the controlling outlet of the basin is constantly shifting.

Lewis et al. (2001) found that during the middle Holocene, closed basin conditions in Lake Winnipeg, another remnant of Lake Agassiz that experienced post-glacial isostatic rebound, resulted in a prolonged period of desiccation in the southern basin but continued inundation in the northern basin. A similar situation might be expected for LOTW. It is possible that mid-Holocene arid conditions produced lower lake levels than what is represented in Figure 9, which would have delayed inundation of the southern basin.

2.4 Seismic-Reflection Data from Lacustrine Environments

The use of seismic-reflection techniques in lacustrine environments has proven to be a useful method for mapping subaqueous sediment stratigraphy (Colman et al., 1994; Todd et al., 1997; Abbott et al., 2000). A review of the methods and field techniques involved in seismic-reflection data reconnaissance can be found in Stoker et al. (1997) and a collection of interpreted seismic profiles was presented by Davies et al. (1997). Methods used for this research will be outlined and described in Chapter 3.

Todd et al. (1997) collected a series of seismic-reflection profiles from Lake Winnipeg using boomer and sleevegun systems. The profiles show three main sequences that they have termed (1) acoustic basement, (2) Agassiz sequence, and (3) Winnipeg sequence (Figure 10). They have broken the Agassiz sequence further into the Lower, Middle, and Upper Reflective Intervals (Figure 10, left side). In all profiles, an angular unconformity lies between the Agassiz and Winnipeg sequences. Their interpretation is that this unconformity formed by wave erosion either during the waning of Lake Agassiz or the advance of Lake Winnipeg. Because both Lake Winnipeg and LOTW formed under similar conditions, these sequences may also exist in the LOTW seismic record.

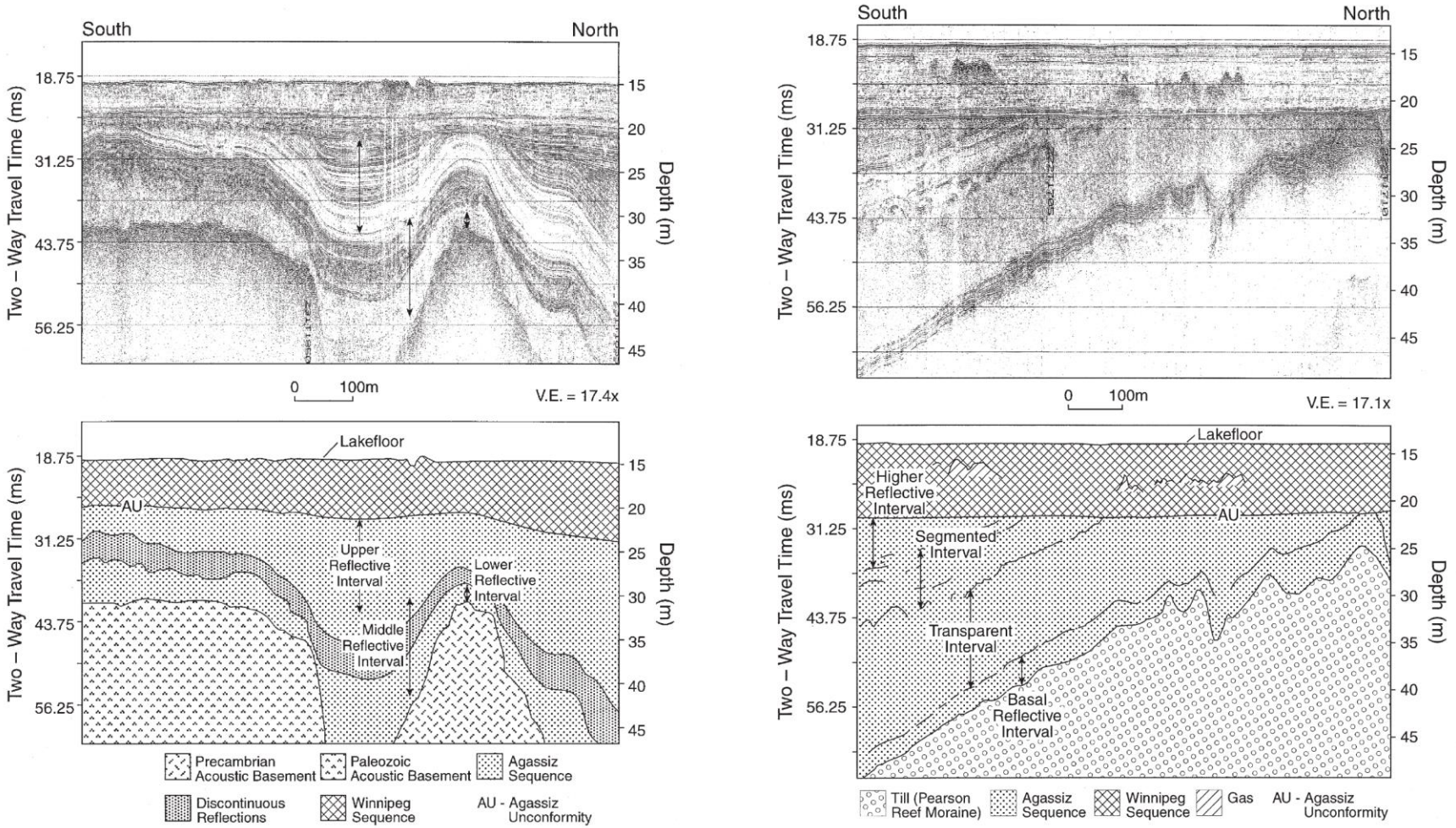

Figure 10 Seismic-reflection profiles from Lake Winnipeg. (Left) Examples of seismic-reflection data and interpretations from Lake Winnipeg. Lake Agassiz reflective intervals draped over the underlying basement vary in thickness. Agassiz Unconformity separates Agassiz from Winnipeg sediments. (Right) Lake Agassiz reflective intervals are truncated by the Agassiz Unconformity (from Todd et al., 1997).

Chapter 3: Methods

3.1 Seismic-Reflection Data

3.1.1 Acquisition

Preliminary seismic-reflection data were collected aboard a research skiff operated by the Minnesota Pollution Control Agency (MPCA) in October, 2011, to assess the character of LOTW sediment. The two-day survey acquired several short seismic lines from Big Traverse Bay and Muskeg Bay. The majority of the seismic data described in this thesis were collected during an eight-day cruise aboard the R/V *Arctic Fox* in August, 2012. A map with all the survey lines collected during both cruises is shown in Figure 11.

3.1.2 CHIRP Sub-Bottom Profiler

Both surveys were conducted using a single-channel EdgeTech 3100P CHIRP sub-bottom profiler (Figure 12) using an EdgeTech SB424 towfish. The CHIRP signal is a swept frequency that operates at 4-24 kHz and can be adjusted to a specific range by the user. For these surveys, the frequency was generally set to 4-20 kHz pulses lasting 10 ms in duration. Survey speeds were kept between 2 and 4 knots (5-8 km/hr) with the profiler 0.5 m below the water surface throughout the survey.

Vertical and horizontal resolutions are dependent upon the wavelength (λ) of the seismic signal and were calculated using Equations 1 and 2 and shown in Table 3. The minimum distance between two features so that they can be seen as separate reflectors (vertical resolution) is between ¼ and ½ wavelength. Assuming an average sound velocity of 1450 m/s for fresh lake water and water-saturated sediments and using frequencies of 4-20 kHz, the vertical resolution was calculated to be about 10 cm using the Equation 1 (Sheriff, 1977):

Equation 1

$$\left(\boldsymbol{\lambda} * \frac{\mathbf{1}}{\mathbf{4}}\right) = \left(\frac{\mathbf{1450}\,\frac{\boldsymbol{m}}{\boldsymbol{s}}}{\mathbf{4{-}20}\ \boldsymbol{kHz}} * \frac{\mathbf{1}}{\mathbf{4}}\right)$$

To determine the horizontal resolution, the first Fresnel zone must be taken into account. The first Fresnel zone is the area of a reflector that returns energy to the receiver within half a cycle of the first reflection. Features within the width of the first Fresnel zone cannot be resolved on a seismic section. Assuming the same velocity and frequencies as above, and an average depth of 10 m below the source and receiver, the width of the first Fresnel zone (horizontal resolution) was calculated at about 3 m using Equation 2 (Table 3):

Equation 2 $$w^2 = 2d\lambda + (\frac{\lambda^2}{4})$$

The relatively high frequencies allow for high horizontal and vertical resolution but limit the penetration to ~100 m. This proved to be more than sufficient for LOTW, where in most areas the total sediment thickness was less than 50 m.

Table 3 Vertical and horizontal resolutions for the SB424 sub-bottom profiler. Calculated vertical and horizontal resolutions using Equations 1 and 2. Features within the calculated vertical and horizontal resolutions constructively interfere and cannot not be independently resolved.

	CHIRP min	CHIRP max	Unit
Frequency (f)	4000	20000	Hz
Velocity (v)	1450	1450	m/s
Wavelength (λ) = v/f	0.36	0.07	m
Minimum Vertical Resolution (1/4λ)	0.09	0.02	m
Maximum Vertical Resolution (1/2λ)	0.18	0.04	m
First Fesnel zone (10m)	2.70	1.20	m

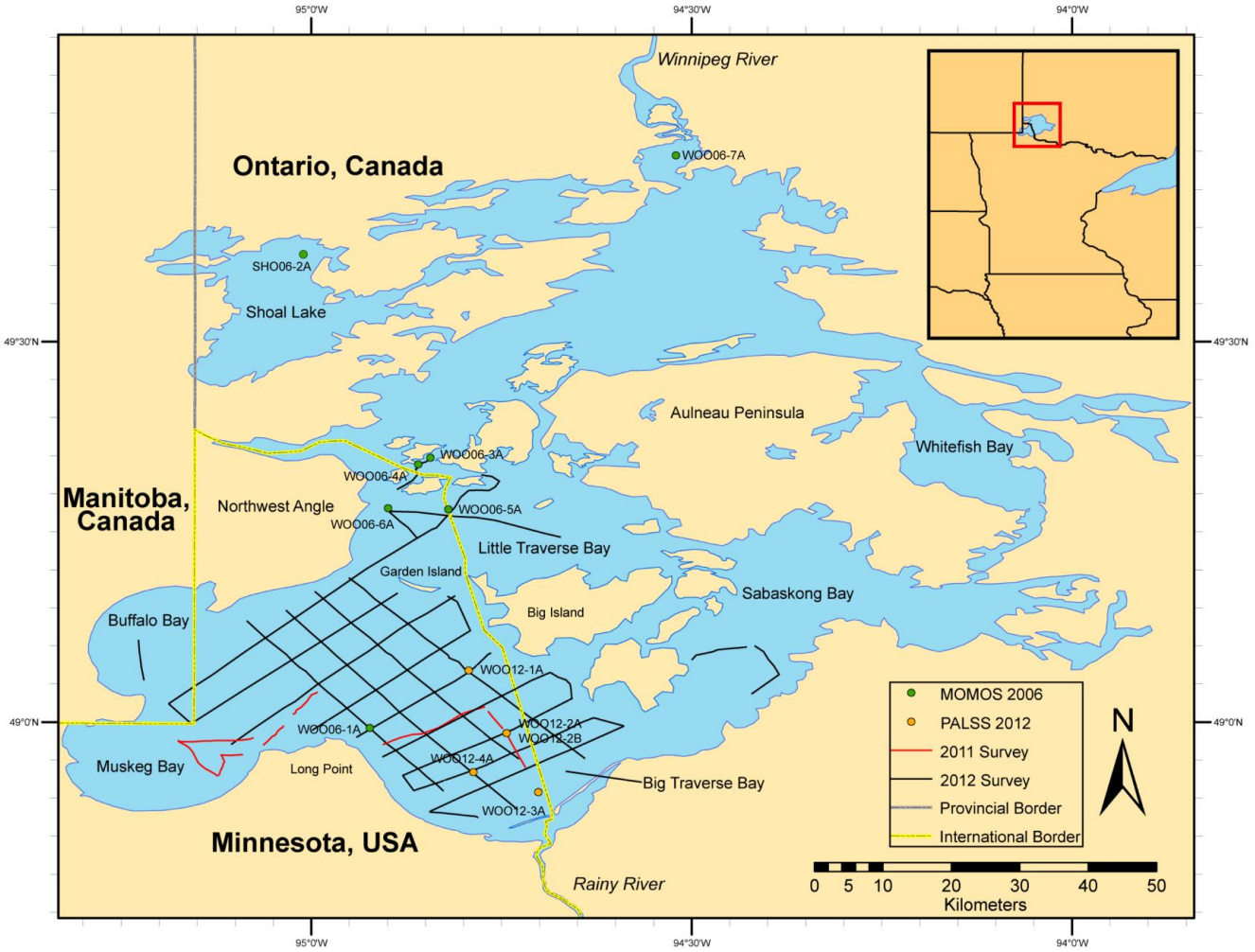

Figure 11 Survey map of Lake of the Woods. Map of Lake of the Woods showing the locations of the 2011 seismic survey lines (red), the 2012 seismic survey lines (black), the four sediment cores taken for this project in 2012 (PALSS, orange circles), and seven sediment cores taken by Mellors et al., 2010 (MOMOS, green circles). Complete core ID numbers are also shown.

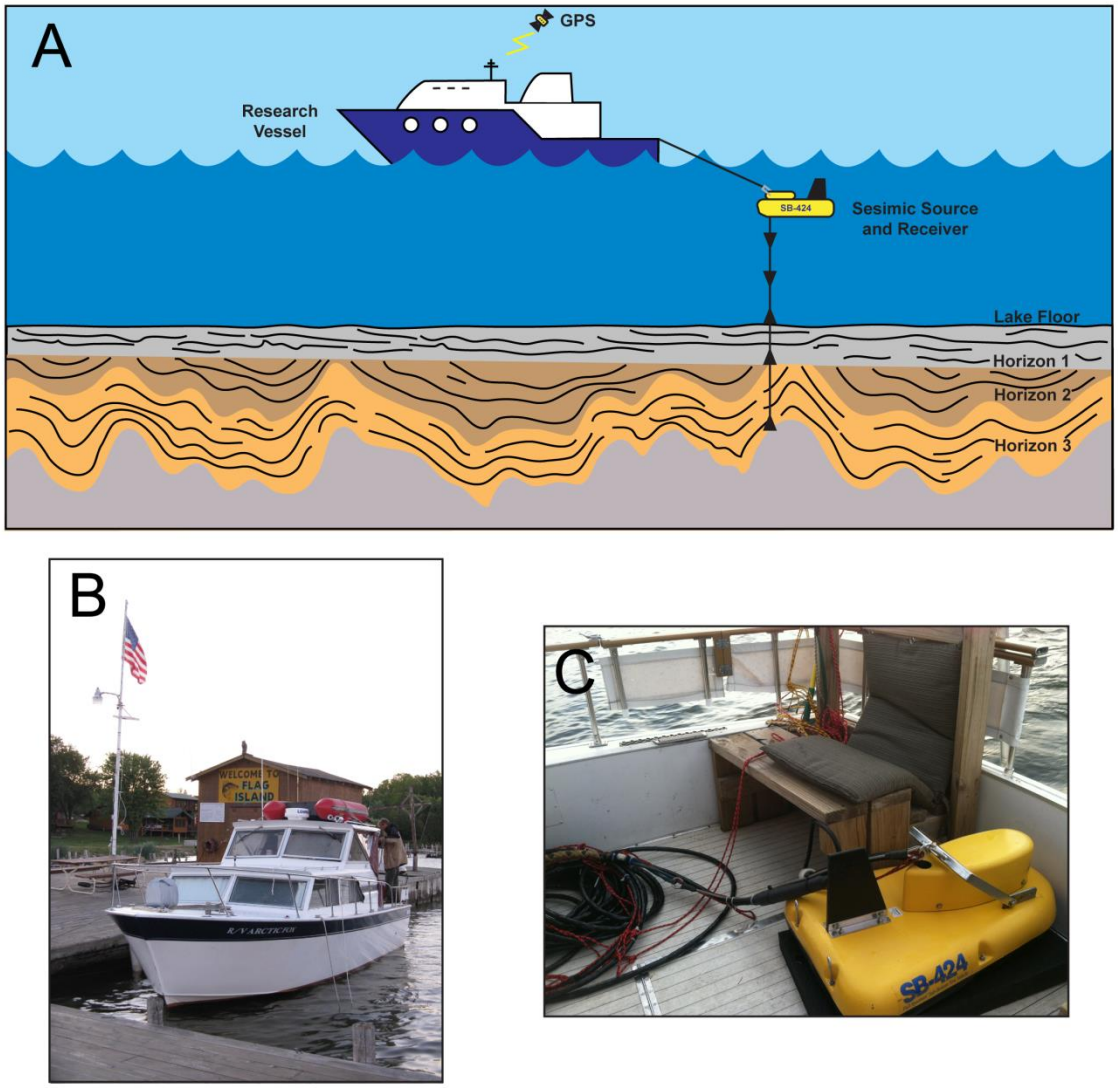

Figure 12 CHIRP sub-bottom profiler. (A) Schematic showing the 3100P CHIRP sub-bottom profiler being towed behind a research vessel. The SB-424 towfish contains both the source and the receiver minimizing the amount of equipment needed to conduct a survey. (B) Photo of the R/V Arctic Fox. (C) Photo of the SB-424 aboard the R/V Arctic Fox before deployment.

3.1.3 Survey Design

The main objective of the preliminary survey was to establish how well-suited the 3100P CHIRP system was for imaging and characterizing LOTW sediments. The three conclusions of this survey were: (1) The 3100P CHIRP system worked well and captured high resolution images of the lake sediments, especially offshore, (2) the high frequency signal attenuated extremely quickly in coarse or well-compacted sediments, limiting the signal's penetration in those regions. This

was observed below the upper boundary of the lower most seismic unit and near the mouth of the Rainy River, and (3) acoustic blanking occurred widely throughout the lake but was most pronounced in shallower regions. This is largely associated with gas bubbles that form from the decomposition of *in situ* organic matter. The gas bubbles tend to absorb the acoustic energy by compression, which attenuates the energy passing down through the sediment and reduces or limits penetration (Stoker et al., 1997).

The second and more extensive survey was designed to identify large-scale basin-wide features and to define the depositional regions of the basin. The survey focused in the southern basin for the following reasons: (1) large-scale features are more likely to be identified using multiple intersecting survey lines taken in open water (navigating around the thousands of islands that occupy the northern basin would have produced a fragmented dataset), (2) the seismic profiles could be compared to sediment cores previously taken from the southern basin, (3) the 3100P CHIRP system had already proven itself capable of producing high resolution images in the southern basin, and (4) access to the northern basin was extremely limited.

Over 475 km of data were collected for this project, 90 percent of which was from Big Traverse Bay. Survey routes were created in Google Earth and their coordinates were entered into the onboard Global Positioning System (GPS) of the R/V *Arctic Fox*. Nine lines were oriented NE-SW (parallel to the direction of isostatic rebound) intersected by four lines oriented NW-SE producing a ~5 x 5 km spaced grid (Figure 11). Additional lines were collected in Sabaskong Bay, Buffalo Bay, and Little Traverse Bay to determine the character of the sediments at the margins of the basin. Muskeg Bay was avoided due to the large amounts of gas found in the preliminary survey. Lines were carefully selected to pass over the locations where sediment cores had been collected.

3.1.4 Processing

Data processing occurred during acquisition with EdgeTech's Discover software so very little post-acquisition processing was required. Coordinates were

converted from geographic Latitude-Longitude to Universal Transverse Mercator (UTM) using the WGS 1984 standard for UTM zone 15N in the seismic processing system SPW (Parallel Geoscience Corporation, Long Creek, OR). This step allowed for the data to be imported into the seismic workstation in SEG-Y format along with the correct coordinates. The processed data were interpreted at the Geophysical Lab of the Large Lakes Observatory (LLO) in Duluth, MN using Kingdom Software Suite (IHS, Houston, TX), an industry standard interpretation package.

All seismic data were collected in time. Time-to-surfaces were converted to depth-to-surfaces using an average velocity of 1450 m/s. The depth-to-surfaces were then used to create Isopach maps, or maps showing regions with the same thickness. This was done by first creating a polygon outlining the survey area. Next, a flex grid algorithm was used to produce a grid, or surface, for selected horizons. The algorithm mathematically interpolated the input data values (traced horizons) and produced a three-dimension grid bounded by the created polygon. Because each isopach is defined by the vertical difference between two horizons (grids) within the seismic data, the spatial extent of the isopachs is dependent upon the continuity of the horizons. Bounding polygons were adjusted for each isopach according to the extent of the horizons of interest to show a more accurate depiction of the sediment thickness variations. Little Traverse Bay was only included in the depth to acoustic basement and bathymetric maps, even though several unique seismic units were observed, because (1) the absence of sediment between Big Traverse Bay and Little Traverse Bay prevented the correlation of seismic units other than the acoustic basement between the two bays and (2) a large portion of the survey area was obscured by shallow gas.

3.2 Sediment Core Data

3.2.1 Core Recovery

Four long (3-7 m) piston cores were collected from Big Traverse Bay through ice in March 2012 for the purpose of correlating seismic-stratigraphic units with lithological units. Core sites were chosen along a roughly N-S striking transect in an attempt to observe sedimentological evidence of shoreline migration as the lake

progressively transgressed southward across the basin. Core site PALSS 2A/2B was selected to capture a particular onlapping sequence identified from the preliminary seismic data). This is the only site where two overlapping cores (2A and 2B, spaced one meter apart) were taken. Core locations are shown in Figure 11.

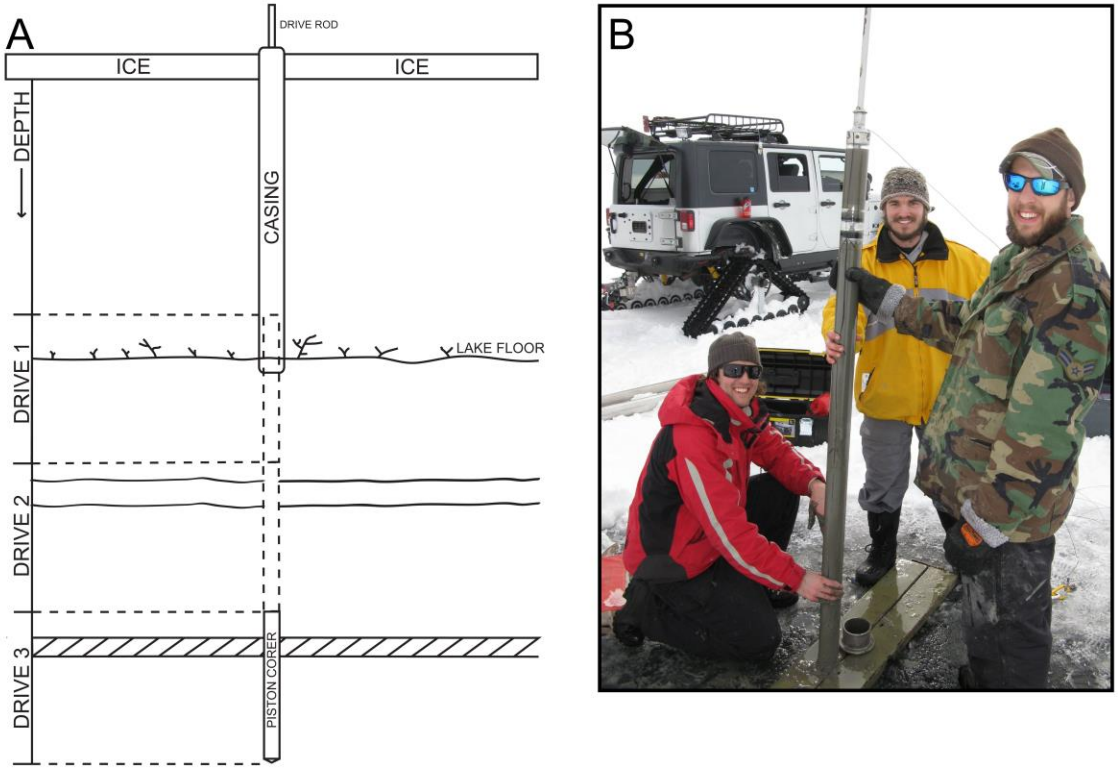

Figure 13 Sediment core recovery. (A) Schematic showing a typical drive sequence using a Bolivia or Livingstone-type piston corer through ice. The first drive captures the sediment-water interface and subsequent drives capture sequentially deeper sediment. Casing is used to prevent the drive rod from deviating from the coring hole after each drive. (B) Photo of a Lake of the Woods sediment core using a Bolivia-type piston corer shortly after recovery.

Bolivia and Livingstone-type piston corers were used for sediment recovery (Figure 13). A detailed description of the equipment and recommended coring techniques used can be found in a review by Myrbo and Wright (2008). In short, the piston corer is manually pushed into the lake sediment while a piston maintains pressure to keep the sediment preserved in its original orientation so it can be brought to the surface and extruded. After each drive and recovery, the corer reenters the same hole, where it sequentially penetrates (with the piston locked),

and collects (with the piston unlocked), deeper and deeper sediment, until the corer reaches the bottom of the lake sediment or encounters impenetrable material and cannot be pushed further.

Data from additional cores collected by Mellors (2010) are used as supplemental material in this project. These cores were collected using a Kullenberg corer during the summer of 2006. Core locations are shown in Figure 11.

3.2.2 Core Processing

The cores were split, imaged, and logged at the LacCore laboratory at the University of Minnesota. Density measurements were conducted on whole-core drives encased in either polycarbonate (Bolivia) or PVC (Livingstone) core liners using a gamma ray source (Cesium-137) and detector. Low-field magnetic susceptibility data were collected using a point source sensor directly on each core after they were split and imaged. Both measurements were simultaneously collected using a Geotek Multi-Sensor Core Logger (MSCL). Corrections for temperature and core liner properties were calculated using the Geotek software.

Magnetic susceptibility is a measure of how easily a material can be magnetized in an external magnetic field. It is primarily used as a relative proxy indicator for changes in the concentration of magnetite, though a detailed magnetic properties study can yield a wealth of information (Sandgren and Snowball, 2001). For this project, however, the magnetic susceptibility data were used for core-to-core and core-to-seismic correlations. The data here are expressed as a ratio per unit volume and the units are dimensionless units, described as 'SI units'.

The density of lake sediment is defined by the ratio of mass to volume, which in turn, depends on the mineralogy and the degree of compaction of the material. Density information is a useful tool for core-to-core correlations and for the identification of lithological changes in sediment cores. It can also be used to detect subtle changes in sediment composition that visual analysis may miss. Though invisible to the human eye these subtle perturbations often cause contrasts in the acoustic impedance of a seismic signal if they exceed the vertical resolution of seismic signal. Therefore, the density data can be used for core-to-seismic

correlation in addition to core-to-core correlation. Units for density are typically expressed as kg/m^3 but are given as g/cm^3 here.

Sediment cores were described using visual and textural analysis at the Sedimentology Lab of the LLO according to the classification scheme outlined by Schnurrenberger et al. (2003). Major changes in lithology were defined in terms of grain-size and classified as clay, mud, silt, or sand. Minor changes in lithology were indicated by the presence or absence of sediment characteristics such as laminations, peat, fossils, and desiccated clay.

Materials for radiocarbon dating were preferentially selected if they were located near a major change in lithology. Wood macrofossils and fragmented peat were preferred because of their dating reliability. Charcoal and terrestrial seeds were used where macrofossils were absent. Eight samples were rinsed with deionized water before being processed by an Accelerator Mass Spectrometer (AMS) at the Woods Hole Oceanographic Institute's radiocarbon lab (NOSAMS). Radiocarbon ages (^{14}C) were converted to calendar years before present (cal BP) using Calib v.5.0.1 (Stuiver and Reimer, 1986) and IntCal13 calibration data. MOMOS radiocarbon data were taken from Mellors (2010).

Chapter 4: Results

4.1 Seismic-Reflection Data Description

4.1.1 Classification and Procedure

Seismic profiles are not geologic cross-sections, but rather they portray contrasts in acoustic impedance. These contrasts are represented as seismic reflections within the geological succession. Seismic-reflection profiles only detect lithological boundaries if there is a change in acoustic impedance (the product of density and velocity) across the boundary.

When analyzing seismic-reflection data, three parameters are typically described: (1) the individual reflection characteristics, (2) the internal reflection configuration of a sequence, and (3) the external form or geometry of a sequence (Stoker et al., 1997). A detailed explanation of these terms is given below and examples of common reflection patterns are shown in Figure 14.

Reflection Character: Reflection character is described in terms of amplitude and continuity. *Reflection amplitude*, or reflection strength, is a function of the magnitude of change in acoustic impedance between strata. It is described as low, moderate or high. Reflection amplitude is higher if there is a greater change in the velocity, density, or both, such as in interbedded sequences of sand and mud or at the interface between bedrock and Quaternary sediments. *Reflection continuity* of stratal surfaces can be used as an indicator of the environment of deposition and is described as high, moderate or low. High reflection continuity, where no major changes disrupt reflection surfaces, is often a characteristic of tranquil, argillaceous lacustrine conditions. Conversely, low reflection continuity, where reflections lack continuity, is often a characteristic of higher energy, sandy sequences. Material composed of large clasts, such as a diamicton, commonly contain many point sources and scatter acoustic energy resulting in low continuity. Shallow gas also effects reflection continuity by obscuring the acoustic signal.

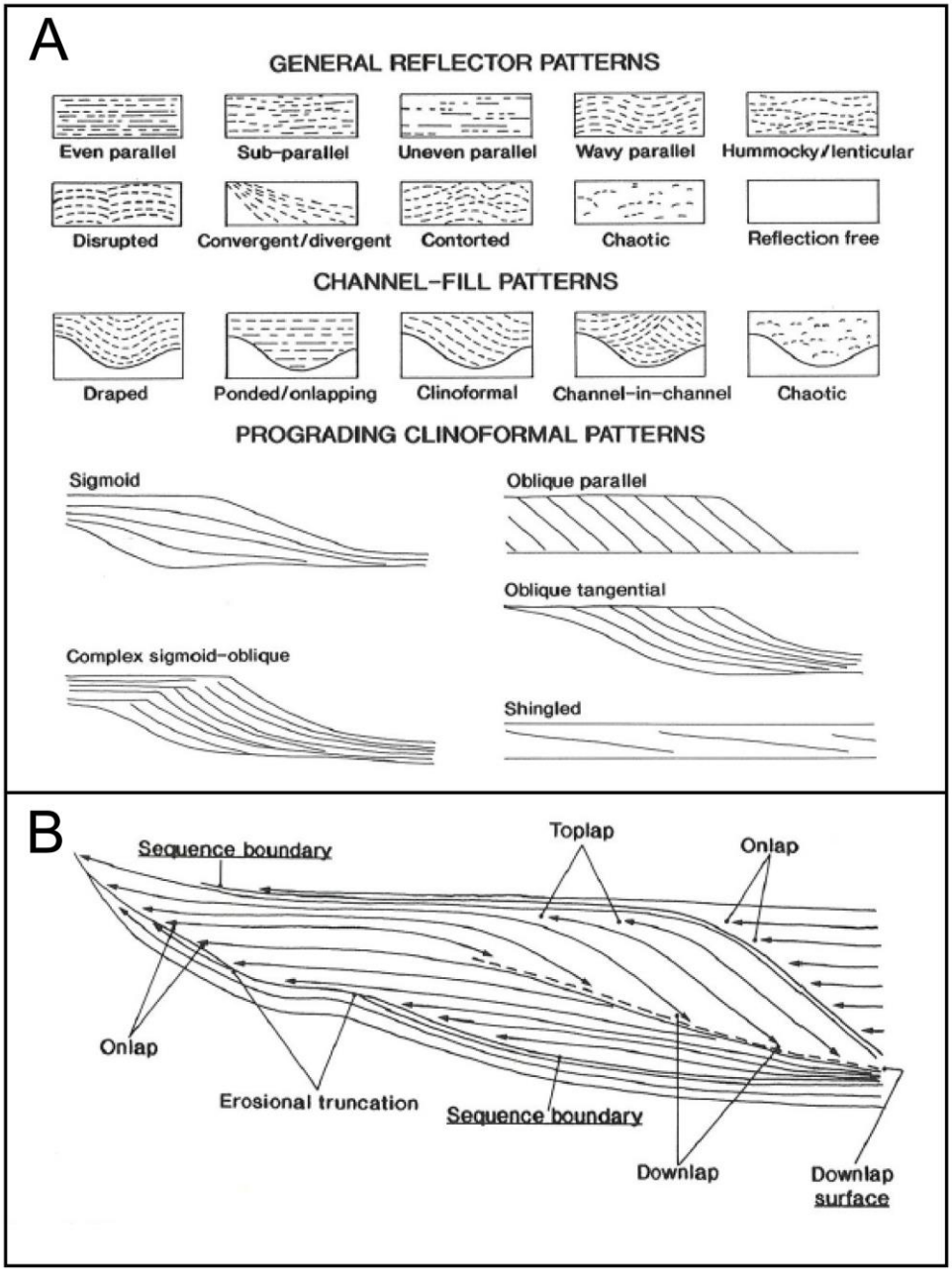

Figure 14 Seismic-reflection patterns. (A) Examples of common reflection configuration patterns observed on seismic profiles, and (B) different types of reflection termination patterns commonly used to distinguish between depositional sequences (from Mitchum et al., 1977).

Reflection configuration: Reflection configuration addresses the shape of the reflection and can be used to infer bedding patterns, depositional processes, erosional surfaces and paleotopography. There are three main types of reflection configurations: stratified, chaotic, and reflection-free (Figure 14A). *Stratified configurations* can occur in many forms. Parallel and sub-parallel patterns typically

form sheet or sheet drapes on the underlying topography. This configuration implies uniform suspended sedimentation found in tranquil environments. Ponded basin-fill patterns contain horizontally stratified reflectors formed under more dynamic conditions. Divergent patterns where the spacing between reflectors increases downslope, can indicate tectonic tilting of the basin, a change in sedimentation rates, differential in erosion and sedimentation, or simply sediment focusing. *Chaotic configurations* display a chaotic arrangement of reflectors and can occur in a variety of settings such as mass-flow deposits or channel fills. *Reflection-free configurations*, as implied, contain no reflections and are generally assumed to represent uniform lithology that lacks a change in density or velocity.

External Geometry: The external geometry of a seismic unit or facies can provide large-scale information such as the gross depositional environment, the sediment source, and the geologic setting. They are three-dimensional features that require a two-dimensional grid of seismic profiles to be constructed. The external geometry of a unit can be described quantitatively by creating isopach (thickness) maps. This is done by first tracing the upper and lower boundaries of a unit and then converting the boundaries from time-to-surface into depth-to-surface. The difference in depth between horizons can then be used to look for geometric patterns if there is a 2-dimensional grid of profiles. Horizons (reflections) for this project were picked, traced, and examined for geometry using Kingdom Software Suite.

Assuming an average sound velocity of 1450 m/s for fresh lake water and water-saturated sediments, depth-to-surface was calculated for each horizon using the following equation:

Equation 3 $$\boldsymbol{D = \frac{t*v}{2} + 0.5}$$

where D=depth-to-surface (m), t=two-way-travel-time (TWTT) in (s), v=sound velocity through medium in (m/s), and 0.5 m is the average depth in the water column at which the sub-bottom profiler was towed.

When used together, reflection character, reflection configuration, and external geometry can help the interpreter define individual seismic units within the seismic data. The terms 'unit' and 'facies' differ slightly from one another though they are often used interchangeably. The term 'unit' describes a group of reflectors that share common seismic characteristics, are distinguished from adjacent units, and are usually, but not always bounded by an erosional surface. Units may or may not be linked to a specific depositional environment. The term 'facies' relates reflection character, configuration, and geometry to a genetic depositional environment. For continuity purposes, however, the term 'unit' will encompass both definitions when describing the seismic profiles for this project.

4.1.2 Description of Seismic Units

The seismic data from LOTW have been separated into five individual units according to their reflection character, reflection configuration, and external geometries. They are labeled seismic units (SU) A, B, C, D, and E from oldest to youngest and are shown in two intersecting basin-wide profiles (Figures 16 and 18) and in a higher resolution profile located ~10 SW of Big Island (Figure 19). All figures include raw seismic data to show more clearly the sediment characteristics prior to interpretation. Selected sections from Figure 16 are shown in greater detail in Figure 17 and are referred to throughout the text. A base map of the study area is provided to locate the survey lines (Figure 15).

Isopach maps are also provided for each unit to spatially show thickness variations across the basin through time (i.e., depositional basins for SU's B-E). Not all isopach maps cover the entire basin, in many cases because shallow gas obscures the seismic signal, which prevents mapping underlying reflections. In other cases, seismic units pinch out and do not fully extend to the margins of the basin. Because it is difficult to distinguish between these scenarios from the sediment thicknesses alone, descriptions are included to help explain the limitations of each isopach map. Depths to surfaces were calculated from the lake floor unless noted otherwise.

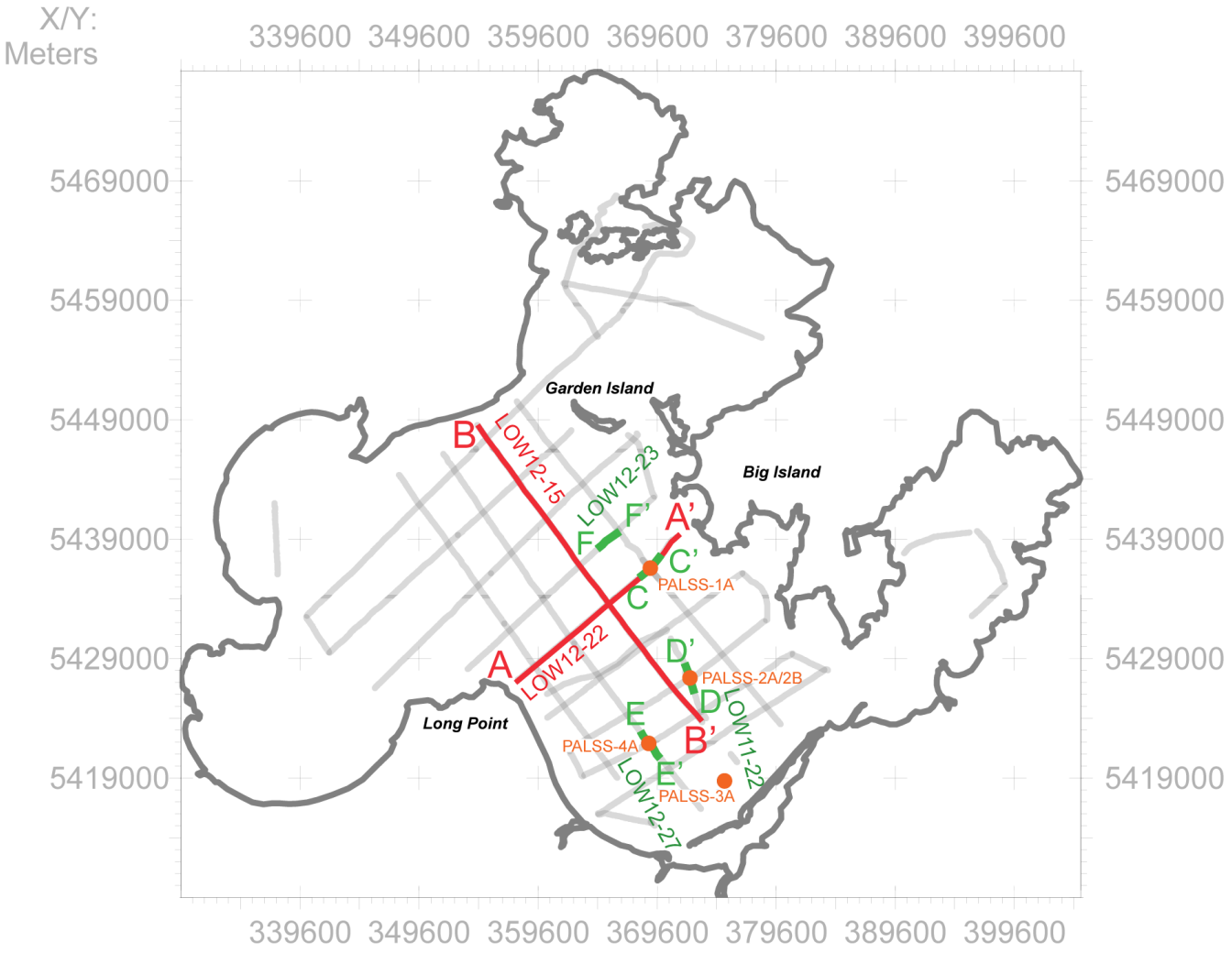

Figure 15 Basemap of survey area. Basemap of the southern basin of Lake of the Woods showing the location and orientation of selected basin-wide profiles (red), local seismic profiles (green), and the locations of four sediment cores collected in 2012 (orange). Axes indicate northing and easting coordinates corresponding to UTM Zone 15 N.

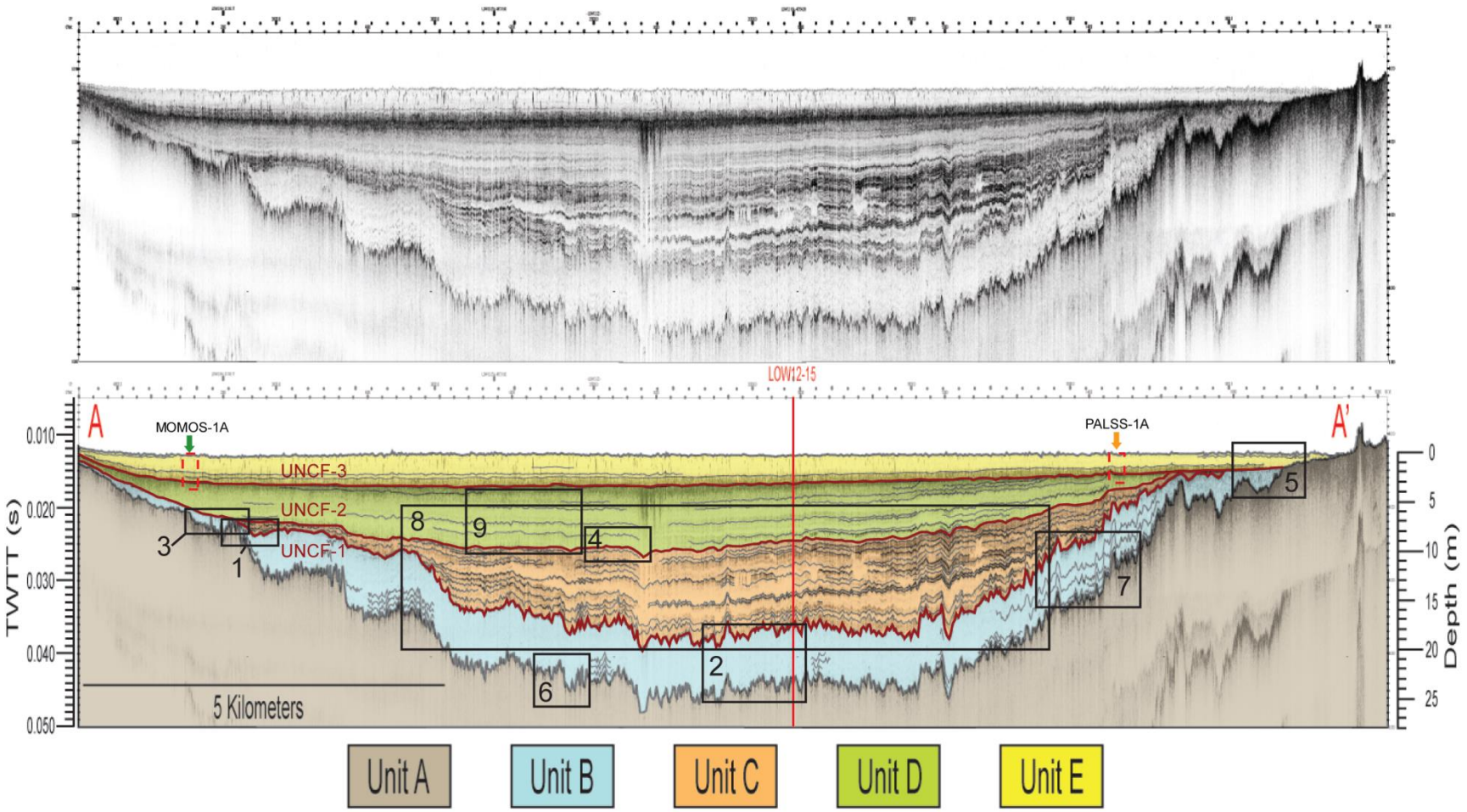

Figure 16 Seismic profile LOW12-22. Uninterpreted (top) and interpreted (bottom) seismic image from a basin-wide profile (LOW12-22) oriented SW-NE and roughly parallel to ice flow direction. The interpreted section shows the spatial relationships between SU's A-E (color coded) and unconformable surfaces (UNCF) 1-3 (maroon colored lines). Smaller scale images of selected regions (black boxes) display critical relationships in greater detail (Figure 17). Core locations are indicated by dashed red boxes. The intersection with seismic profile LOW12-15 is indicated by the vertical red line. Vertical exaggeration (V.E.): ~73x.

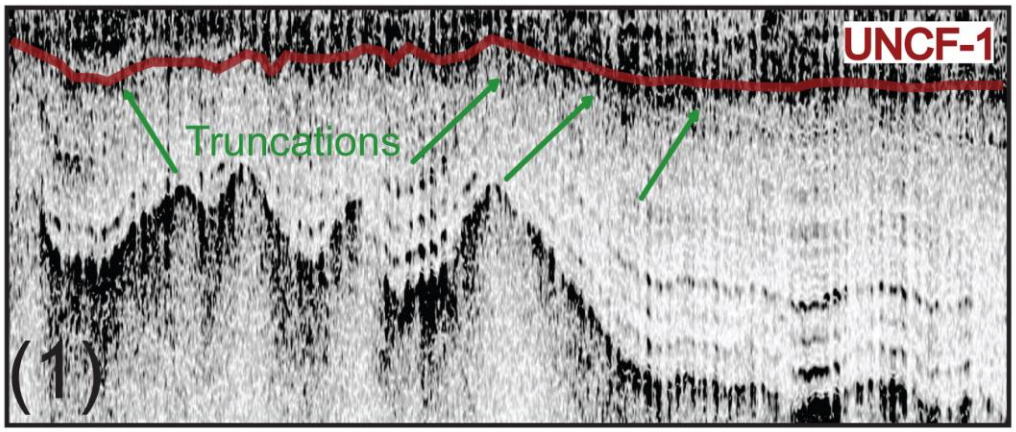
UNCF-1
Truncations
(1)

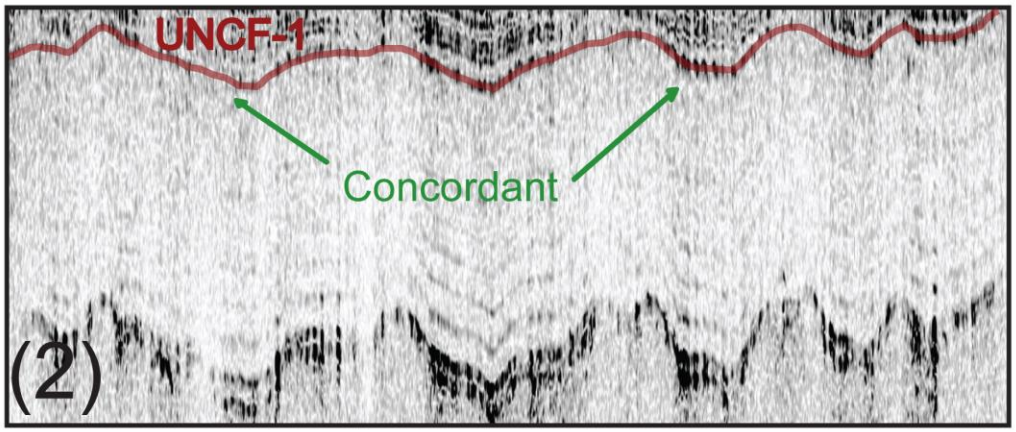
UNCF-1
Concordant
(2)

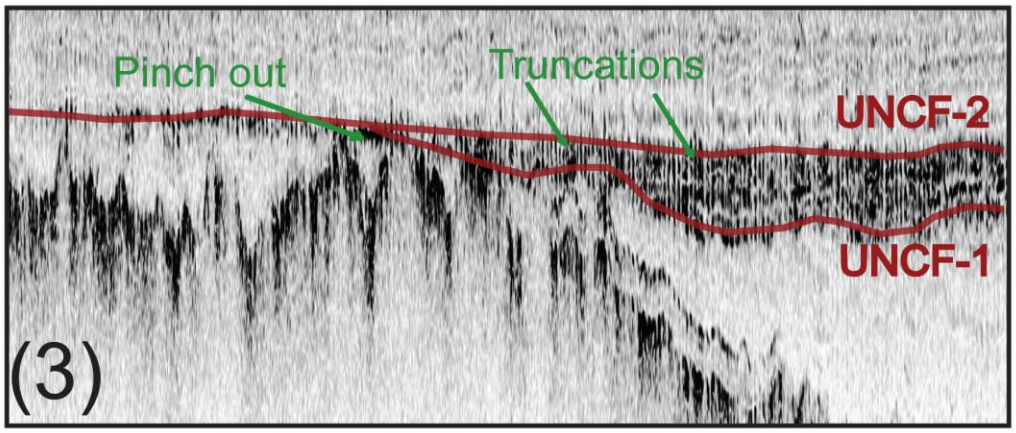
Pinch out
Truncations
UNCF-2
UNCF-1
(3)

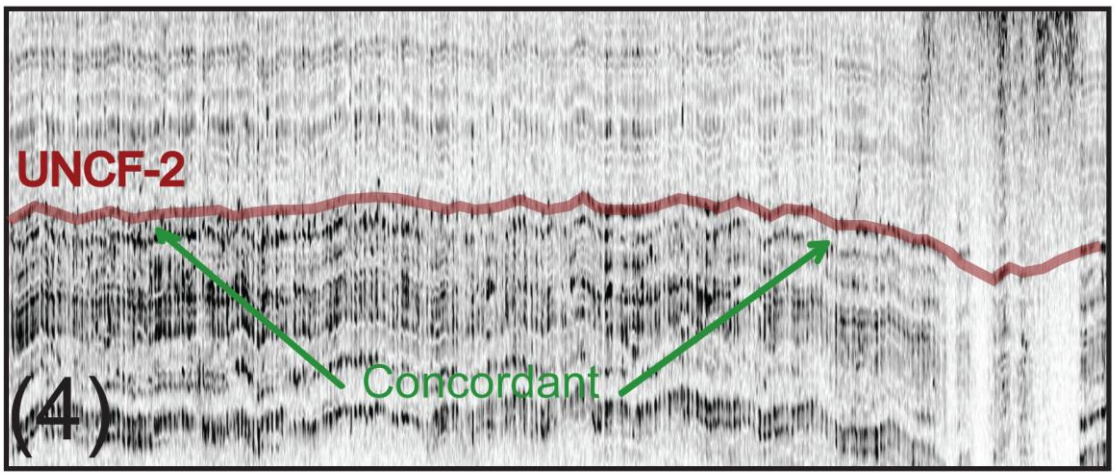
UNCF-2
Concordant
(4)

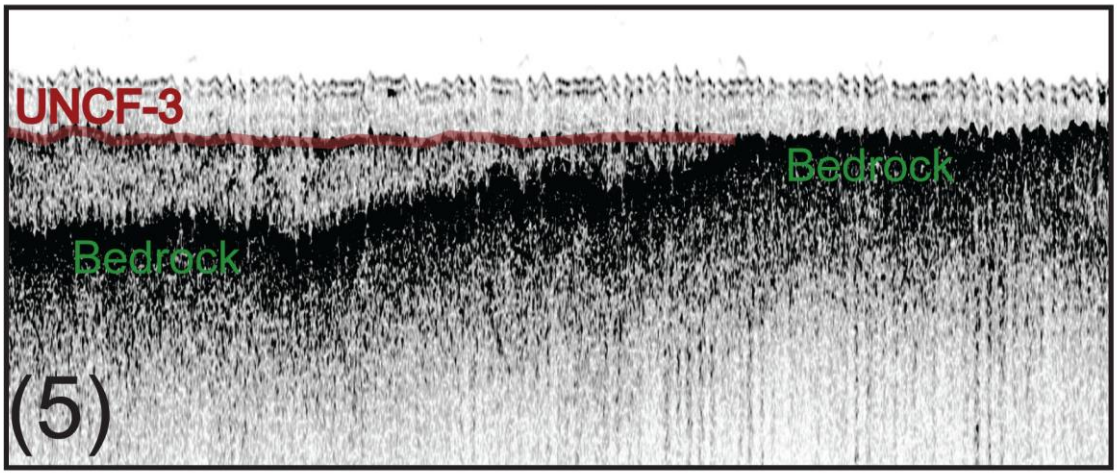
UNCF-3
Bedrock
Bedrock
(5)

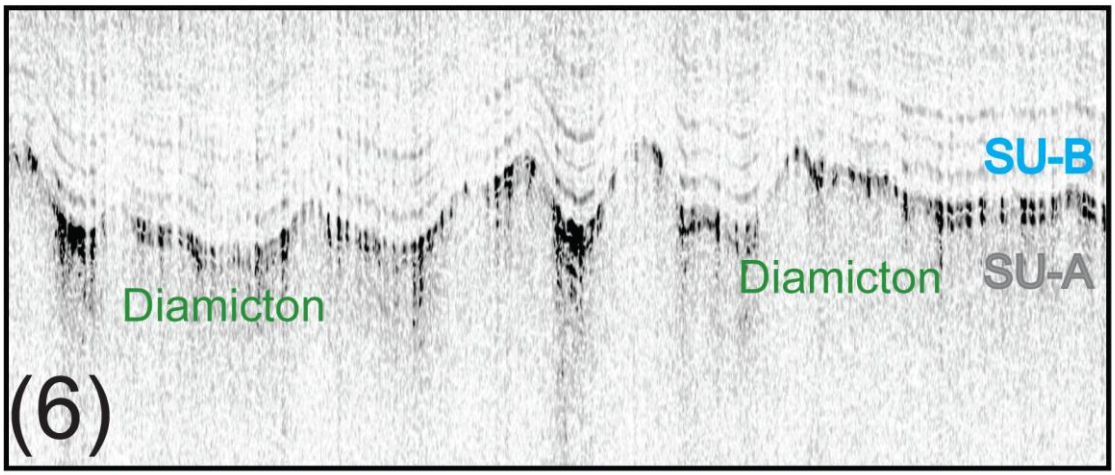
SU-B
Diamicton
Diamicton
SU-A
(6)

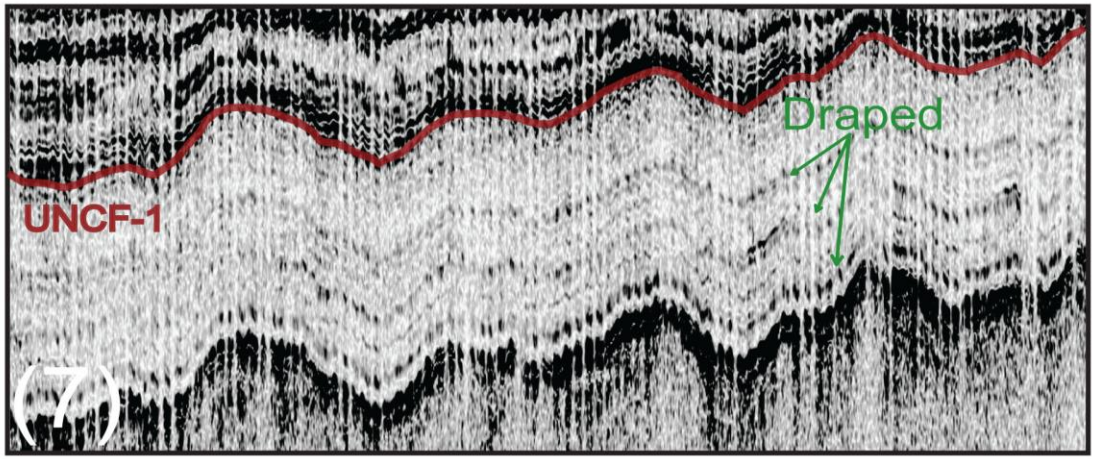
Draped
UNCF-1
(7)

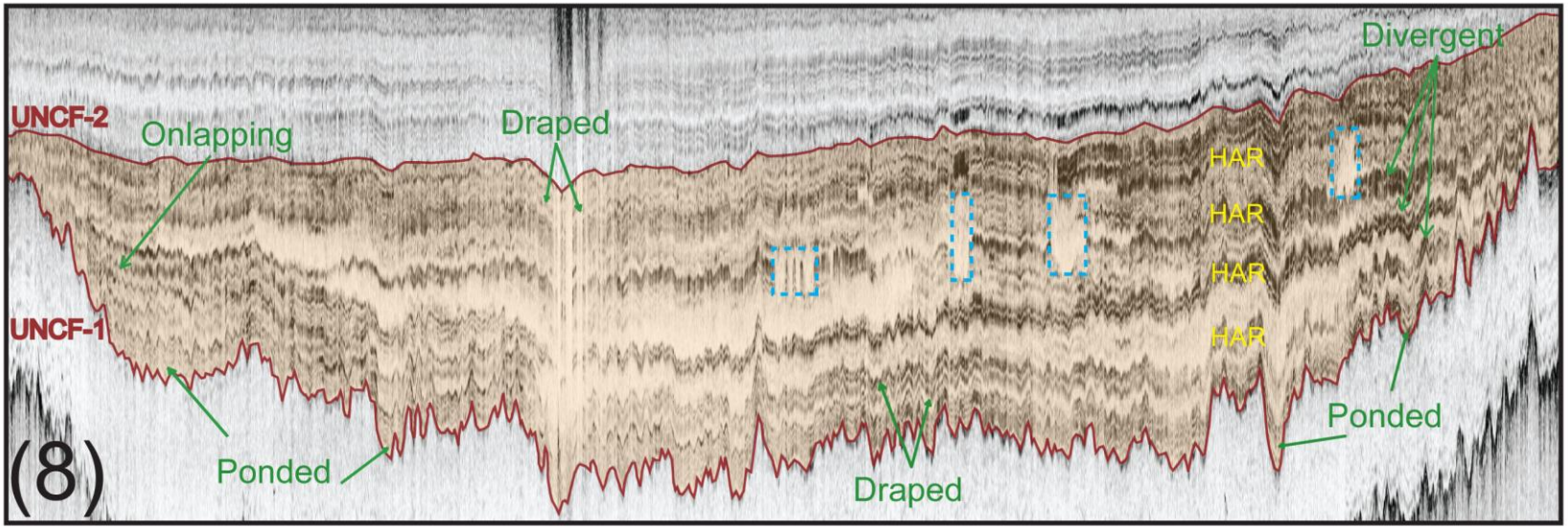
Divergent
UNCF-2
Onlapping
Draped
HAR
HAR
HAR
HAR
UNCF-1
Ponded
Draped
Ponded
(8)

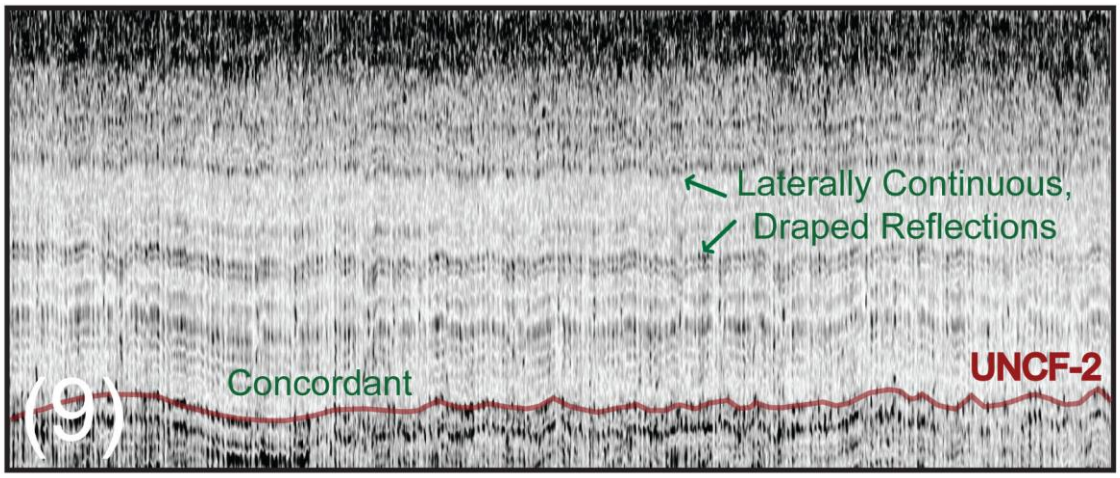

Figure 17 Selected images from seismic profile LOW12-22. (1) UNCF-1 truncates internal reflections of underlying SU-B near the margin of the basin but (2) lies concordant with the same reflections in the middle of the basin. (3) Similarly, UNCF-2 truncates underlying reflections at the margins of the basin, including UNCF-1, causing SU-C to pinch out at several locations. (4) Internal reflections within SU-C lie concordant with UNCF-2 in the middle of the basin. (5) The reflection amplitude strength of the acoustic basement (SU-A) is very high at the margins of the basin and becomes chaotic with depth, suggesting bedrock. The reflection configuration is generally smooth but becomes (6) highly irregular, with abrupt changes in relief inward of the margins, suggesting diamicton lithology. In the middle of the basin the reflection amplitude strength is lower than at the margins of the basin, and stratified wavy parallel reflections are occasionally observed at the top of SU-A. (7) Low-amplitude reflections within SU-B lie draped over underlying SU-A. They are best observed near the margins of the basin where the overlying sediment package is relatively thin and the seismic signal is not as attenuated as in the middle of the basin. (8) SU-C contains a complex arrangement of seismic reflections. Reflections in lower part of SU-C are ponded in the topographic lows onlapping onto the lower boundary moving up sequence and at the margins of the basin. The middle and upper part of the unit predominately contain stratified wavy parallel reflections that lie draped over underlying reflections. Several high amplitude reflections (HAR) diverge to the southwest and are separated by reflection free to low-amplitude zones. Wipe-out features (blue dashed boxes) are observed in the middle of SU-C and suggest the internal composition in these locations is relatively uniform. (9) SU-D contains abundant laterally continuous reflections that are strongly stratified parallel to sub-parallel. Internal reflections onlap onto UNCF-2 at and near the margins of the basin (not shown) but lie draped above UNCF-2 and underlying reflections in the middle of the basin.

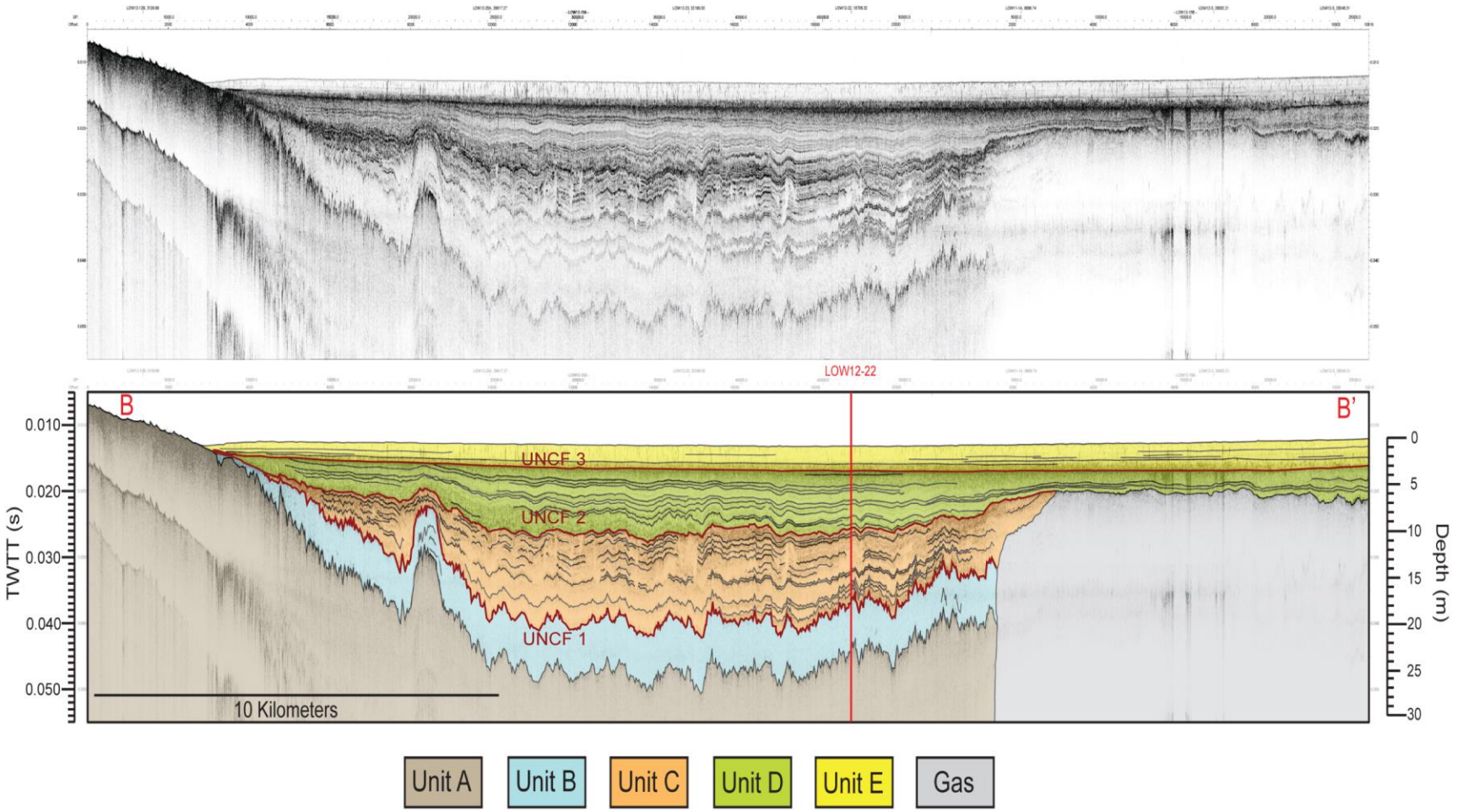

Figure 18 Seismic profile LOW12-15. Uninterpreted (top) and interpreted (bottom) seismic image from a basin-wide profile oriented NW-SE and roughly perpendicular to ice flow direction. Similar to LOW12-22, the interpreted section shows the spatial relationships between SU's A-E (color coded) and unconformable surfaces (UNCF) 1-3 (maroon colored lines). Relatively shallow gas on the right side of the image (between Units D-C) obscures lower reflections. The intersection with seismic profile LOW12-22 in indicated by the vertical red line. V.E.: ~195x.

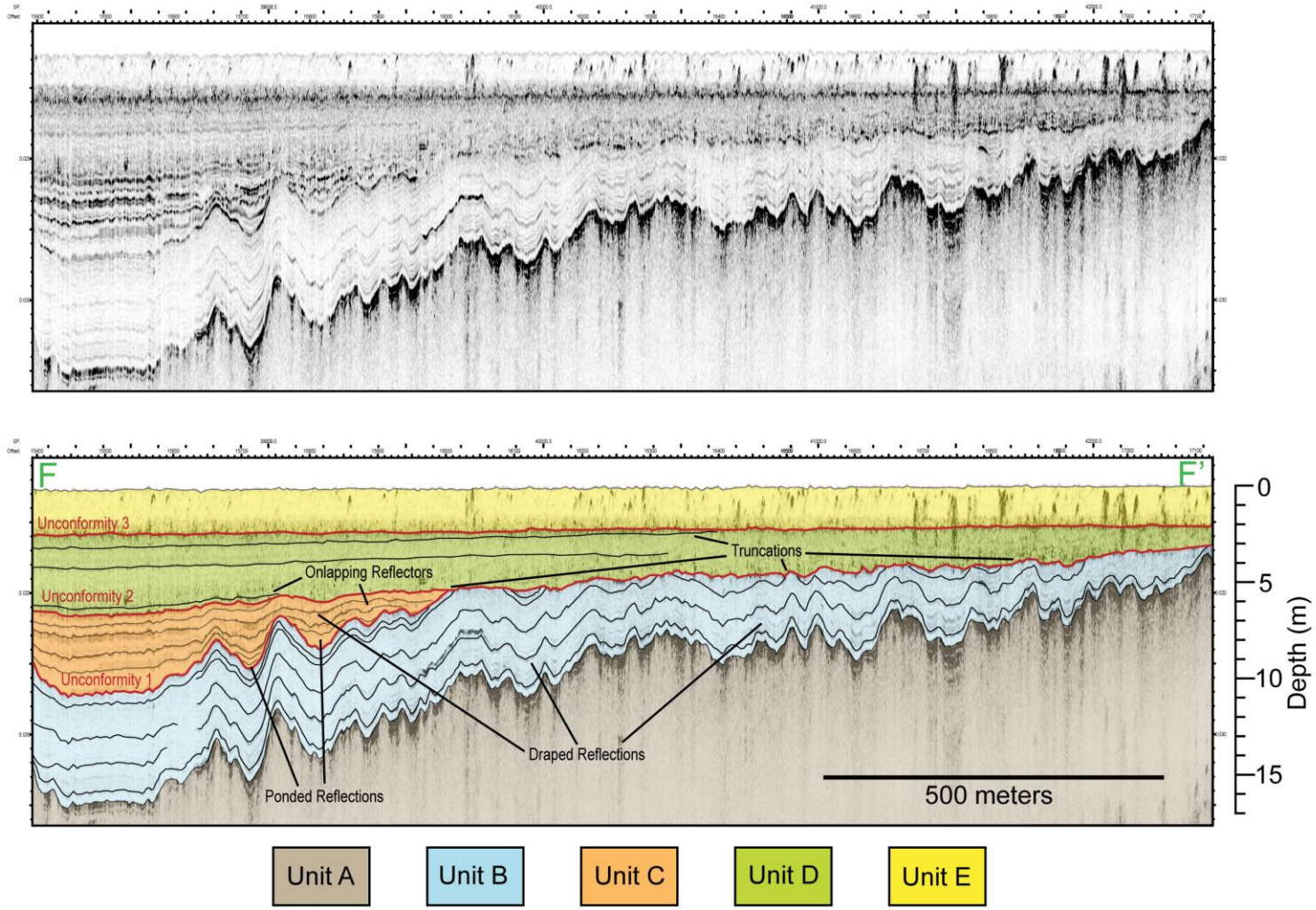

Figure 19 Seismic profile LOW12-23. Uninterpreted (top) and interpreted (bottom) seismic image from ~10 km SW of Big Island in the southern basin. This section shows the relationships between SU's A-E (color coded) and UNCF-1, -2, -3 (maroon colored lines) near the NE margin of the southern basin. V.E.: ~28x.

Table 4 Description of Seismic Unit A.

		Seismic Unit A
Reflection Character	Amplitude	Generally high with higher amplitudes at the margins of the basin and lower in the middle. Signal tends to diminish rapidly with depth below the upper boundary.
	Continuity	High to moderate though occasional discontinuities exist. Reflections are obscured by shallow gas or noise in Buffalo and Sabaskong Bays.
Reflection Configuration		Occasionally stratified sub-parallel or uneven parallel where penetration occurs beneath upper boundary. Upper boundary itself is very irregular in shape, displaying relatively high topographic relief in the middle part of the basin and smoothed surfaces at the margins of the basin. No stratification occurs where the configuration is smooth.
External Geometry		The upper surface of this unit forms the acoustic basement in most areas and the unit is observed everywhere within the survey area with the exception of gassy regions. It is deepest in the middle of Big Traverse Bay and shallowest near Garden Island marking the separation of Big Traverse Bay and Little Traverse Bay. Local variations in depth are observed across the survey area with some occurring abruptly.

Table 5 Description of Seismic Unit B.

		Seismic Unit B
Reflection Character	Amplitude	Low to moderate.
	Continuity	Internal reflections are mostly discontinuous but occasionally are laterally continuous for several kilometers near the margins of the basin. Much of this unit is obscured by shallow gas or background noise outside of Big Traverse Bay.
Reflection Configuration		Nearly reflection-free but weakly stratified wavy parallel in some areas. The upper part of the unit is concordant with Unconformity 1 in the middle of the basin but is truncated by Unconformities 1, 2, or 3 near or at the margins of the basin.
External Geometry		Seismic Unit B is observed mostly in the central part of Big Traverse Bay where it is not obscured by noise or gas. It displays a sheet drape geometry over Unit A and is spatially uniform in thickness where not truncated by Unconformities 1, 2, or 3. It is thinnest near Long Point and in the northwest part of Big Traverse Bay.

Table 6 Description of Seismic Unit C.

		Seismic Unit C
Reflection Character	Amplitude	High to moderate, though, some low-amplitude reflectors are visible in the center of the seismic unit. A few high-amplitude reflections are sandwiched between low-amplitude and reflection free zones.
	Continuity	Moderate to highly continuous. Some reflections are discontinuous in the center of the seismic unit and occur where the seismic signal is "wiped-out". Much of this unit is obscured by shallow gas or background noise outside of Big Traverse Bay.
Reflection Configuration		Strongly stratified wavy parallel with regions that are reflection-free to faintly stratified. Internal reflectors frequently onlap onto Unconformity 1 and are ponded at topographic lows. Seismic profiles striking NE to SW display some internal reflections that have a divergent configuration. The magnitude and direction of divergence varies vertically in the seismic unit. In the middle of the basin, the upper part of this seismic unit is concordant with Unconformity 2. Near the margins, however, it is truncated by Unconformities 2 and 3 causing seismic Unit C to pinch out. Reflections become increasingly more planar moving up the seismic unit.
External Geometry		Seismic Unit C is observed mostly in the central part of Big Traverse Bay. It has characteristics of a sheet draped geometry (wavy configuration), a ponded geometry (onlapping reflections), and a divergent geometry (lateral thickening between high-amplitude reflectors). It is thickest in the center of Big Travers Bay and thins more rapidly to the NE than other direction. It is thinnest where Unconformities 2 and 3 truncate internal reflections, to the north and south of the middle of the basin.

Table 7 Description of Seismic Unit D

		Seismic Unit D
Reflection Character	Amplitude	Low to moderate. Reflection amplitudes are highest near Unconformities 2 and 3. High-amplitude acoustic noise is frequent directly below Unconformity 3 and reflections often fade into the background noise.
	Continuity	Mostly continuous, though, some discontinuous reflectors are observed throughout the seismic unit. Seismic Unit D is sometimes obscured by shallow gas or background noise (i.e. Buffalo and Sabaskong Bays).
Reflection Configuration		Strongly stratified parallel to sub-parallel. Internal reflections drape Unconformity 2 in the middle of the basin and onlap onto Unconformity 2 near the margins of the basin. Internal reflections in the upper part of the unit are truncated by Unconformity 3 in all survey lines. This relationship is most pronounced at the margins but internal reflections are truncated as much as 8 km into the middle of the basin.
External Geometry		Unit D is observed across the majority of the survey area. It is thickest in the center of Big Traverse Bay and thins radially towards the modern day shoreline. This unit mainly lies unconformably over Unit C but also lies unconformably over Unit B in regions where Unit C pinches out (margins). It always underlies Unit E unconformably.

Table 8 Description of Seismic Unit E.

		Seismic Unit E
Reflection Character	Amplitude	The upper two-thirds of seismic Unit E is mostly reflection-free with occasional moderate-amplitude reflectors. The lower third contains high-amplitude noise that increases in strength towards Unconformity 3. A few high amplitude reflectors are present through the noise. The upper boundary (i.e., the lake floor) is moderate-amplitude.
	Continuity	Internal reflections are mostly discontinuous. A few reflectors in the lower part of the seismic unit are laterally continuous for tens of kilometers. Shallow gas is common in this unit, obscuring any underlying reflections.
Reflection Configuration		Weakly stratified parallel. Low angle internal reflections onlap onto Unconformity 3 over tens of kilometers and occur more frequently in the southern part of the basin. The upper two-thirds of the seismic unit is mostly reflection-free. The lower third of the unit contains background noise that increases in thickness towards the middle of the basin.
External Geometry		Seismic Unit A is the uppermost unit and is observed over the majority of the survey area when not obscured by shallow gas. It distinctly increases in thickness from NE to SW within the survey area and the thicker regions wrap around Long Point. This seismic unit primarily lies unconformably over seismic Unit D but also lies unconformably over seismic Units C, B, and A at or near the margins.

4.1.3 Description of Unconformable Surfaces

Unconformable surfaces indicate hiatuses in deposition. Their relationship with underlying reflections indicates the process by which the unconformity formed. Unconformable surfaces either lie concordant to, indicating non-depositional conditions, or truncate underlying reflections, indicating erosional conditions. Erosional unconformities are commonly formed in the high-energy littoral zone where waves can easily erode underlying material. Because the energy state of lacustrine and marine environments is often laterally variable, unconformable surfaces can be concordant in one region but erosional in another. Additionally, horizons can be unconformable in the littoral zone but conformable (no hiatus) in the low-energy distal regions where sedimentation remains continuous. The point or zone at which a horizon transitions from being unconformable to conformable, together with an estimate of wave base, can be used to delineate the paleoshoreline of a former lake (Colman, 2012). Unconformities are

interpreted to be related to lowstands, specifically, as in marine environments, the transgressions following lowstands.

Identifying unconformable surfaces from conformable surfaces in seismic profiles can be difficult. Unconformable surfaces that are concordant (hiatus) and conformable surfaces (no hiatus) may express similar reflection character and configuration at a given location. Therefore, it is important to also use the characteristics of adjacent reflections (both laterally and vertically) to help understand the mechanism in which the surface formed.

Three major unconformities were identified in the LOTW seismic record. Each unconformable surface marks the boundary between two or more seismic units. They display different reflection character and configuration properties than the seismic units they bound and have therefore been described separately. Unconformable surface 3 (UNCF-3) was erosional across the majority of the basin, exhibiting a high amplitude reflection strength, and mapping its extent was straightforward. Unconformable surface 1 (UNCF-1) and unconformable surface 2 (UNCF-2) were erosional only at or near the margins of the basin. Inward of the erosional zone the amplitude strengths of UNCF-1 and UNCF-2 remain greater than the overlying and underlying reflections for the majority of the basin and mapping their extent was also fairly straightforward. Occasionally, in the middle of the basin, UNCF-1 and UNCF-2 were not noticeably different than those of the overlying and underlying reflections and mapping their extent was more challenging. At these locations, the two surfaces (UNCF-1 and UNCF-2) were also conformable with underlying reflections making them *conformable surfaces* rather than *unconformities* (Figure 17(2), (4) and (9)). However, to avoid confusion, each of the three surfaces are referred to as UNCF-1, -2, and -3. Contour maps of the three major unconformable surfaces (below) show that the amount of relief across the basin decreased through time as the higher elevation regions were eroded and the topographic lows were filled. Depths to surfaces were calculated from the lake surface.

Unconformable Surface 1 (Figure 20)

UNCF-1 separates SU-B and SU-C (Figures 16, 18, and 19). The reflection amplitude of UNCF-1 is high at the margins of the basin decreasing towards the middle of the basin. At the margins, where reflection amplitudes are highest, the surface is erosional and the surface truncates internal reflections of underlying SU-B (Figure 17(1)). In the middle of the basin the surface is concordant with the internal reflections in SU-B (Figure 17(2)). Red to light-green regions (Figure 20) indicate where truncations occur and dark-green to dark-blue indicate where the surface is concordant. At the margins of the basin UNCF-1 is always truncated by UNCF-2 or UNCF-3.

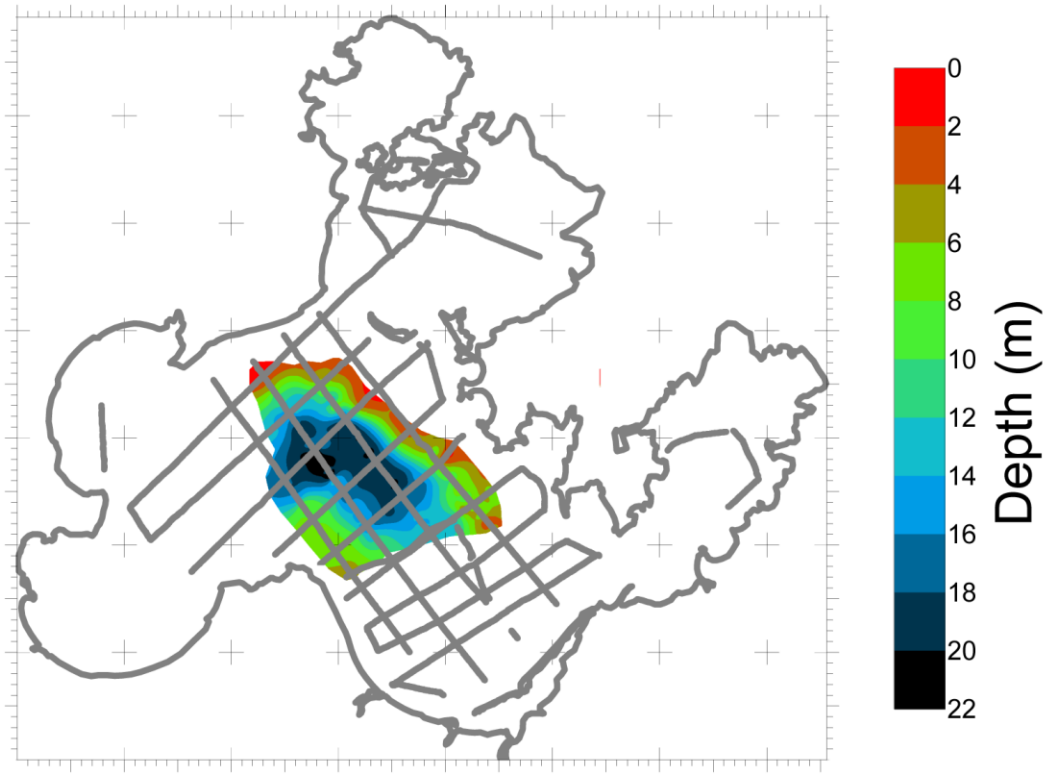

Figure 20 Contour map of depth to UNCF-1.

Unconformable Surface 2 (Figure 21)

UNCF-2 separates SU-D from SU-C and SU-B. Like UNCF-1, its reflection amplitude decreases from the margins to the middle of the basin but to a lesser degree than UNCF-1. The related reflection is typically broad and laterally continuous, though, occasional discontinuities are observed in the middle of the basin. UNCF-2 truncates internal reflections of underlying SU-C and SU-B near the margins of the basin (Figure 17(3)) but is concordant with reflections within SU-C in the middle of the basin (Figure 17(4)). UNCF-2 also frequently truncates UNCF-1, causing SU-C to pinch out (Figure 17(3)). The topographic relief of UNCF-2 is less than that of UNCF-1 (Figure 20) and is more continuous across the survey area. At the basin's margins UNCF-2 is frequently truncated by UNCF-3 (red to yellow, Figure 21).

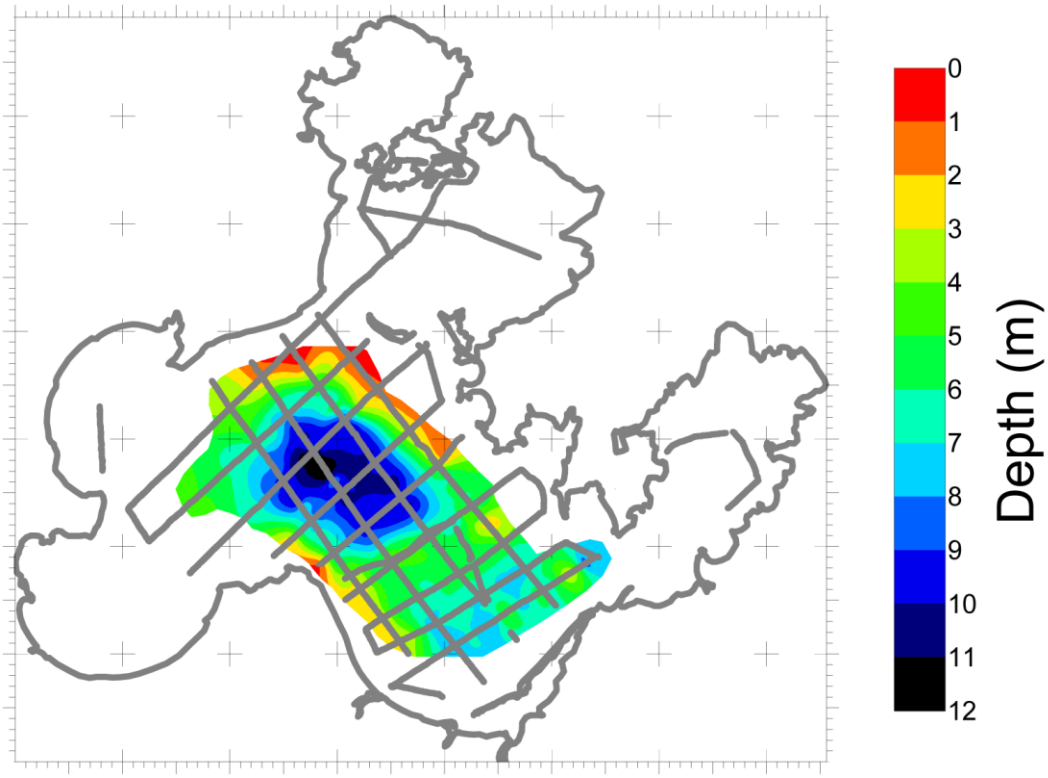

Figure 21 Contour map of depth to UNCF-2.

Unconformable Surface 3

UNCF-3 separates SU-E from underlying SU-B, SU-C, and SU-D. Because the lake floor has so little relief (Figure 27), the contour map of depth to UNCF-3 is virtually identical to the isopach map of SU-E (thickness between the lake-floor and UNCF-3, Figure 26) and is therefore not included here. UNCF-3 is continuous and forms a very high-amplitude reflection across the basin. Underlying seismic units and unconformable surfaces are truncated by UNCF-3 at the margins of the basin (Figures 16, 18, and 19). There is very little variation (< 4 m) in topographic relief on the unconformity. UNCF-3 is noticeably farther from the lake floor in the southwestern part of Big Traverse Bay (black regions) where SU-E is thickest.

4.1.4 Description of Isopach Maps

Thickness of Sediments above the Acoustic Basement (Figure 22)

This map represents the distance from the lake floor to the acoustic basement (upper boundary of SU-A), equivalent to the total sediment thickness above the acoustic basement within the survey area. The geometry of sediment package is an elongated mass with its long axis striking NW-SE. The thickest region reaches 28 m in the middle of the southern basin. A few isolated regions 20-22 m thick occur on the eastern edge of the survey area. The acoustic basement rises to the lake floor forming two distinct non-depositional strips, to the north and south of the thickest region (red colored regions, Figure 22). The northern strip is 7-10 km wide and separates the southern basin (Big Traverse Bay) from the NW Angle basin (Little Traverse Bay).

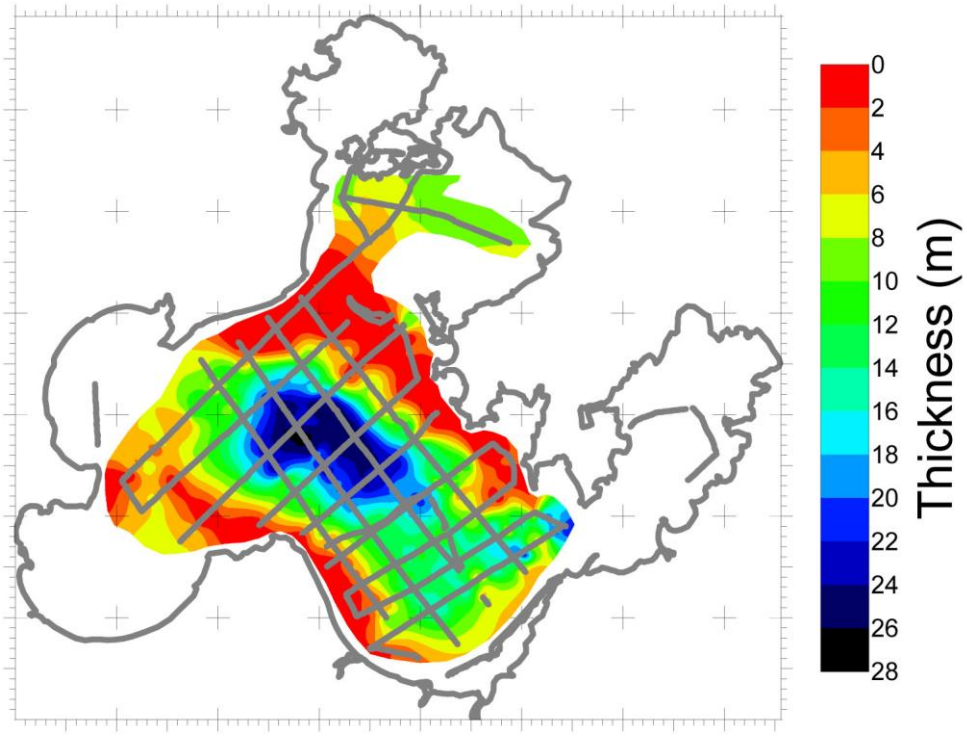

Figure 22 Isopach map of total sediment thickness. Sediment thickness above acoustic basement (sediment thickness between the lake floor and the top of SU-A).

Isopach of Seismic Unit B (Figure 23)

This isopach shows the sediment thickness between the upper bounding surface of SU-B (unconformable surface (UNCF) 1, 2, or 3 depending on the location) and the acoustic basement. SU-B is visible primarily in the middle of Big Traverse Bay where seismic reflections are apparent. Outside of this central region, this SU-B is often obscured by shallow gas. The reflection amplitude of internal reflections and the upper bounding surface also tend to diminish in strength outside of the middle of the basin, making the reflections difficult to distinguish from the ambient background noise. In these locations, the external geometry is impossible to identify. Where SU-B is identifiable, the unit is extremely uniform in thickness averaging about 5.5 m. Shallower regions near the modern-day shoreline indicate where the upper bounding surface erodes into internal reflections (green to red, Figure 23).

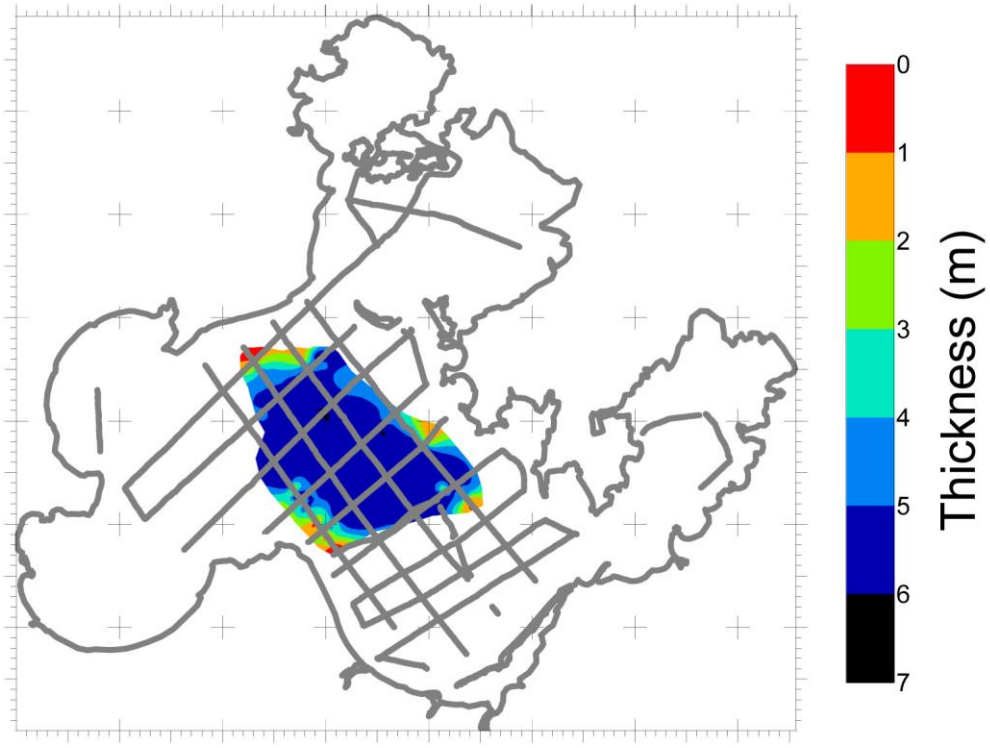

Figure 23 Isopach map of Seismic Unit B.

Isopach of Seismic Unit C (Figure 24)

The sediment thickness for SU-C is constrained by the upper boundary of SU-C (UNCF-2 or 3 depending on location) and unconformable surface 1 (UNCF-1). SU-C is more variable in thickness (0-11 m) than any other seismic unit and its geometry is markedly different than underlying SU-B. It resembles the geometry of the total sediment thickness of the basin (Figure 22) displaying a similar elongated shape that strikes NW-SE. Thicknesses reaching 10.5 m are common in the middle of the basin but the unit thins rapidly away from this region. Multiple seismic profiles, such as LOW12-22 (Figure 16), LOW12-15 (Figure 18), and LOW12-23 (Figure 19) indicate that SU-C is often truncated by UNCF-2 or 3, causing SU-C to pinch out in the northern and southern parts of the survey area (orange to red, Figure 24).

Shallow gas obscured SU-C reflections outside of Big Traverse Bay. In some cases penetration into SU-C was achieved but the return signal diminished with depth until fading into background noise at the bottom of the unit. Thickness data for these locations could not be calculated because of the absence of a lower bounding surface (i.e., UNCF-1). As a result, the extent of this isopach map is similar to the isopach map of SU-B.

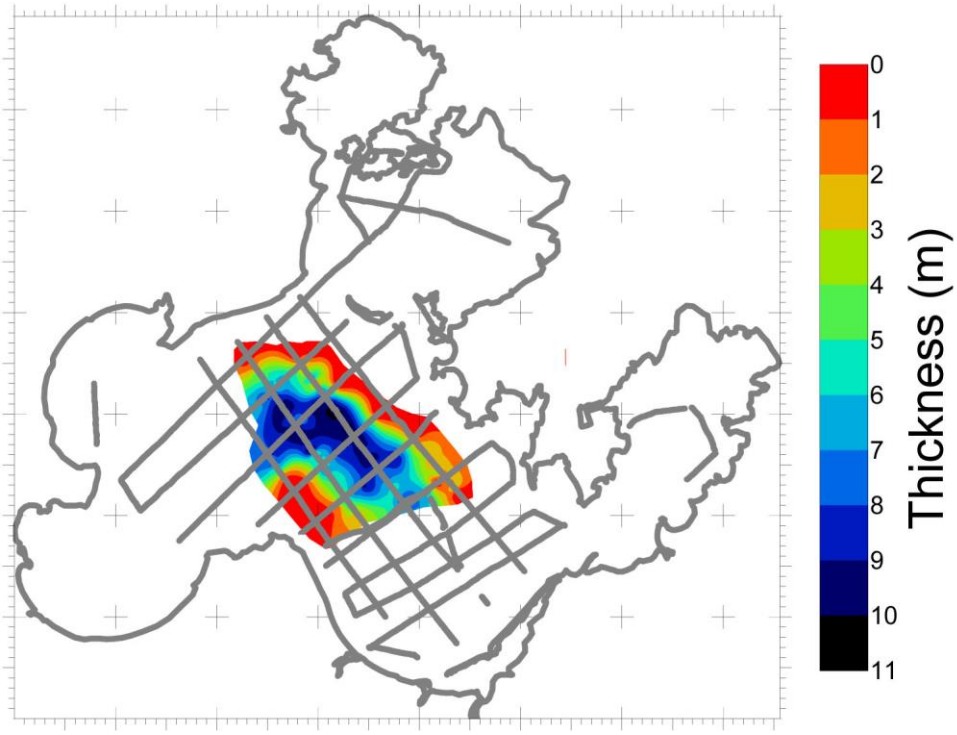

Figure 24 Isopach map of Seismic Unit C.

Isopach of Seismic Unit D (Figure 25)

The bounding surfaces for SU-D are UNCF-3 (upper boundary) and UNCF-2 (lower boundary). Both bounding surfaces were observed across the majority of the survey area, resulting in a relatively extensive isopach map. The unit is thickest in the center of the basin (7-9 m) where the isopachs are quasi-circular (blue region, Figure 25). Outside of the center of Big Traverse Bay, SU-D is fairly uniform, averaging 3-4 m in thickness (light to dark-green, Figure 25). SU-D is thinnest to the north and south of the survey area where UNCF-3 truncates internal reflections well into the unit (Figure 16). A locally thick region (7 m) is apparent between Big Traverse Bay and Sabaskong Bay (Figure 25).

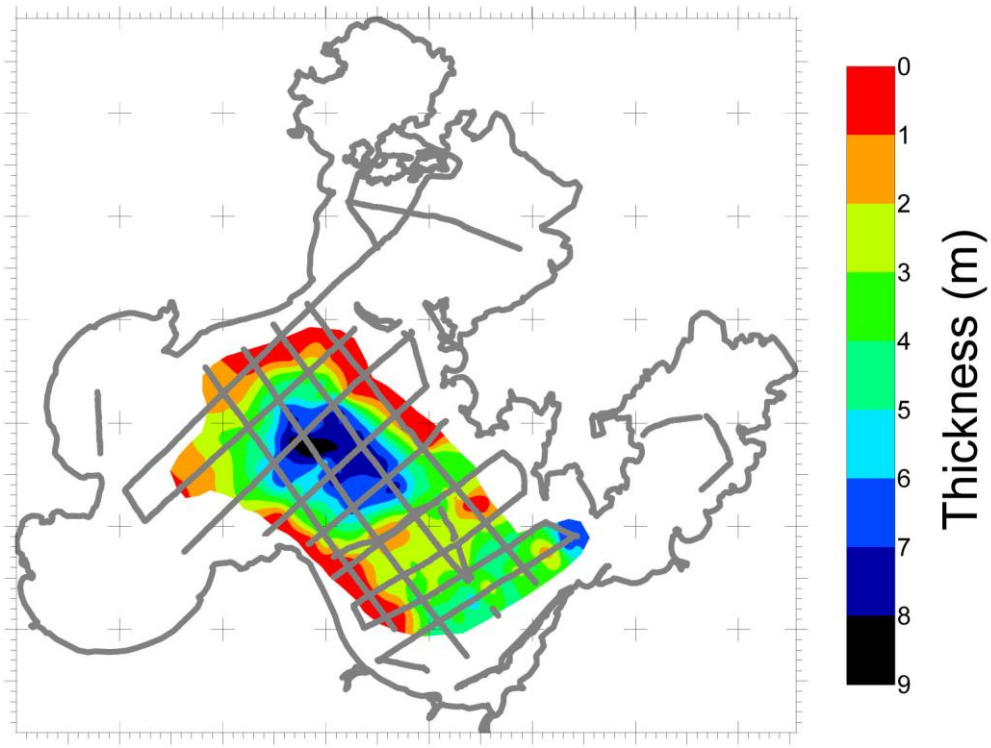

Figure 25 Isopach map of Seismic Unit D.

Isopach of Seismic Unit E (Figure 26)

The isopach map of Unit E shows the sediment thickness between the lake floor and the lower boundary of SU-E (UNCF-3 or the acoustic basement). With a maximum thickness of 4 m, SU-E is the thinnest of the seismic units. Sediment thickness is relatively uniform throughout the survey area. However, subtle changes in sediment thickness indicate that, unlike all underlying units, SU-E is not thickest in the center of Big Traverse Bay. Instead, there are two main thick regions that link together and wrap around Long Point (black color). Red colors (Figure 26) indicate regions where there is no sediment overlying the acoustic basement.

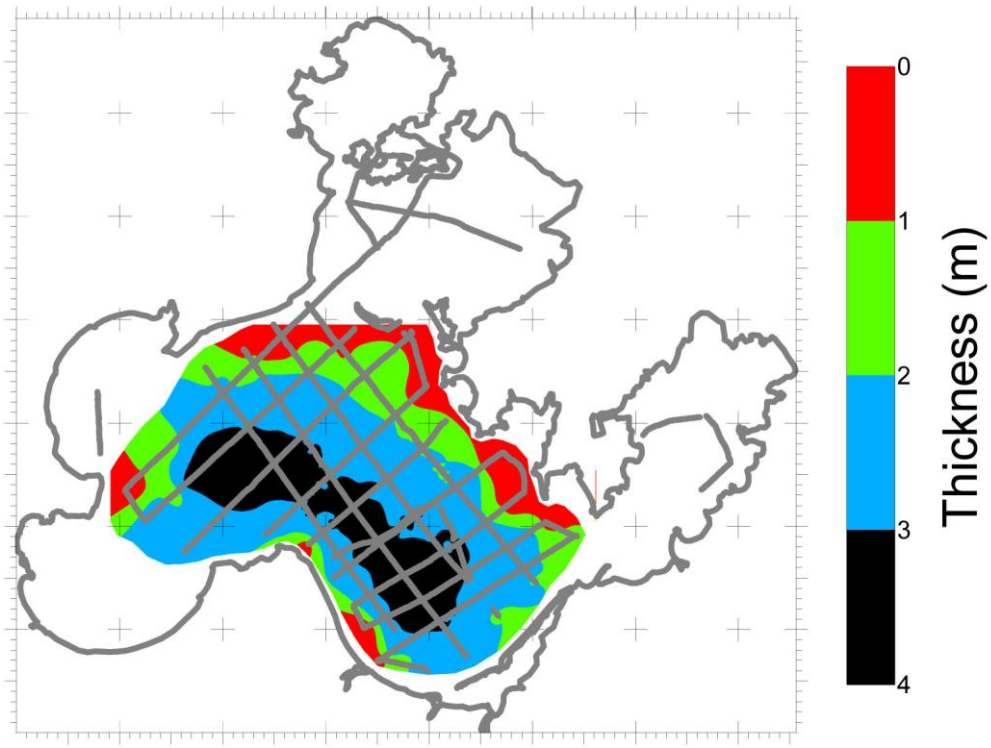

Figure 26 Isopach map of Seismic Unit E (Contour map of depth to UNCF-3).

Bathymetry (Figure 27)

The bathymetry expresses very little relief within the survey area of Big Traverse Bay. The areas of greatest relief occur at the margins of the basin where the rocky shoreline slopes into the lake basin (red colored regions, Figure 27). The lake floor lies between 9.5 and 10 m below the surface lake surface (green colors, Figure 27) in the southern basin and is extremely flat (Figures 16 and 18). The bathymetry in the NW Angle basin is slightly more variable and this area contains the deepest part of Lake of the Woods (~25 m) located in Little Traverse Bay.

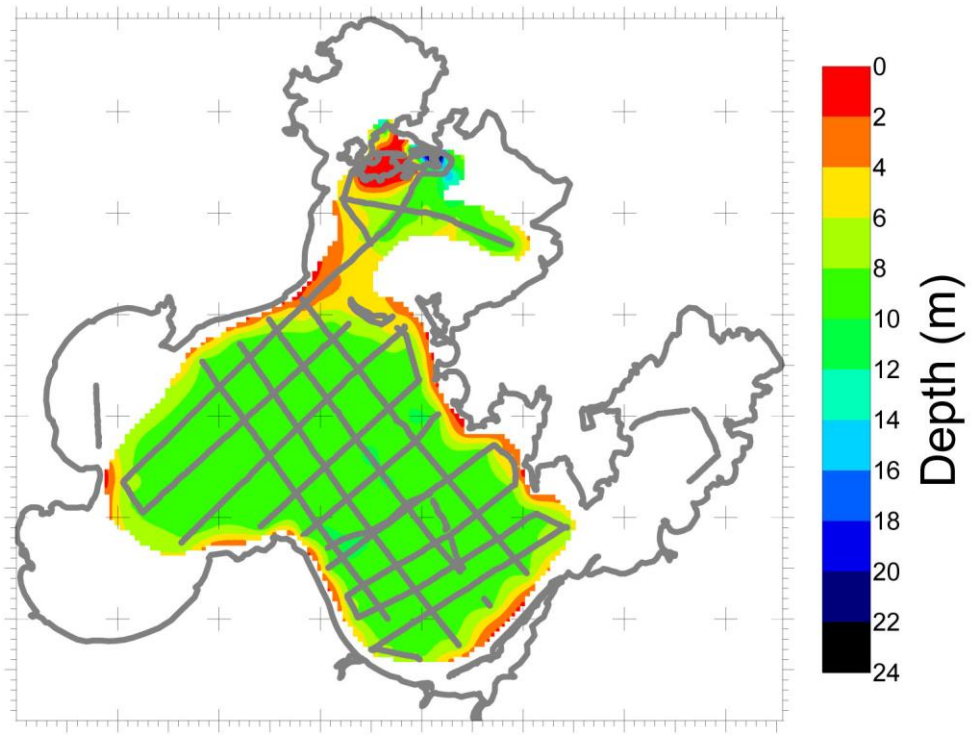

Figure 27 Bathymetric map of Lake of the Woods. Measured from the surface of the lake.

4.2 Sediment Core Description

Descriptions of sediment cores were based primarily on visual and textural analysis. Magnetic susceptibility (MS) and density data were helpful for identifying subtle features, such as minor lithologic changes, that visual and textural analysis missed. These data served primarily for core-to-core and core-to-seismic correlations. The sediment core descriptions presented here, though limited, serve the purpose of providing the general lithology of LOTW sediment as a means to "ground truth" the seismic-reflection data in this project.

The lithology of each core is presented alongside the magnetic susceptibility and density data. Barrel sheets are also provided to show images of individual drives. Large spikes in MS and density data were removed if they occurred at breaks in the core (i.e. tops and bottoms of individual drives) or if they occurred in sediment infill at the top of a drive. A digital copy of the metadata for all cores is included in DVD at the end of this thesis.

Two cores were taken at site PALSS-2A/2B with the intent of creating one continuous composite stratigraphic section, independent of breaks between individual drives. The two cores are similar above a depth of 3.5 m. Below that depth, however, it is difficult to correlate between them. Unique stratigraphic features that should have otherwise been easy to identify within a sediment core, such as fossil-bearing sand layers, were either absent in one of the two cores or could not be correlated across the short distance between cores below 3.5 m. Therefore, instead of presenting them as one combined core, they are described in detail individually to highlight the differences between them. This presents issues with core-to-seismic correlations below ~3.5 m, and possible reasons for the non-correlations are discussed in this chapter and Chapters 5 and 6.

Seismic profiles from each coring location (Figures 33, 44 and 61) are provided to show how the stratigraphic and seismic records were correlated. Important horizons are identified (represented by a green letter H followed by a number starting from the top of the section and increasing down section, i.e., H1, H2, etc.) and their approximate depths are indicated by shaded gray bars.

4.2.1 Sediment Core PALSS-1A

PALSS-1A (49.06775^0 N, 94.79328^0 W) is the northern-most core taken, ~5.5 km west of Big Island in Big Traverse Bay (Figures 11 and 15). Total sediment recovery was 2.1 m (Figures 28-31). From 0-1.38 m the core is composed of brownish-gray, massive, mud containing weak color banding (light and dark) 5-10 cm thick. A diffuse boundary occurs at 1.38 m, below which the sediment changes to light-gray, mud with light colored silt and clay laminations 1-3 cm thick from 1.38-1.96 m. A sharp boundary at 1.96 m marks a major change in lithology from mud-dominated sediment to light-gray clay containing laminated silts 1-2 cm in thickness from 1.96-2.01 m. A minor lithology change occurs at 2.01 m where the clay becomes massive and contains no silt from 2.01-2.11 m.

Magnetic susceptibility (MS) is relatively constant (between 0-10 SI units) from the top of the core until about 1.15 m where it gradually increases (from 20-70 SI units) until ~1.38 m. After 1.38 m, MS is much more variable but tends to decrease in value to the base of the core. Several abrupt excursions appear between 1.38-1.96 m corresponding to silt laminations. A large peak in MS at 1.96 m (ranging between 40-60 SI units) corresponds to the change from mud dominated sediment to clay dominated sediment.

Density is relatively constant (between 1.0-1.3 g/cc) from the top of the core until about 1.15 m. From 1.15-1.38 m the density gradually increases until peaking at 1.8 g/cc (1.38 m), where the sediment becomes laminated with silt. From 1.38-2.1 m the density is variable but stays between 1.5-1.9 g/cc. The largest peak (1.9 g/cc) occurs from 1.96-1.99 m, corresponding to a lithologic change from mud to clay.

Both major and minor lithology changes correlate well to horizons in the seismic-reflection data (Figures 32 and 33). The minor change in lithology at 1.38 m (first occurrence of laminated silt) occurs within seismic Unit E (H1) at the beginning of a very high amplitude zone. The major change from mud to clay at 1.96 m correlates with UNCF-3 (H2) in the seismic record and separates SU-E from SU-D. Large spikes in MS and density values are present at this boundary.

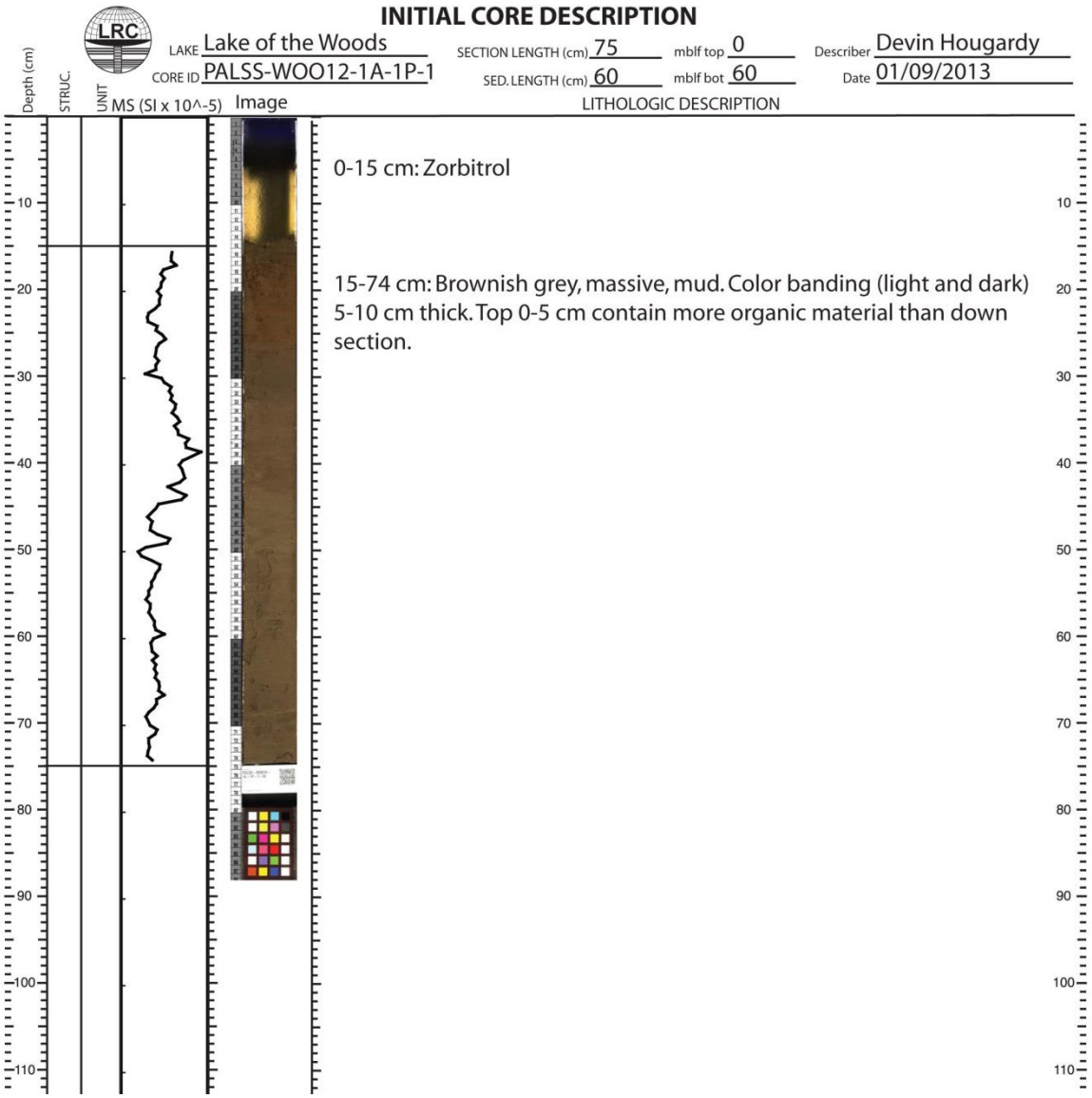

Figure 28 Core barrel sheet for PALSS-WOO12-1A-1P-1.

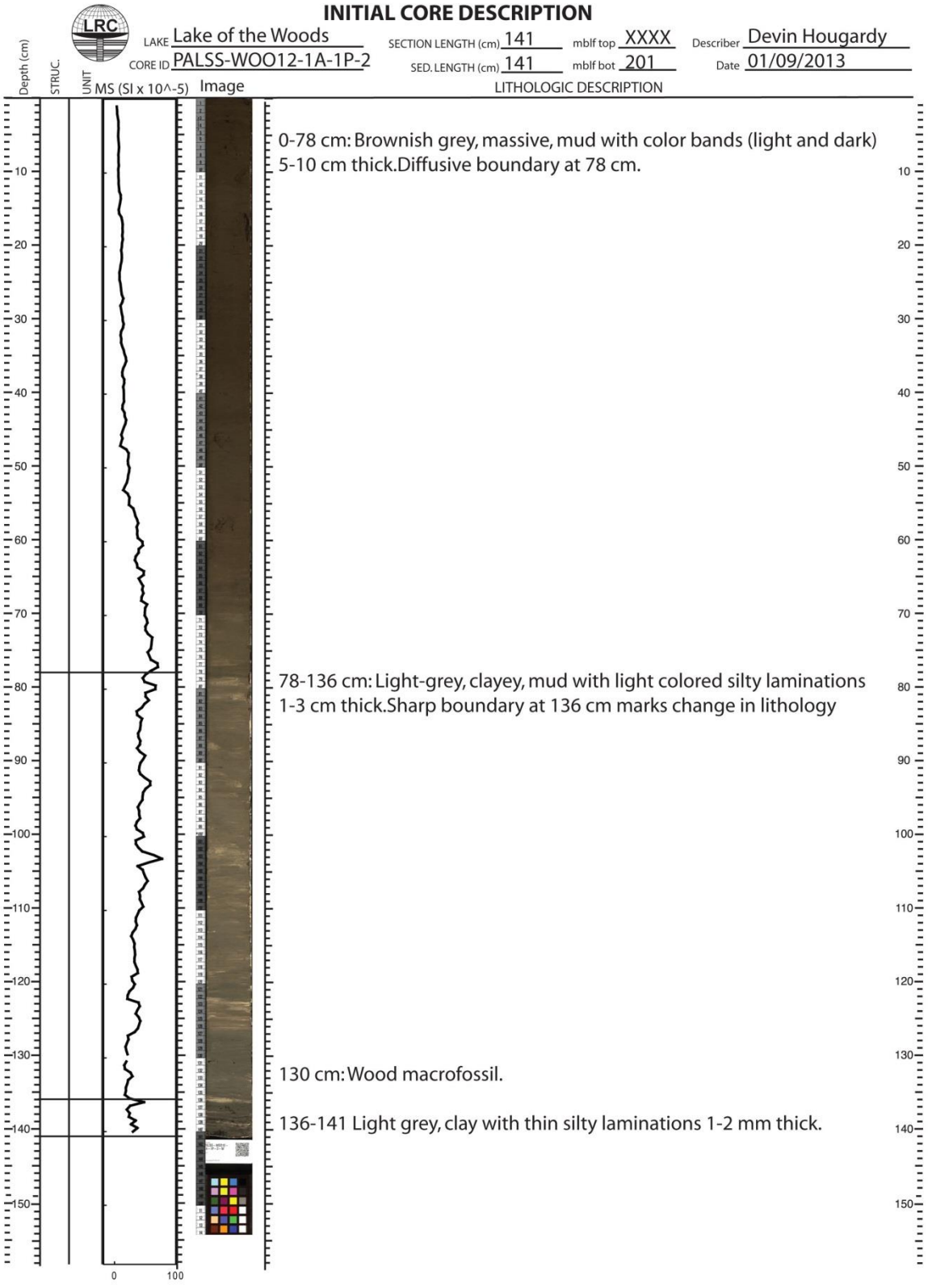

Figure 29 Core barrel sheet for PALSS-WOO12-1A-1P-2.

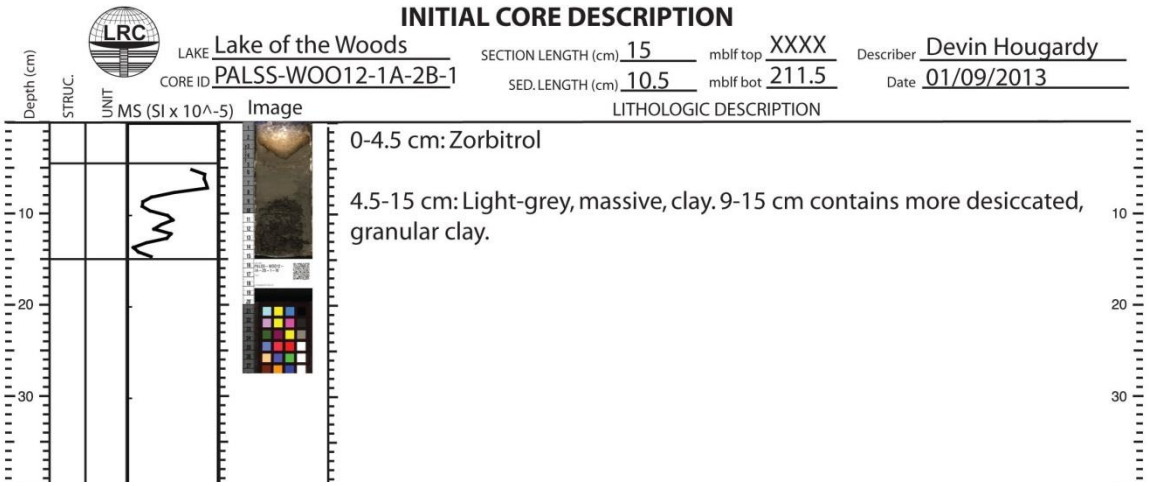

Figure 30 Core barrel sheet for PALSS-WOO12-1A-2B-1.

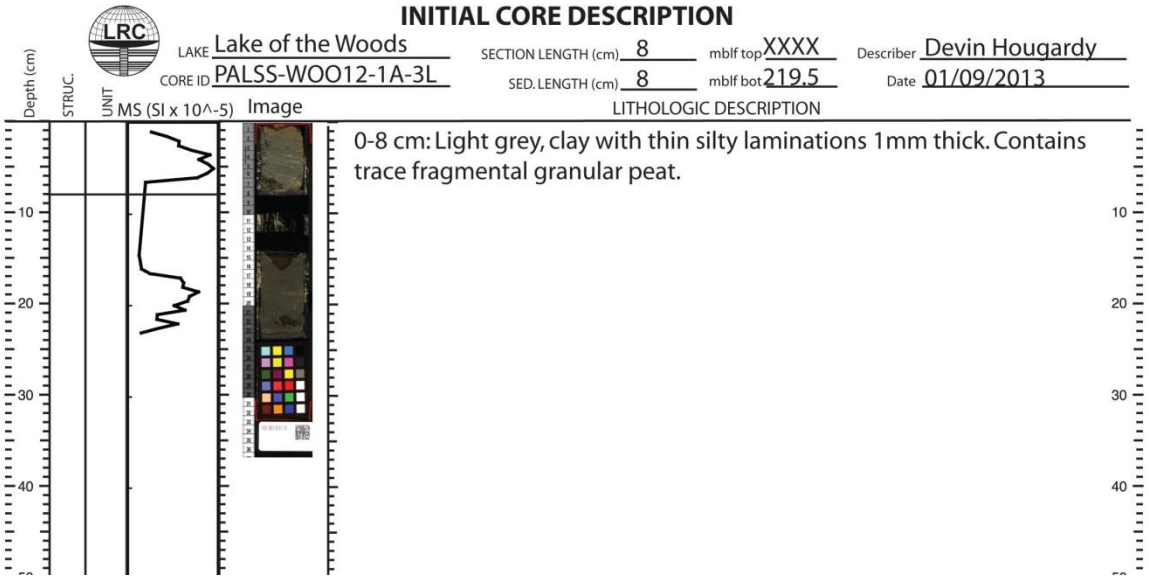

Figure 31 Core barrel sheet for PALSS-WOO12-1A-3L-1.

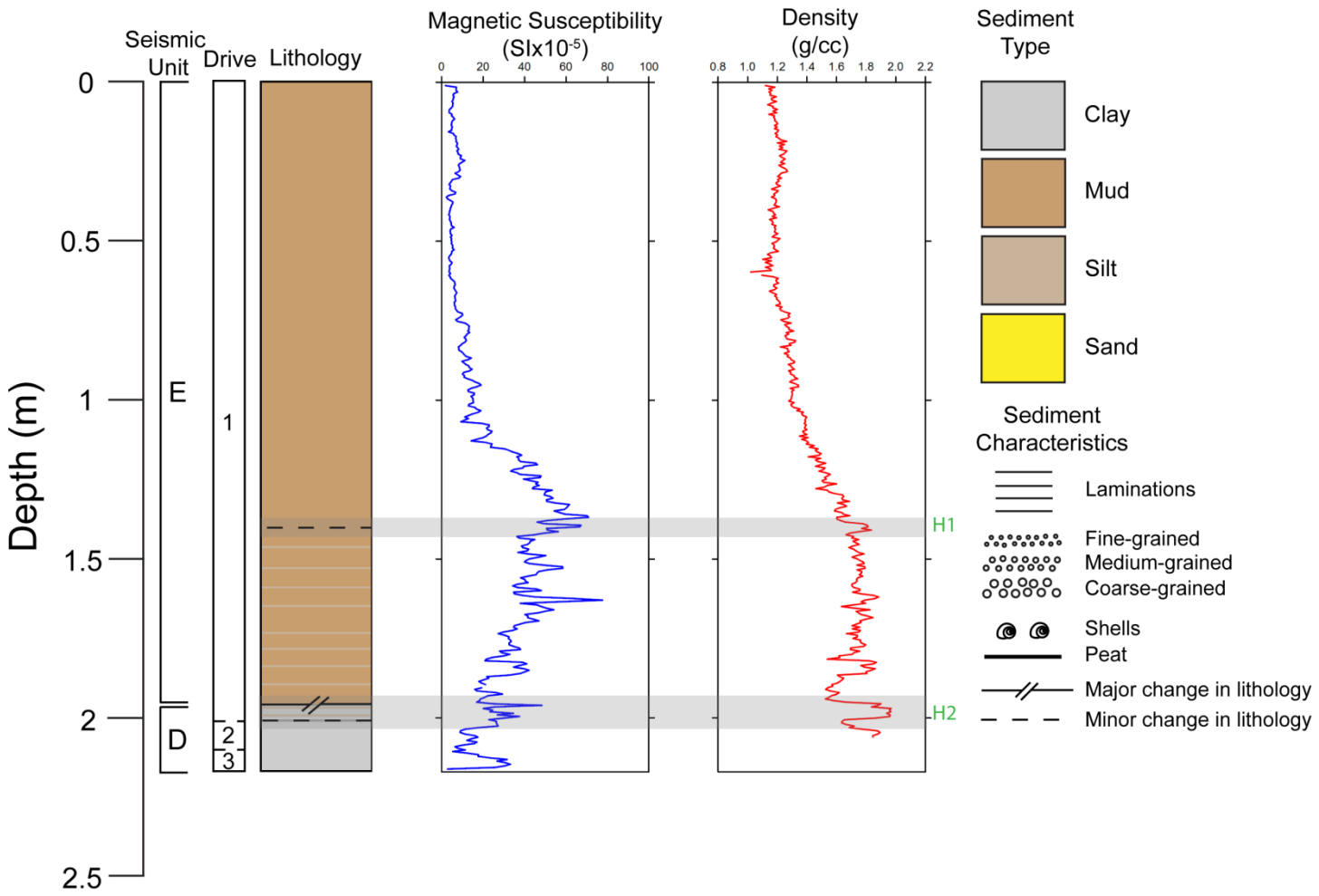

Figure 32 Stratigraphy of PALSS-1A. Drive length, stratigraphic column, magnetic susceptibility, and density data for PALSS-1A.Gray shaded bars and green labels represent prominent contrasts in acoustic impedance identified from seismic-reflection images over the core site (Figure 33). A major abrupt change in lithology occurs at a depth of ~2 m from mud-dominated sediment to clay. The contact (H2) corresponds to UNCF-3. The approximate thicknesses of seismic units are shown at the far left.

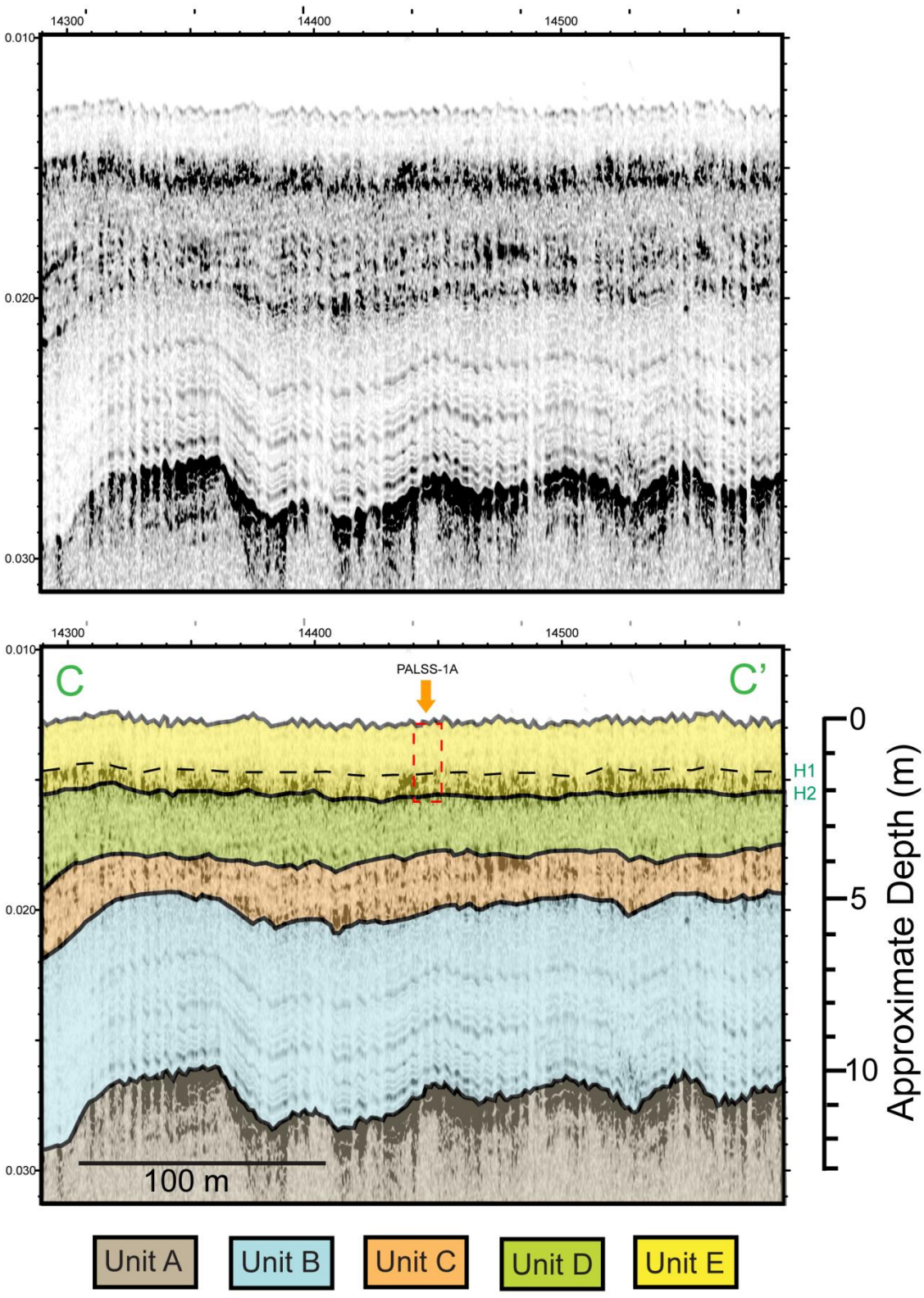

Figure 33 Seismic image of core site PALSS-1A. Interpreted seismic image (bottom) with the location and length of core PALSS-1A (dashed red box). The bottom of the core passes through UNCF-3 (H2) at ~2 m. Total sediment thickness is ~10 m. V.E.: ~15x.

4.2.2 Sediment Core PALSS-2A

PALSS-2A (48.98527^0 N, 94.74361^0 W) was collected at a central location in Big Traverse Bay 10 km offshore in all directions. It was, along with overlapping core PALSS-2B, the only site picked using the preliminary seismic dataset collected in 2011 (Figure 44). Total sediment recovery was 6.6 m (Figures 34-42). From 0-2.42 m the core is composed of brownish-gray, massive mud with weak color banding (light and dark) 5-15 cm thick. At 2.42 m, non-continuous silty laminations 1-2 mm thick appear but are sporadic below until a major change in lithology occurs at 3.05 m (Figure 36). Here the lithology generally becomes silt dominated with frequent parallel to sub-parallel laminations light (silt dominated) and dark (clay dominated) in color. Fragmented woody peat is common throughout the rest of the core including three distinct peat layers at 3.08 m, 4.45 m, and 5.82 m. Five sand layers occur (3.63-3.66 m, 3.74-3.79 m, 4.22-4.43m, 6.07-6.12 m, and 6.52-6.6 m) indicating major changes in lithology from the otherwise laminated silty-clay. The lowermost two sand layers are coarse-grained and contain bivalve fossil shells.

MS in the core can be separated into two sections; one from 0-3.08 m and a second from 3.08-6.6 m. In the first section, from the top of the core until 1 m the MS values stay low between 0-10 SI units with a small peak at 1 m. MS gradually increases from 1-1.75 m but then decreases from 1.75-1.9 m. Here the MS plateaus at ~50 SI units, until 3.08 m but shows a small peak at 2.42 m. In the second section, from 3.08-6.6 m, MS is highly variable with large peaks that tend to correspond with major changes in lithology. The largest of which (375 SI units) appears at a major change in lithology from mud to silt at 3.08 m.

Density in the core can also be separated into the same sections. The first section displays several sub-sections of similar slope interrupted by small peaks or valleys in the density. The peaks and valleys tend to occur at the same depths as peaks and valleys in the MS described above. Below 3.08 m, the range in density is much more variable but the median value is relatively constant (1.7-1.9 g/cc) compared to the overlying section. Peaks in the data commonly occur at the same depths as peaks in the magnetic susceptibility data and generally correspond to changes in lithology.

Materials for radiocarbon dating were collected from the uppermost peat layer at a depth of 3.08 m and from a wood macrofossil in the lowermost sand layer at a depth of 6.52 m (Figure 43 and Table 9). Their ages are 7,750 cal BP (calibrated years before present) (6,930±30 yr BP; ^{14}C years before present) and 7,890 cal BP (7,040±35 yr BP), respectively.

Seven distinct horizons (reflections) have been identified in the seismic-reflection record at coring location PALSS-2A/2B (Figure 44). Reflection amplitude strength varies between the seven horizons, indicating the changes in the physical properties of the sediments vary also. The two most pronounced horizons (H4 and H6) correlate with UNCF-3 and UNCF-2, respectively. H4 occurs at a depth of ~3.0 m and correlates well with the major change in lithology and large peaks in MS and density values at the boundary between mud-dominated sediment and laminated silts and clays at a depth of 3.05 m. This boundary marks the boundary between SU-E and SU-D. No apparent change in lithology, however, occurs at a depth of ~5.3 m, where H6 is observed in the seismic image. MS and density values increase slightly at this depth, but not by an amount greater than what is commonly observed below ~3.0 m. The lack of physical evidence to support a change in sediment properties at a depth where the seismic-reflection record indicates a significant contrast in acoustic impedance is puzzling, but presumably relates to a change in seismic velocity.

The remaining five horizons correlate well with major or minor changes in lithology. H5 (~4.3 m) and H7 (~6 m) occur at depths where sand lenses are interbedded in the laminated silts and clays and H3 (~2.5 m) occurs at the same depth where laminated silts appear in the mud dominated sediment. H1 (~1.0 m) and H2 (~2.0 m) occur where visual or textural changes in lithology are not obvious but coincide with abrupt variations in both magnetic susceptibility and density data.

Two closely occurring sand layers at a depth of ~3.5-3.7 m do not produce a detectable contrast in acoustic impedance in the seismic record. In this case, what is observed as a clear change in sediment lithology is *not* observed as a change in acoustic impedance. MS and density values both peak at a depth of 3.5-3.7 m, corroborating the lithologic interpretation. The thin nature of the sand layers (3 and

5 cm thick, respectively) are not a sufficient explanation for the lack of a change in acoustic impedance in the seismic record for the following reasons. First, the vertical resolution of the 3100P CHIRP towfish is high enough (1-10 cm, see previous chapter) to detect a change in lithology 3-5 cm thick. This is demonstrated several times in this core by the identification of horizons H1, H2, H3, and H4, all of which occur at a transition of less than 3 cm. Second, horizons have been identified where the change in the physical properties of the sediment are much more subtle than at ~3.5 m corresponding to a change in lithology from clayey silt to fine to medium-grained sand. The depths at which H1 and H2 are observed contain minute changes in the MS and density in an otherwise uniform section of mud dominated sediment. MS and density value peaks are much more prominent at 3.5 m, yet there is no corresponding horizon in the seismic record at or near this depth. The question remains, why do some seismic reflections occur (do not occur) where there is no change (change) in the physical properties of the sediment, whereas other reflections occur exactly where there are changes in sediment properties? Possible explanations to this question are discussed in section 5.2.1.

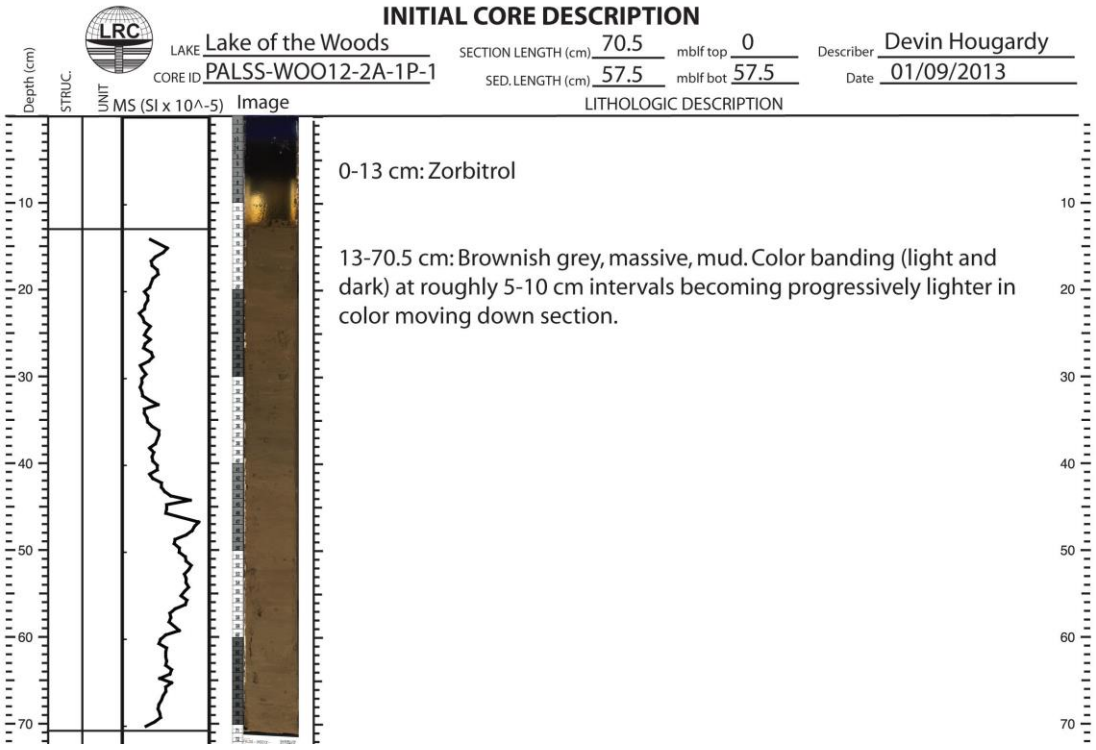

Figure 34 Core barrel sheet for PALSS-WOO12-2A-1P-1

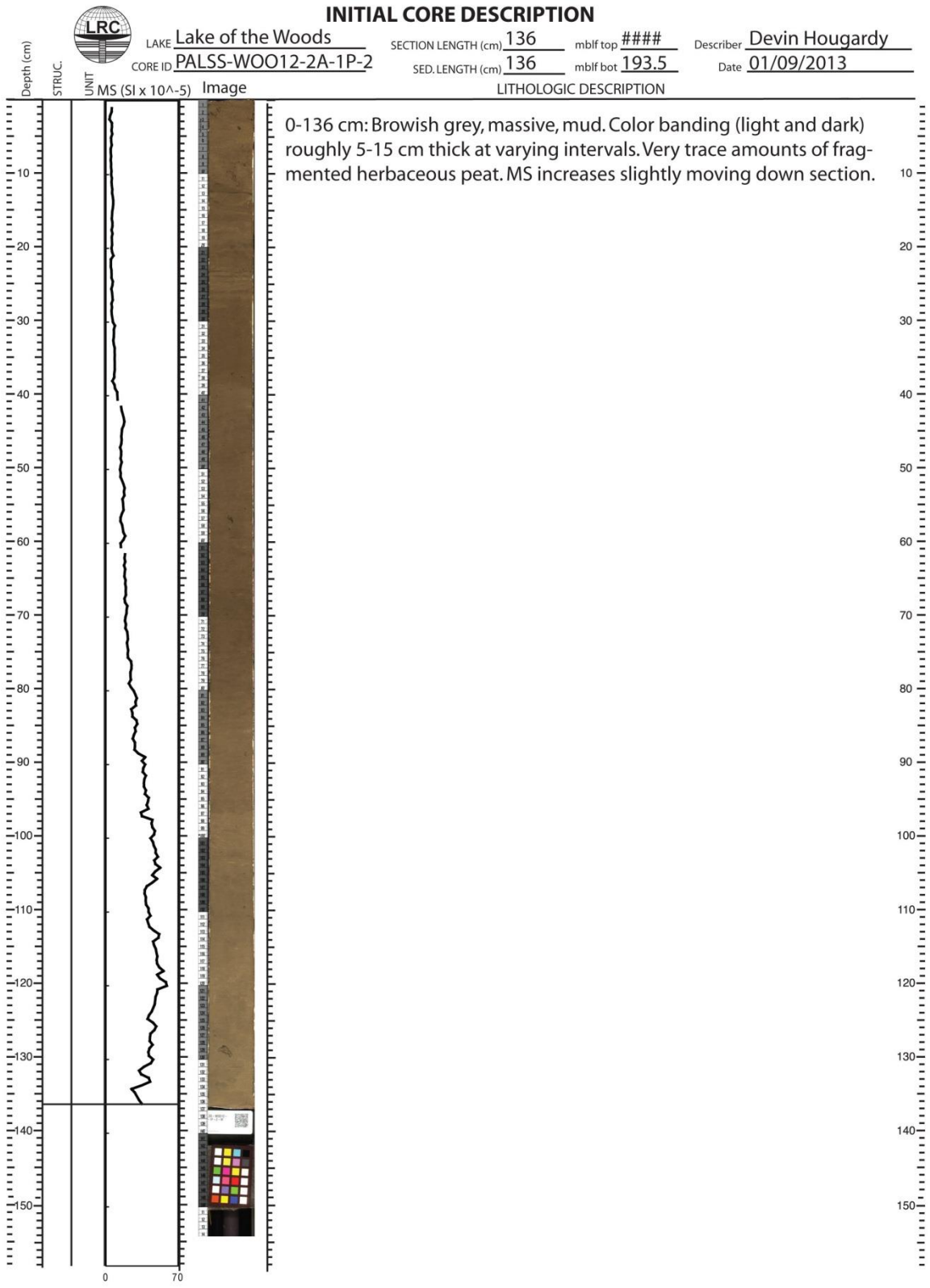

Figure 35 Core barrel sheet for PALSS-WOO12-2A-1P-2

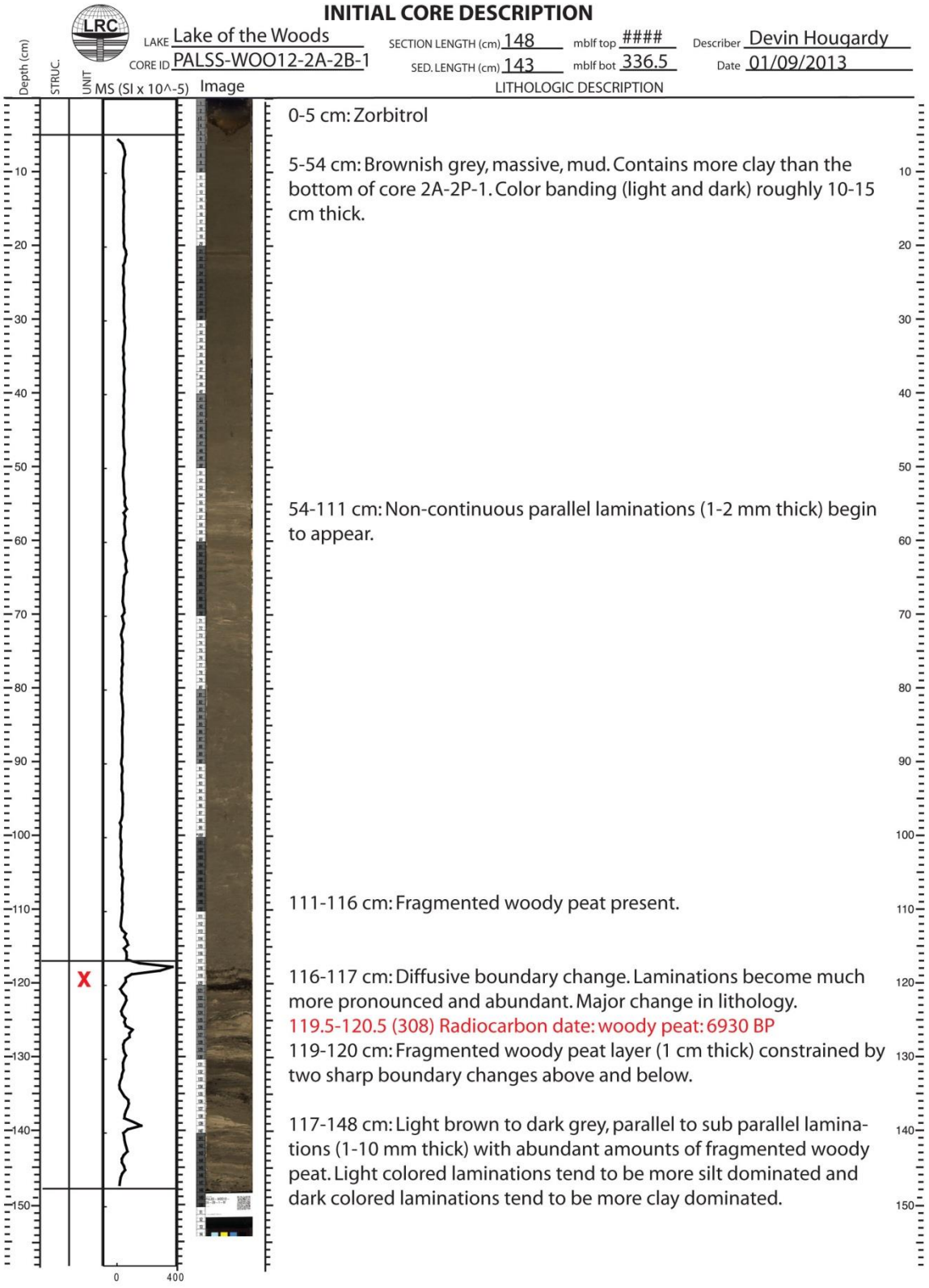

Figure 36 Core barrel sheet for PALSS-WOO12-2A-2B-1.

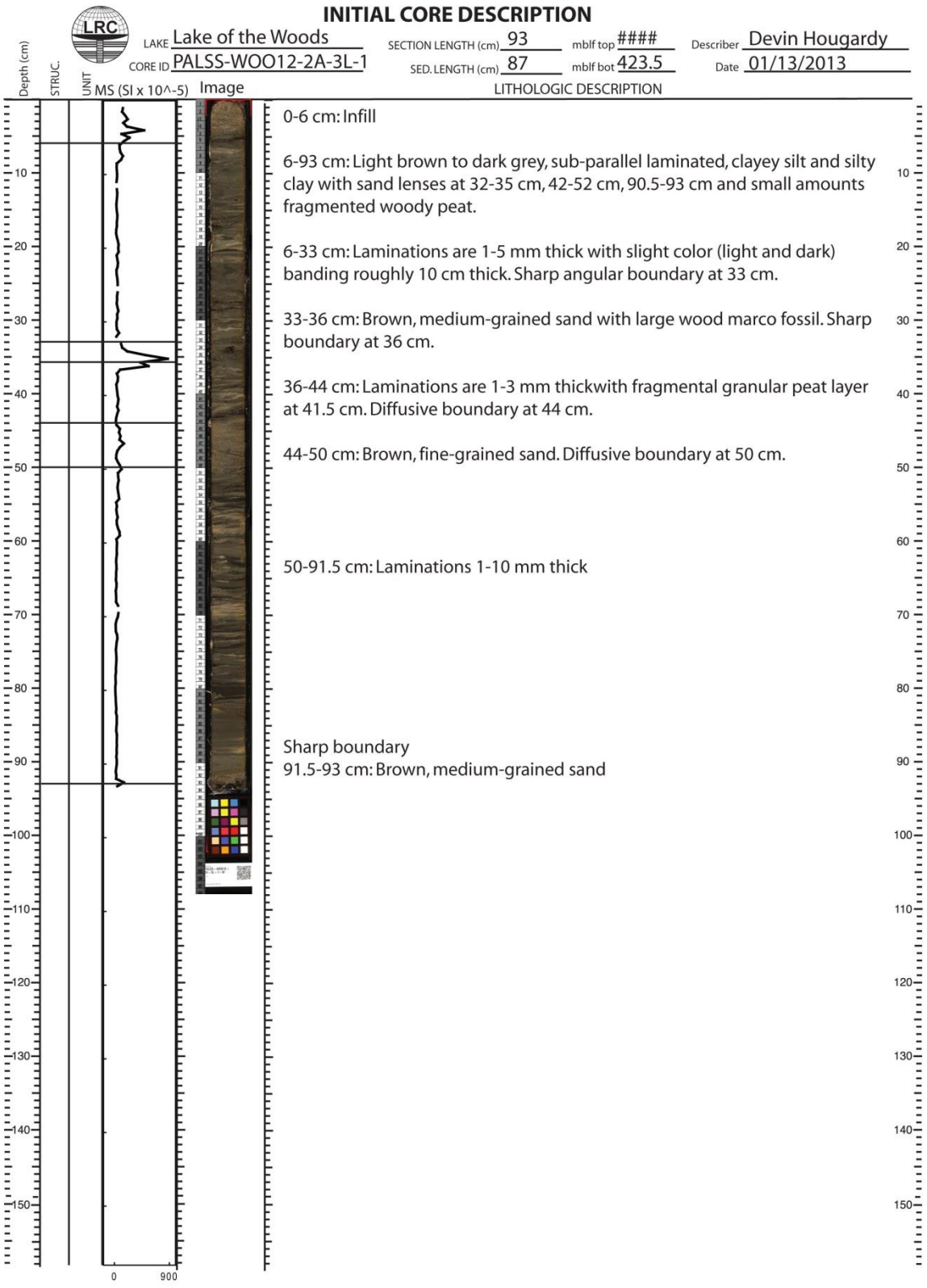

Figure 37 Core barrel sheet for PALSS-WOO12-2A-3L-1.

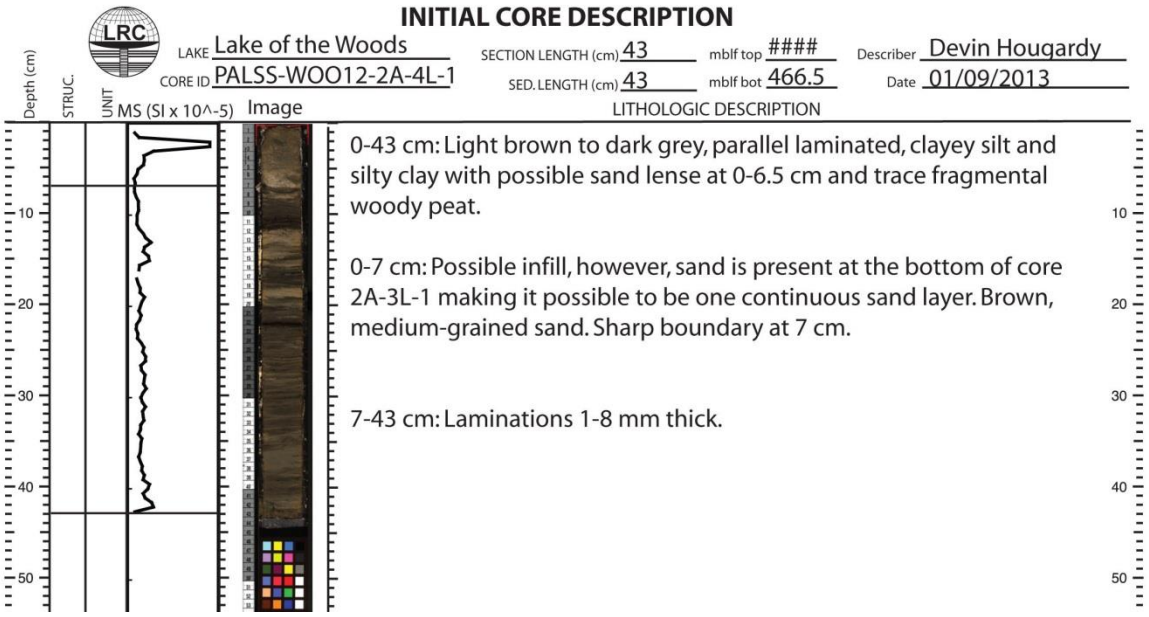

Figure 38 Core barrel sheet for PALSS-WOO12-2A-4L-1.

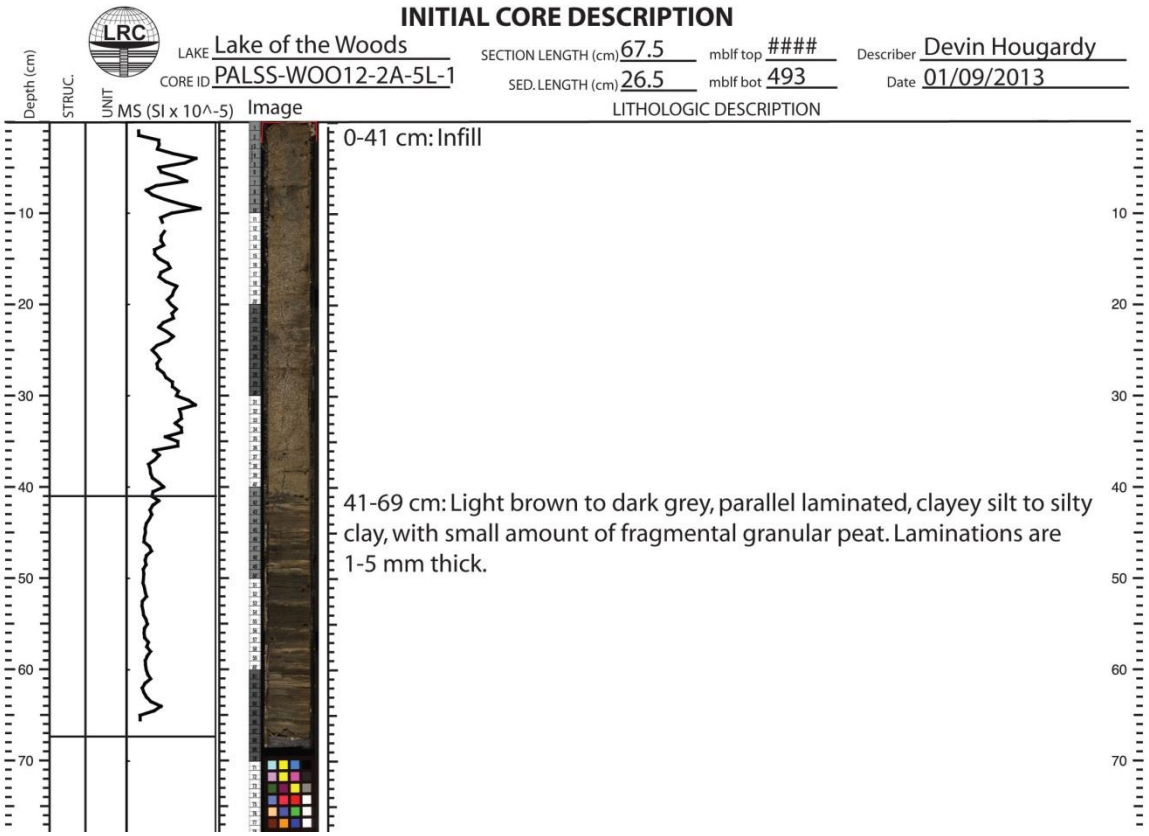

Figure 39 Core barrel sheet for PALSS-WOO12-2A-5L-1.

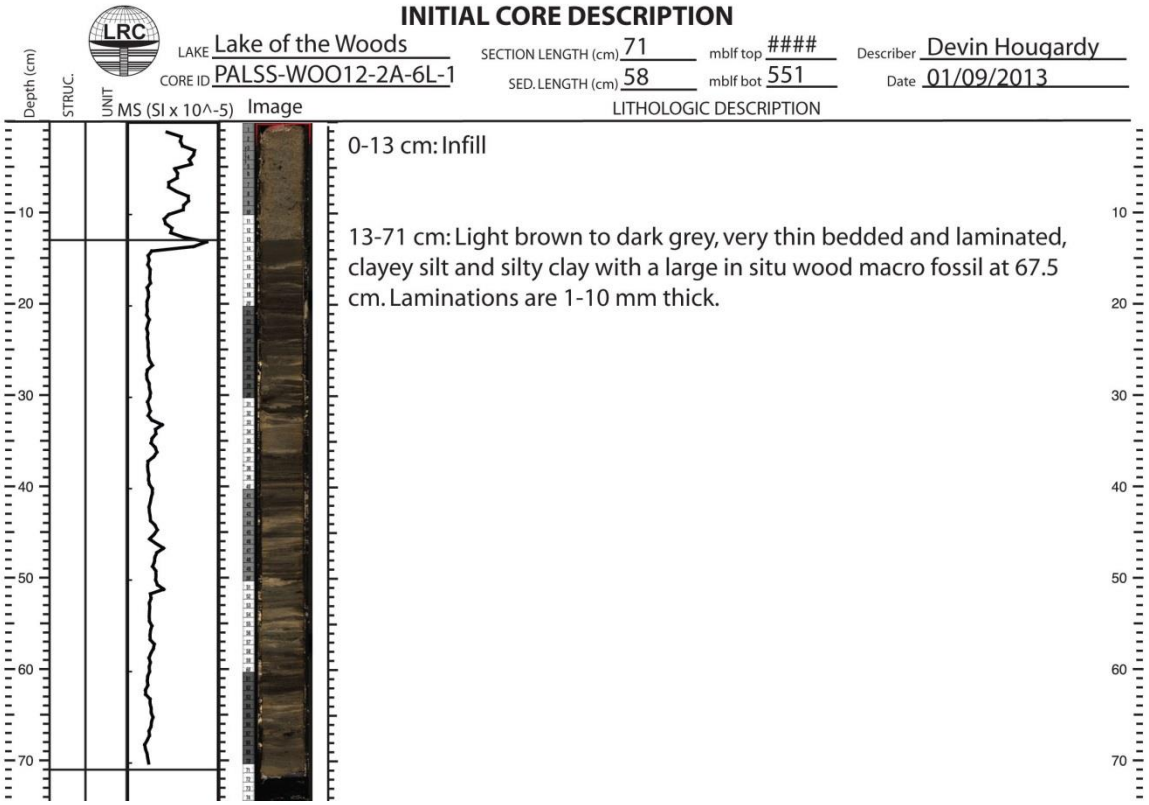

Figure 40 Core barrel sheet for PALSS-WOO12-2A-6L-1.

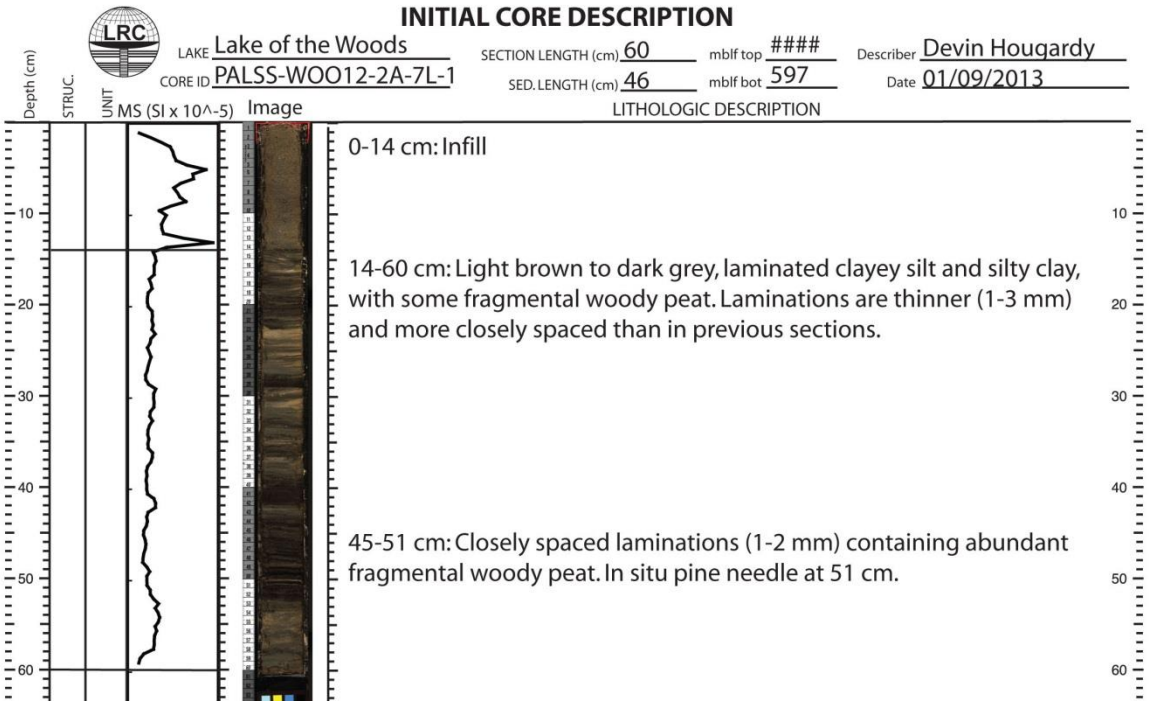

Figure 41 Core barrel sheet for PALSS-WOO12-2A-7L-1.

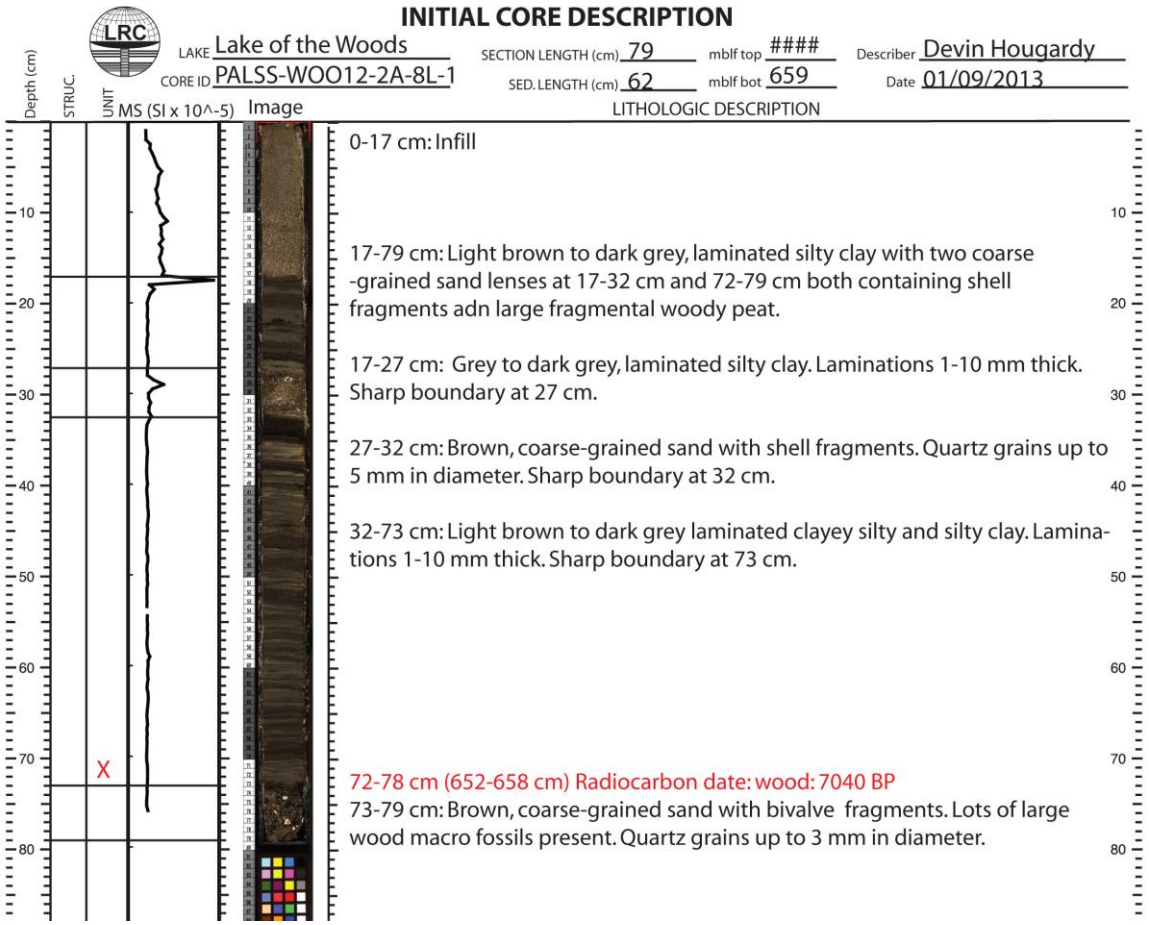

Figure 42 Core barrel sheet for PALSS-WOO12-2A-8L-1.

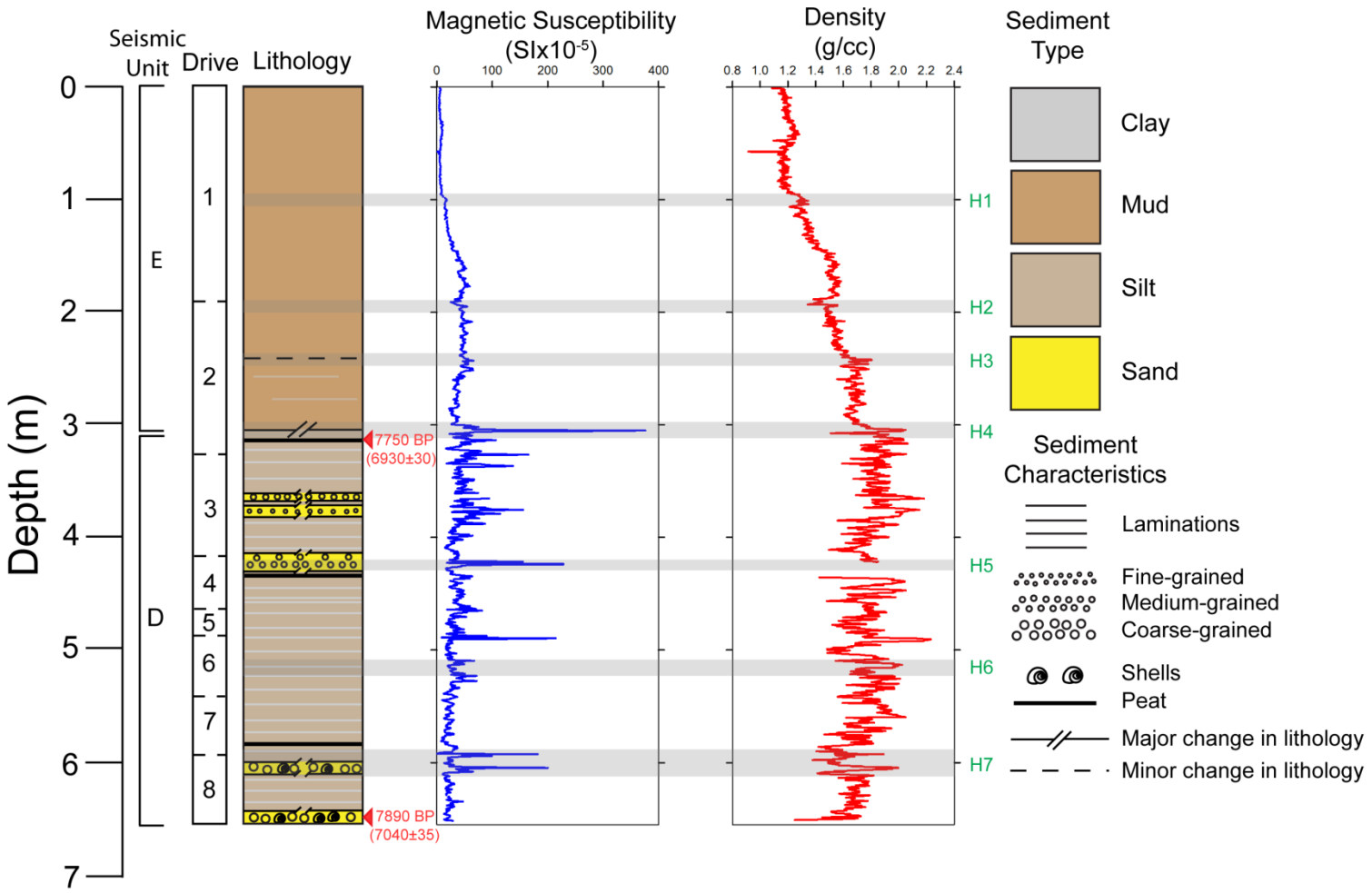

Figure 43 Stratigraphy of PALSS-2A. Drive length, stratigraphic column, magnetic susceptibility, and density data for PALSS-2A.Gray shaded bars and green labels represent prominent contrasts in acoustic impedance identified from seismic-reflection images over the core site (Figure 44). A major abrupt change in lithology occurs at a depth of ~3 m from mud-dominated sediment to laminated silt and clay corresponds to UNCF-3 (H4). The depths at which material was collected for radiocarbon dating are indicated by red triangles.

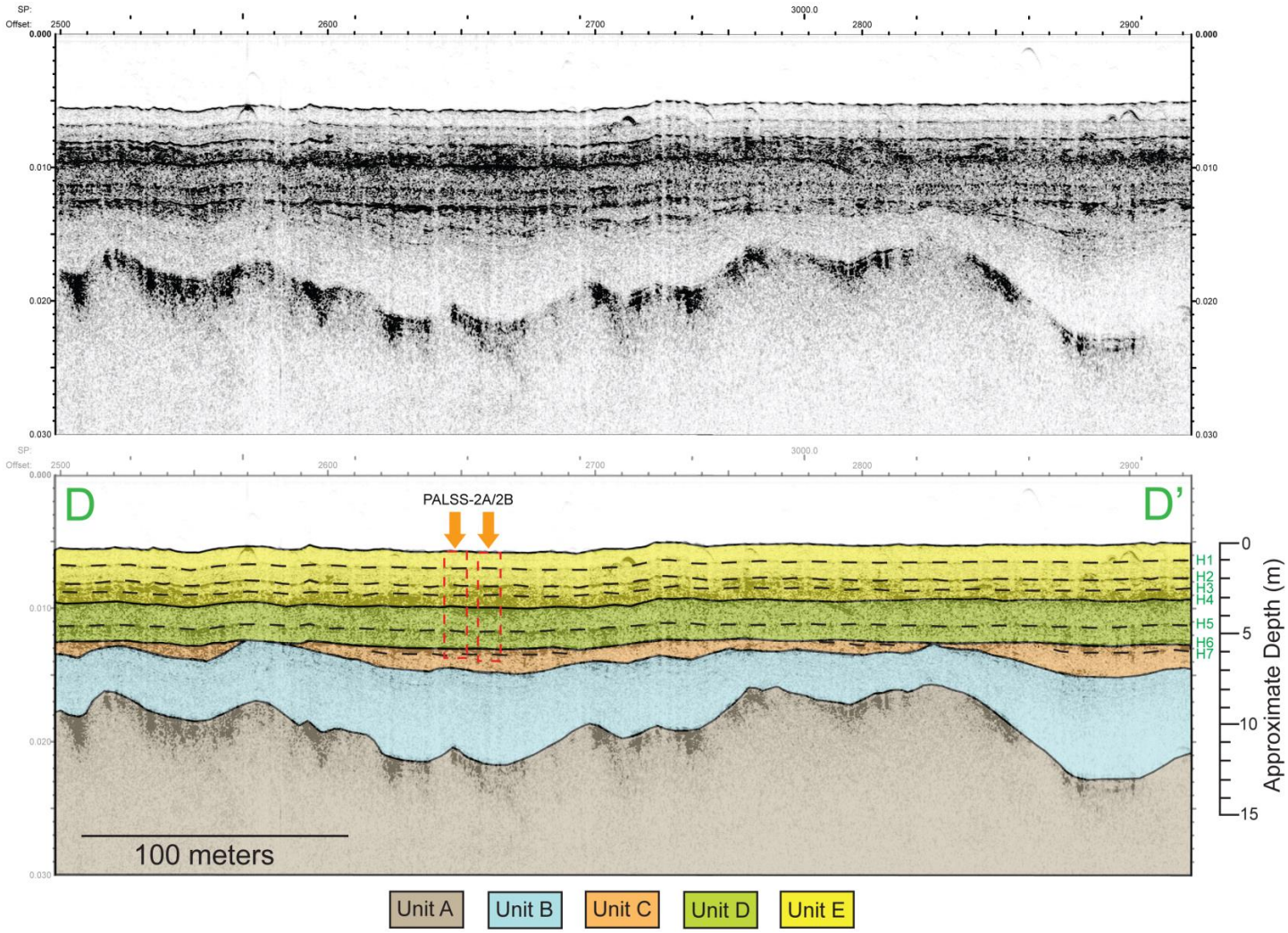

Figure 44 Seismic image of core site PALSS-2A and 2B. Interpreted seismic image (bottom) with the location and lengths of cores PALSS-2A and 2B (dashed red boxes). Seven prominent reflections are labeled (solid and dashed black lines) including UNCF-3 (H4) and UNCF-2 (H6). V.E.: ~9x.

4.2.3 Sediment Core PALSS-2B

Total sediment recovery for PALSS-2B (48.98527^0 N, 94.74361^0 W) was 6.9 m (Figures 45-51). From 0-2.53 m the core is composed of brownish-gray, massive mud with weak color banding (light and dark) 5-15 cm thick. Below 2.53 m, silt laminations 1-5 mm thick appear in groups, becoming progressively more apparent until a major change in lithology occurs at 3.10 m depth. Here, the lithology is silt dominated by parallel to sub-parallel laminations, light (silt dominated) and dark (clay dominated) in color and comparable in form to the laminated silts of PALSS-2A. Similar to PALSS-2A, these laminated silts and clays make up the primary lithology for the entire lower section. Fragmented woody peat occurs as distinct layers (3.22 m and 4.34 m) or in trace amounts throughout the lower part of the core. Four medium-grained sand layers are present at depths of 3.60-3.70 m, 4.43-4.57 m, 5.40-5.46 m, and 5.75-5.77 m. The uppermost two sand layers also contain bivalve fossil shell fragments. Underlying each of these fossil rich sand layers is a mixture of gray clay and coarse-grained sand both 10 cm thick.

Similar to PALSS-2A, MS is broken into two sections; one from the top of the core until 3.1 m and a second from 3.1-6.9 m. The first section shares the same general trends as PALSS-2A containing two small peaks (1 m and 2.53 m) and one small valley (1.9 m) in the MS record. There is a large spike (110 SI units) at 3.1 m corresponding to a major change in lithology from mud to silty clay. In the second section from 3.1-6.9 m, the MS remains fairly uniform (10-50 SI units) with large spikes occurring at the same depths as major changes in lithology (i.e. sand lenses or clay intervals). The two largest peaks (310 and 280 SI units), located at depths of 5.4 m and 3.7 m respectively, occur within medium-grained sand layers.

Density values are also separated into the same two sections. The first section (0-3.1 m) contains several sub-sections separated by small peaks and valleys that correspond to peaks and valleys in MS and are similar in depth and magnitude to density variances in PALSS-2A. The second section (3.1-6.9 m) is characterized by density values that are highly variable but that typically stay within 1.7-1.9 g/cc, also similar to PALSS-2A. The three largest negative deviations (3.3 m, 4.0 m, and 5.0 m) occur at or very close to the boundaries of drives 3, 4, and 5 and are related

to small gaps in the core. Conversely, the three largest positive deviations (3.6 m, 4.5 m, and 5.4 m) all occur in the middle sections of drives and correspond to medium-grained sand layers.

Material for radiocarbon dating was abundant in PALSS-2B and the majority of the ages determined in this study were from this core (Table 9). The material collected includes peat and wood charcoal from a prominent peat layer (3.22 m) directly below the lithologic change from mud-dominated sediment to silty clay sediments (8,350 cal BP; 7500±30 yr BP); terrestrial seeds and charcoal (8,800 cal BP; 7,500±40 yr BP) from within a coarse-grained sand layer a depth of 4.58 m; a large (2.5 cm in length) *in situ* terrestrial twig (11,040 cal BP; 9,650±40 yr BP) collected directly below the coarse-grained sand layer mentioned above and ~40 cm above UNCF-2 at a depth of 4.70 m; an *in situ* wood macrofossil (7,890 cal BP; 7,040±40 yr BP) collected from directly below a medium-grained sand layer and above H7 at a depth of 5.87 m; and an *in situ* macrofossil (7,900 cal BP; 7,080±40 yr BP) collected directly below H7 at a depth of 6.17 m.

The same seven horizons identified for core-to-seismic correlations for PALSS-2A are also used for PALSS-2B. The most prominent horizon H4 (UNCF-3) occurs at the same approximate depth (~3.0 m) as the major change in lithology from mud-dominated sediment to laminated clayey silt and represents the bounding surface between SU-E and SU-D (Figure 52). Horizons H1, H2, and H3 also correlate well with changes in sediment properties. H3 (~2.5 m) occurs at the approximate depth where the silt content increases while H1 (~ 1.0 m) and H2 (~2.0 m) coincide with subtle yet distinct changes in MS and density that are likely related to compaction from the weight of the overlying sediment.

The approximate depths where prominent internal reflections are observed below H4, however, indicate little, if any, changes in the physical properties of the sediment. A thin peat layer does occur at the same depth as H5 (~4.3 m) suggesting that the change in density between the peat and overlying clayey silt is strong enough to produce a prominent reflection. However, other peat layers similar in thickness that occur throughout both PALSS-2B and PALSS-2A do not occur at depths where prominent reflections are observed.

There is no evidence of a lithologic change at the approximate depths to horizons H6 (~5.3 m) and H7 (~6.0 m), though the two horizons do occur within a half a meter of two medium-grained sand layers. It is possible that the boundary between the clayey silt and sand layers, or vice versa, produced these horizons. If so, then either the vertical resolution is larger than the calculated 1-10 cm or the velocity value used to calculate the approximate depth-to-horizons is faster than 1450 m/s. It is unlikely that the resolution is greater than 1-10 cm considering the accuracy of core-to-seismic correlations for the upper horizons (H1-H4) in PALSS-2A and PALSS-2B as well as all horizons in PALSS-1A and PALSS-4A. If an increased sound velocity of 1500 m/s is used for the whole sediment sequence, the depths to horizons below H4 occur 15-20 cm *below* where they occur using a velocity of 1450 m/s. Using Figure 52 as a guide, lowering horizons H5-H7 15-20 cm does not improve the overall core-to-seismic correlations. This can also be seen in Figure 43 when horizons H5-H7 are lowered by 15-20 cm.

It is clear that below ~3.0 m in depth, the correlation between the lithology of cores PALSS-2A and PALSS-2B and prominent seismic reflections is not straightforward. Furthermore, below a depth of ~3.5 m, lithologic correlations between cores PALSS-2A and PALSS-2B are largely not possible. This makes it difficult to reconstruct a detailed depositional history for SU-D at this location. It is possible, however, to make some useful first order observations for this site: (1) the uppermost seismic unit (SU-E) represents a uniform section of brownish-gray mud; (2) a distinct and major change in lithology at a depth of ~3.0 m (UNCF-3) separates SU-E from SU-D; (3) the difference in the internal reflection character between SU-D and SU-E is likely the result of the lithology change from mu- dominated sediment to sediment composed of clayey silt.

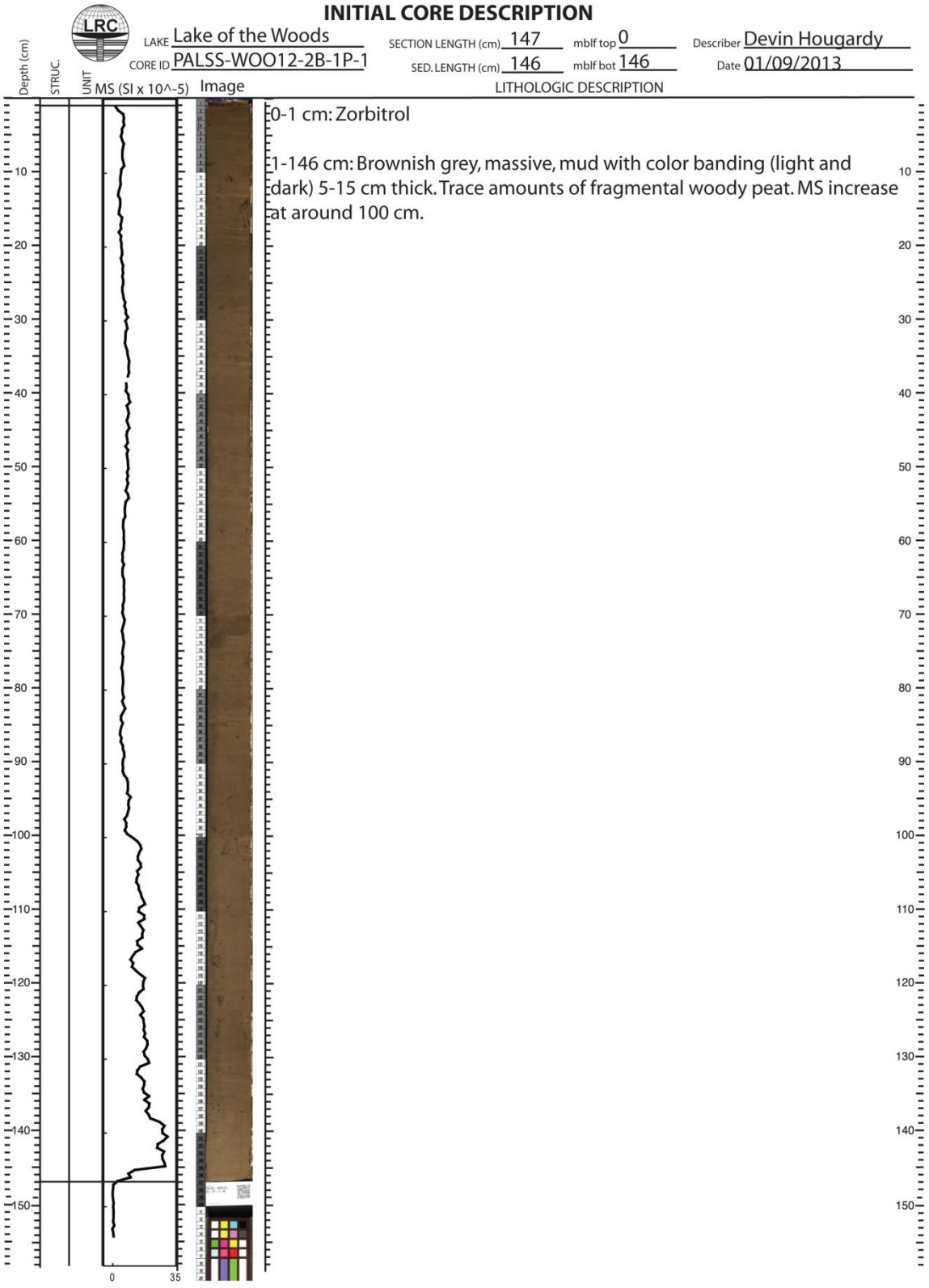

Figure 45 Core barrel sheet for PALSS-WOO12-2B-1P-1.

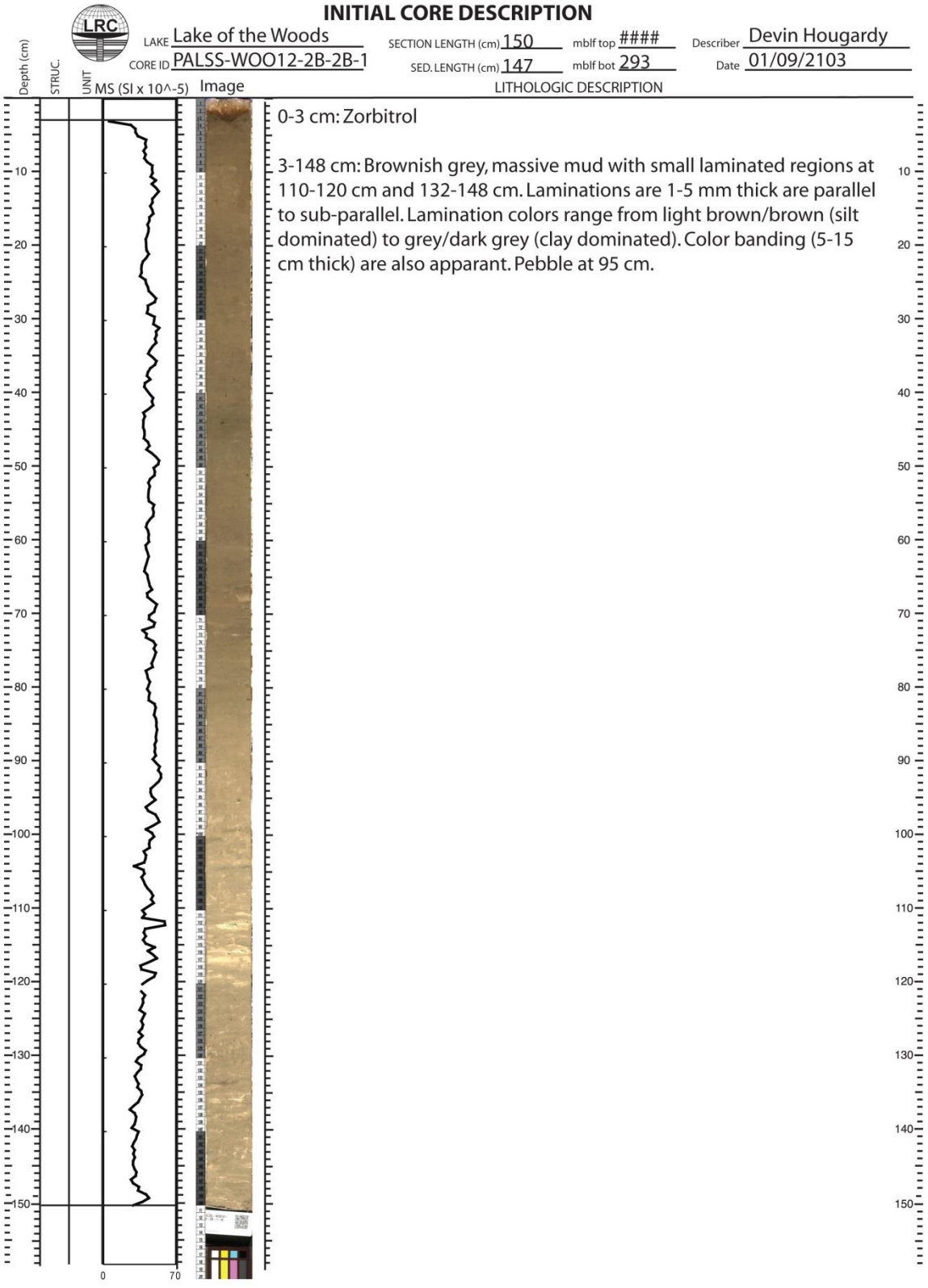

Figure 46 Core barrel sheet for PALSS-WOO12-2B-2B-1.

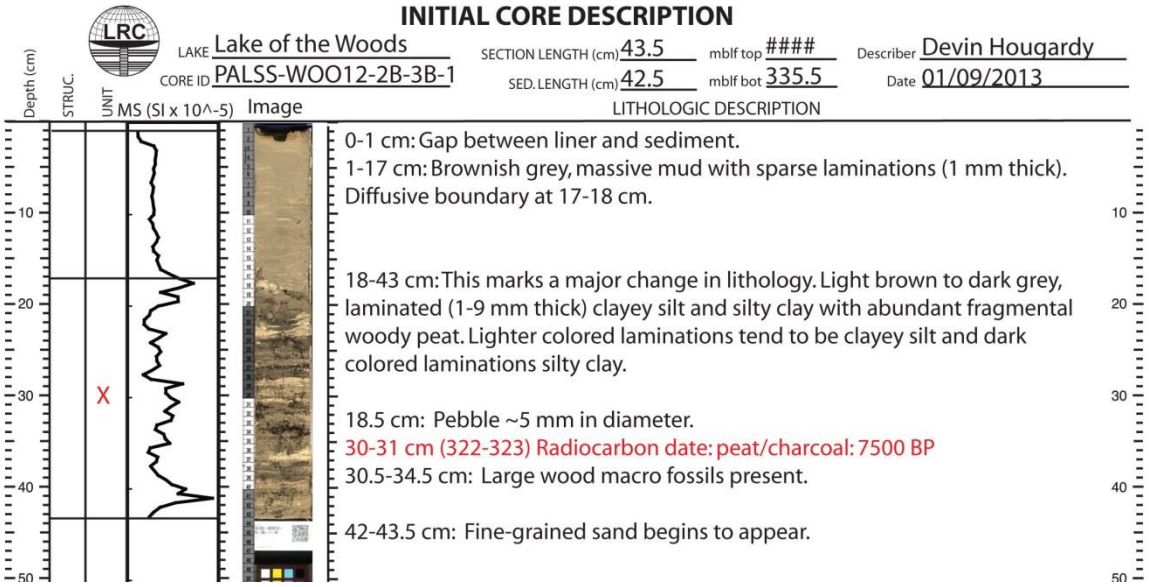

Figure 47 Core barrel sheet for PALSS-WOO12-2B-3B-1.

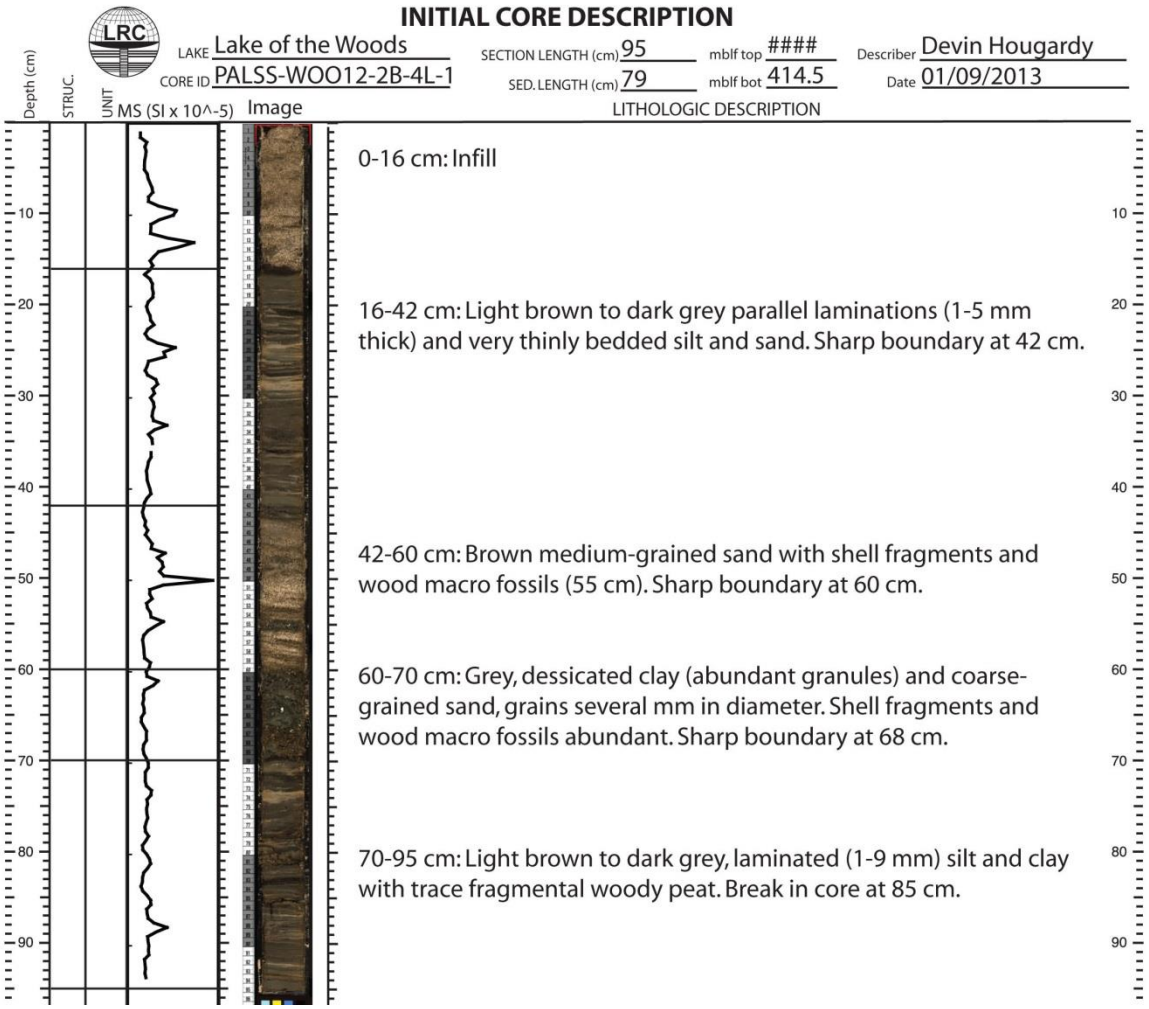

Figure 48 Core barrel sheet for PALSS-WOO12-2B-4L-1.

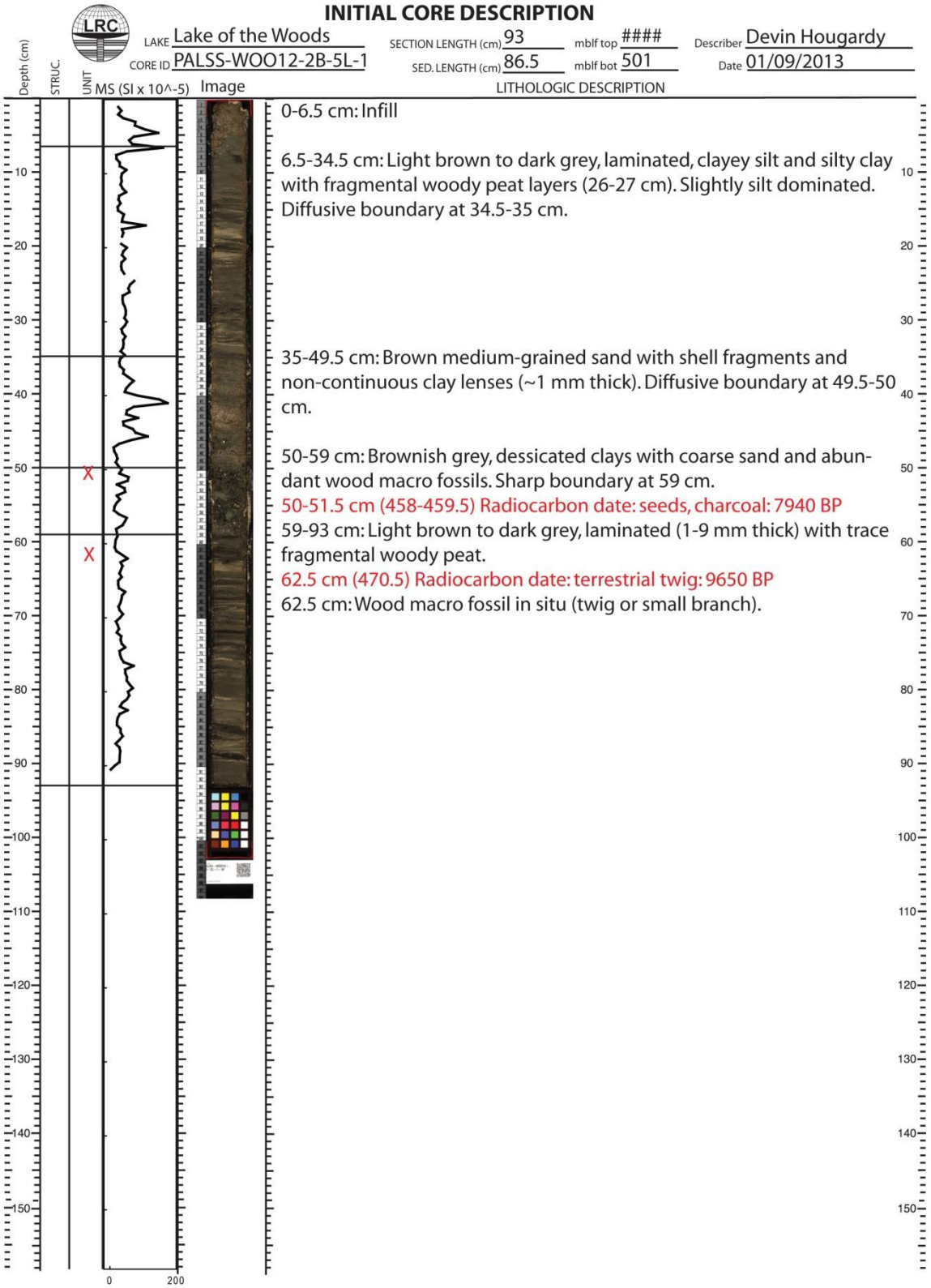

Figure 49 Core barrel sheet for PALSS-WOO12-2B-5L-1.

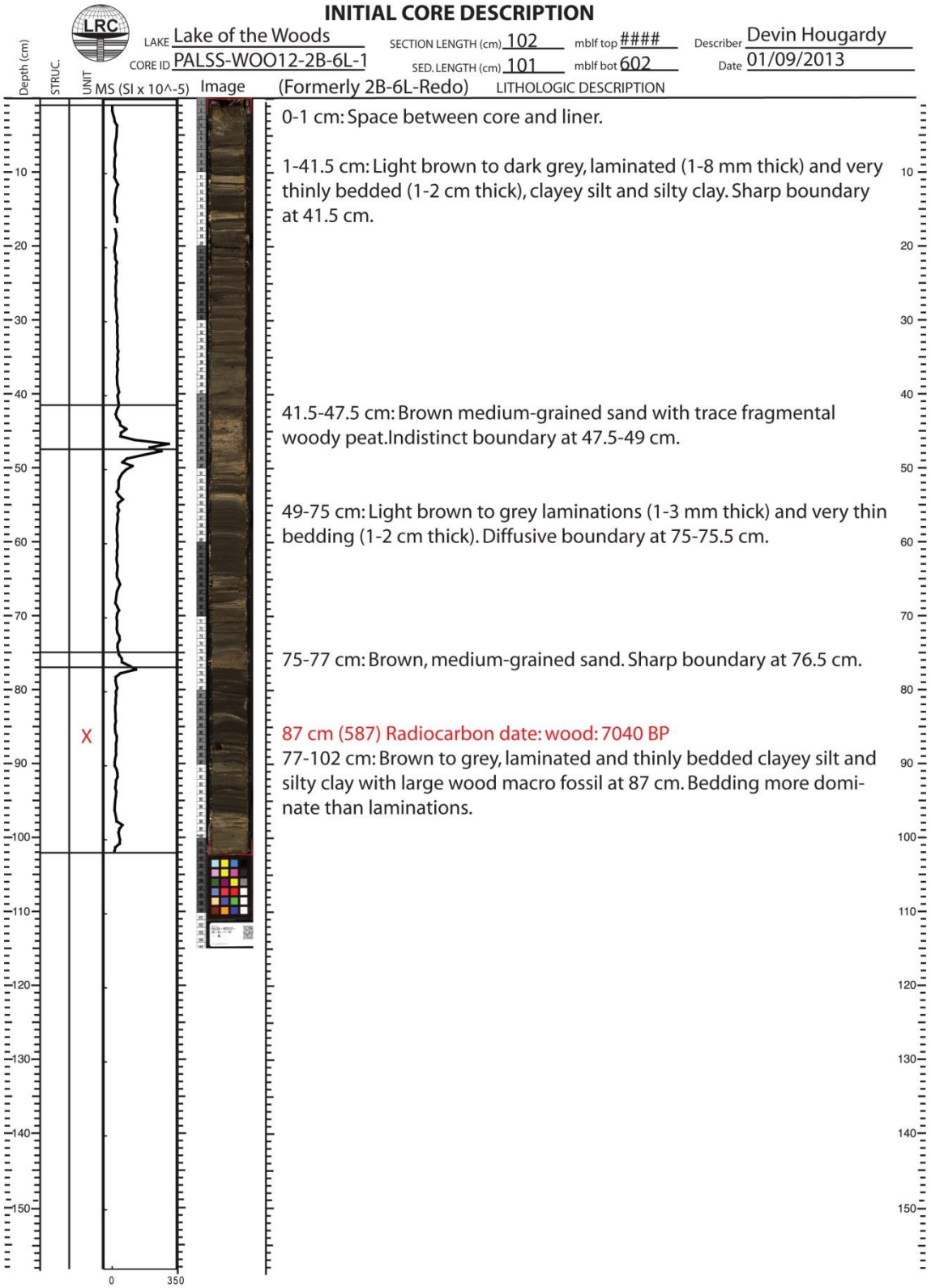

Figure 50 Core barrel sheet for PALSS-WOO12-2B-6L-1.

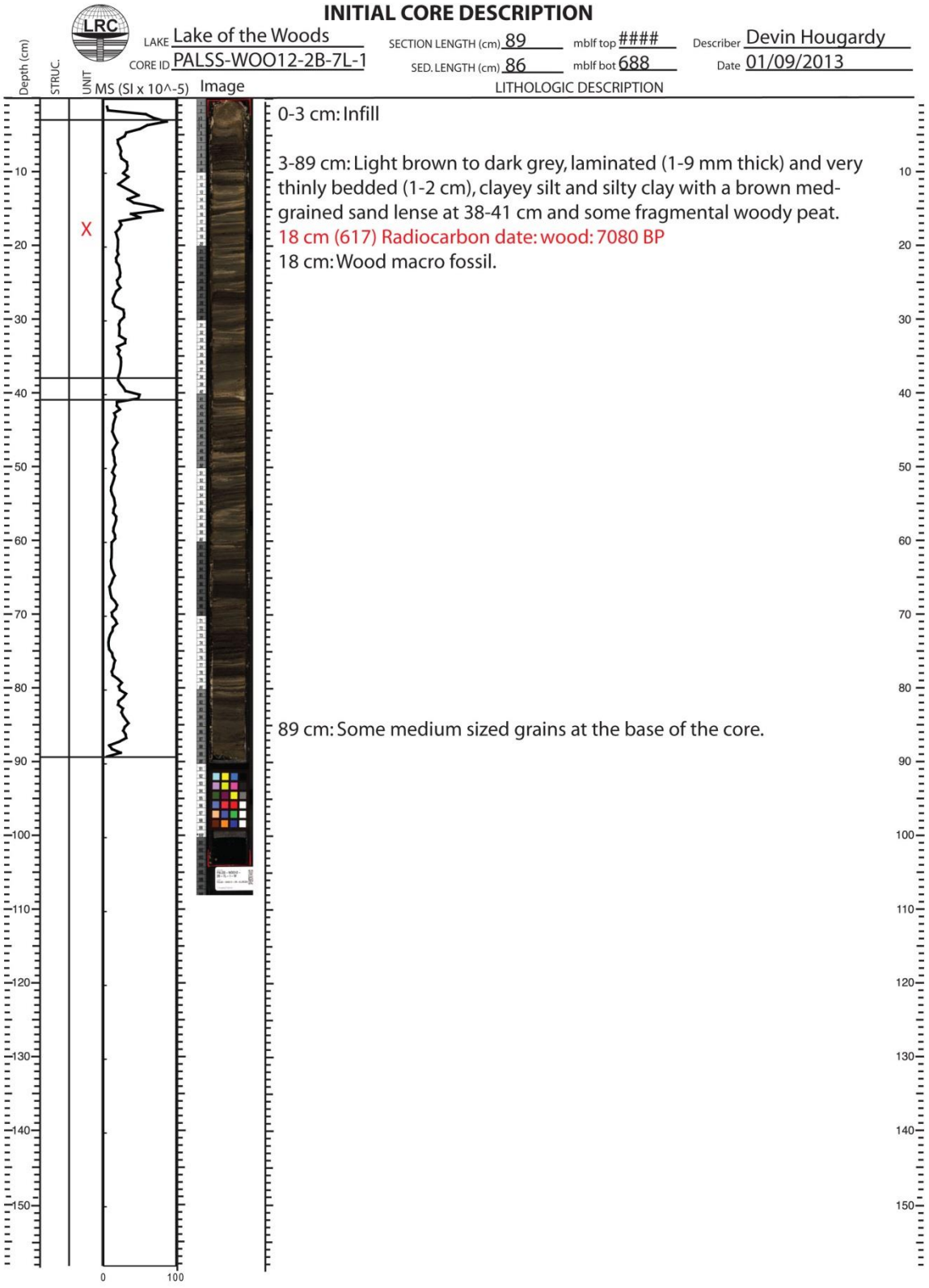

Figure 51 Core barrel sheet for PALSS-WOO12-2B-7L-1.

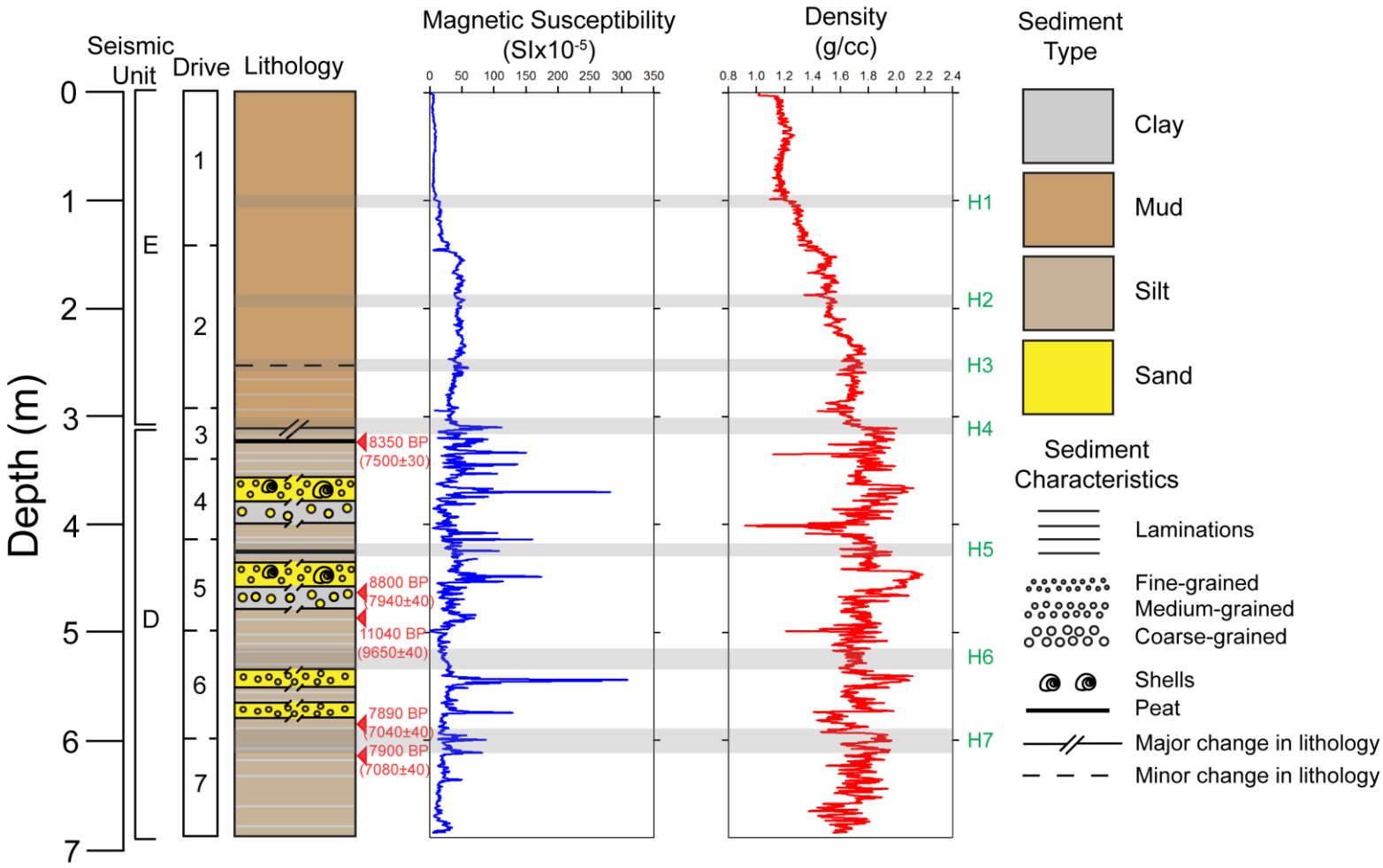

Figure 52 Stratigraphy of PALSS-2B. Drive length, stratigraphic column, magnetic susceptibility, and density data for PALSS-2B.The same seven seismic reflections (Figure 44) are shown with gray bars and labeled in green. A major abrupt change in lithology from mud-dominated sediment to laminated silt and clay occurs at the same depth as PALSS-2A (~3 m). Material from five locations was collected for radiocarbon dating (red triangles).

4.2.4 Sediment Core PALSS-3A

PALSS-3A (48.90773^{0} N, 94.74361^{0} W) represents the southernmost (~7 km north of where the Rainy River drains into Lake of the Woods) and shortest sediment core collected, measuring 0.70 m in length (Figures 53 and 54). From 0-0.24 m, the core is composed of brownish-gray, massive mud with a very thin peat layer at 0.09 m (Figure 55). There is a diffusive boundary from 0.24-0.25 m at which point the sediment lightens in color to light-brown and contains a thin bed of silt from 0.25-0.27 m. Below 0.52 m there is a shift from mud-dominated sediment to clay-dominated sediment containing abundant medium-grained sand marking a major change in lithology. This interval is thin (0.50-0.54 m) with a sharp lower boundary that overlies light-gray to bluish gray, highly desiccated clay for the remainder of the core (0.54-0.70 m).

MS remains relatively constant (0-100 SI units) from the top of the core until 0.45 m but does peak occasionally such as from 0.24-0.27 m (laminated silts). Below 0.45 m there is a large positive excursion for ~10 cm that occurs from 0.45-0.54 m, after which the MS stays relatively constant (0-50 SI units). MS peaks at 0.50 m corresponding to a change in lithology from mud to sand and clay, but then decreases sharply at 0.52 m and stays around 25 SI units where the matrix becomes clay-dominated.

Density values can be partitioned into three sections separated by two positive steps (0.17-0.19 m and 0.45-0.47 m). The density in the first section (0-0.17 m) is relatively constant (1.2-1.4 g/cc) but decreases slightly at 0.09 m corresponding to a peat layer. The second section (0.19-0.45 m) contains a large spike (2.0 g/cc) in density at 0.24 m corresponding to a minor change in lithology but otherwise stays between 1.5-1.7 g/cc. The third section (0.47-0.70 m) increases at 0.50-0.51 m (change in lithology from mud to clay and sand) and an stays relatively constant between 2.0-2.1 g/cc.

No radiocarbon material was identified from PALSS-3A. Seismic-reflection data was collected from this core site (not shown) but a very high signal-to-noise ratio prevented the identification of seismic reflections. Other regions of similar

distances from the Rainy River also displayed a highly attenuated seismic signal and poor penetration.

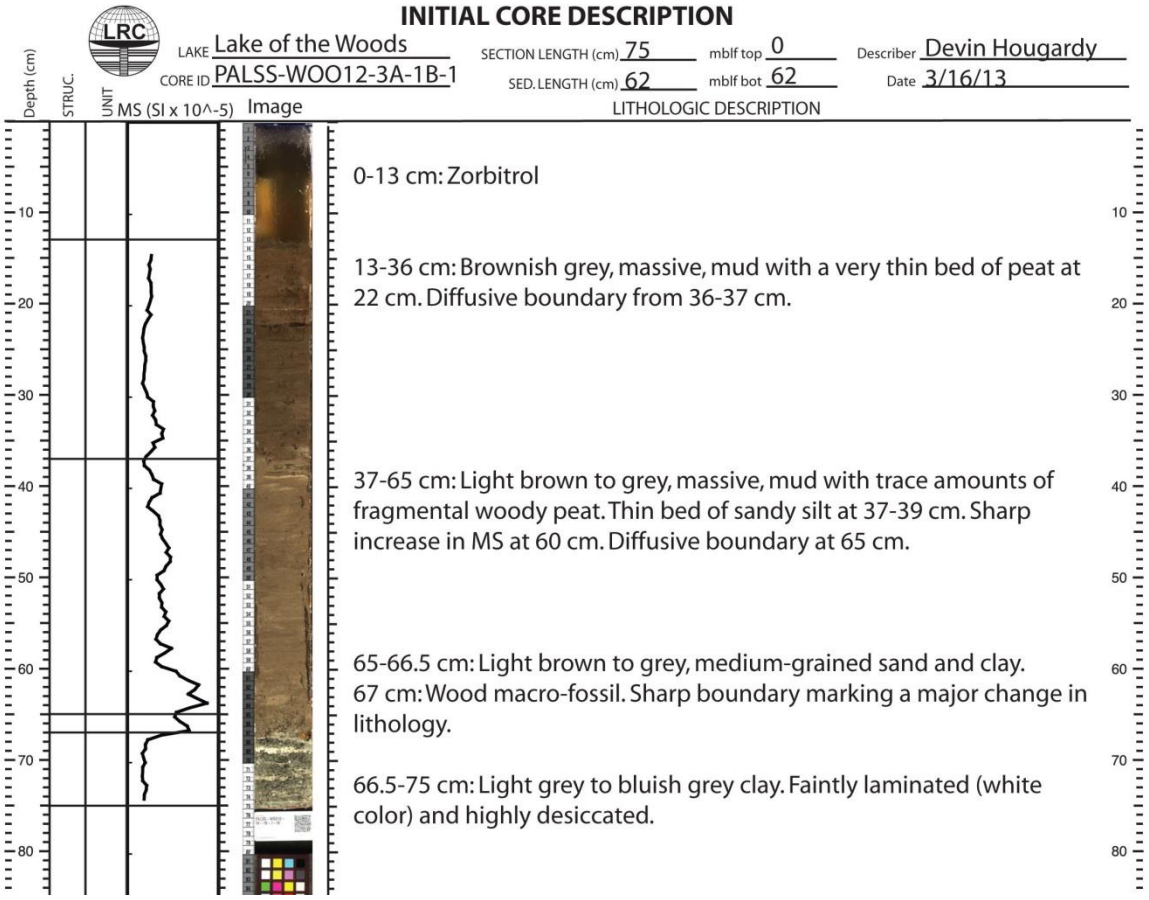

Figure 53 Core barrel sheet for PALSS-WOO12-3A-1B-1.

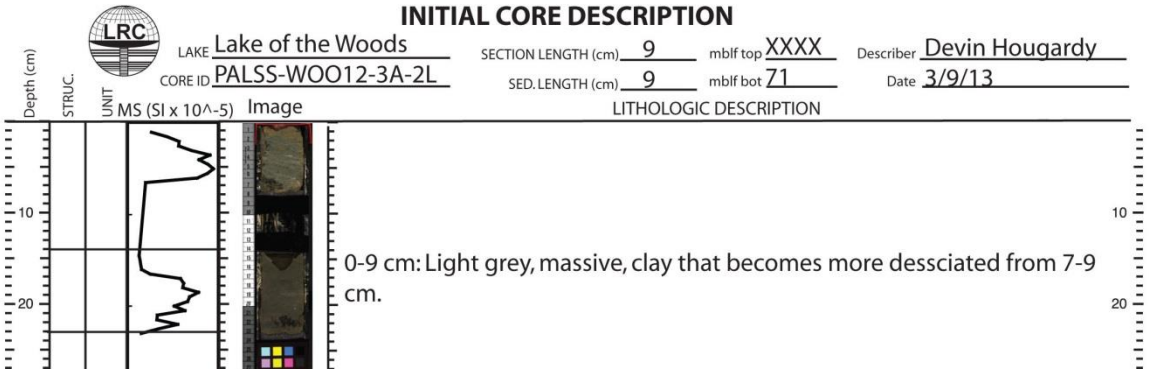

Figure 54 Core barrel sheet for PALSS-WOO12-3A-2L.

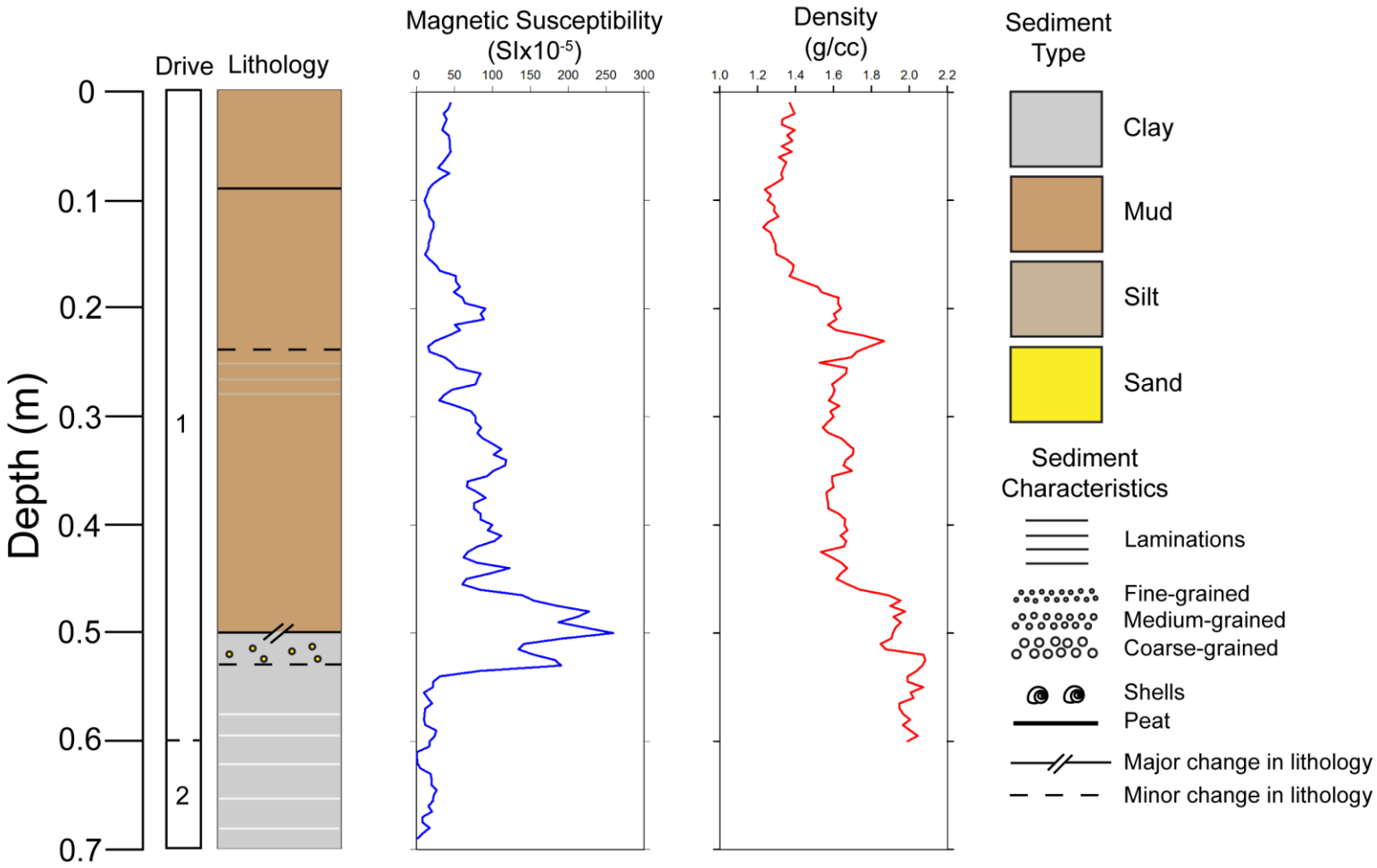

Figure 55 Stratigraphy of PALSS-3A. Drive length, stratigraphic column, magnetic susceptibility, and density data for PALSS-3A. A major change in lithology from mud dominated sediment to clay containing medium-grained sand occurs at ~0.5 m. Seismic-reflection data from this location was highly distorted preventing the identification of reflections.

4.2.5 Sediment Core PALSS-4A

PALSS (48.93400^0 N, 94.78740^0 W) was collected ~8.5 km offshore in the southern region of Big Traverse Bay. Total sediment recovery was 3.9 m (Figures 56-59). From 0-2.75 m, the core is composed of brownish-gray, massive mud with weak color banding (light and dark) 5-15 cm thick. From 2.75-3.57 m, sub-parallel to parallel laminations of silts and clays 1-3 mm thick appear within the mud. At 3.57, m there is a major lithology change from mud-dominated to clay-dominated sediment that is greenish-gray in color, and contains medium-grained sand.

MS values gradually increase from the top of the core until 1.5 m, at which point they plateau at roughly 40 SI units until 3.5 m. Several large spikes occur from 3.5-3.7 m, the largest of which (3.57 m, 150 SI units) probably correspond to a break in the core even though the majority of these data excursions were removed. From 3.7-3.9 m, the MS decreases and remains at around 10-20 SI units, corresponding to a shift in lithology from a mud-dominated to a clay-dominated matrix.

Density values gradually increase from 0-2.75 m (1.2-1.4 g/cc). At 2.75 m there is a small positive deviation that roughly corresponds to a minor change in lithology. A sharp decrease in the density occurs at 3.47 m followed by two peaks, the smaller of which corresponds to a major change in lithology and the largest peak in MS.

An *in situ* terrestrial twig located at a depth of 1.54 m was selected for radiocarbon dating and was measured at 1,750 cal BP (1,800±25 yr BP). Two horizons have been identified in the seismic-reflection data (Figure 61) and correlate well with the core data (Figure 60). The uppermost horizon (H1) occurs at an approximate depth of 2.7 m and corresponds to the depth where laminated silt and clay begin to occur within the mud-dominated sediment. The lower horizons (H2) corresponds to the approximate depth (3.5 m) of a major change in lithology from silt and clay laminated mud to clay and sand.

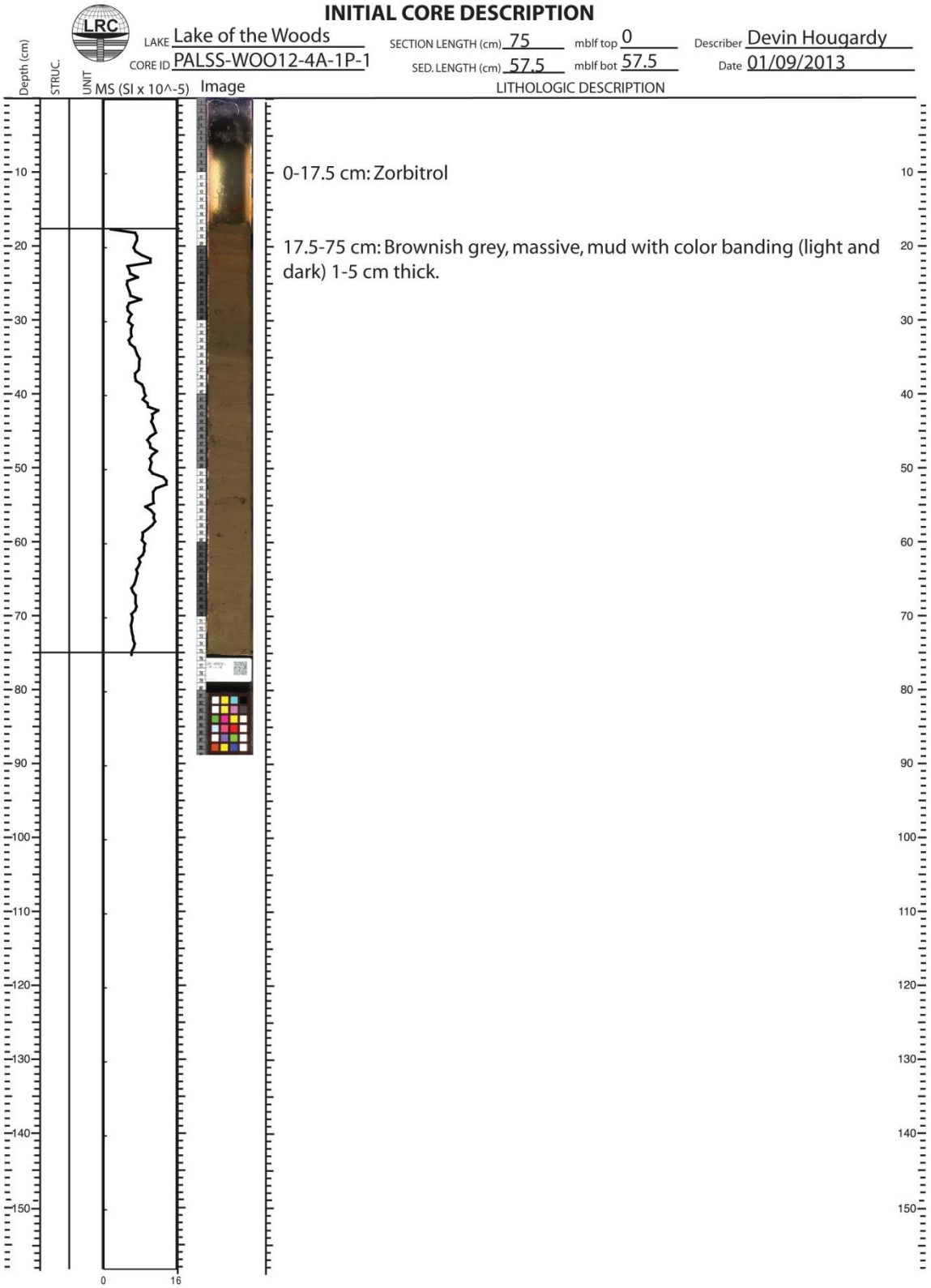

Figure 56 Core barrel sheet for PALSS-WOO12-4A-1P-1.

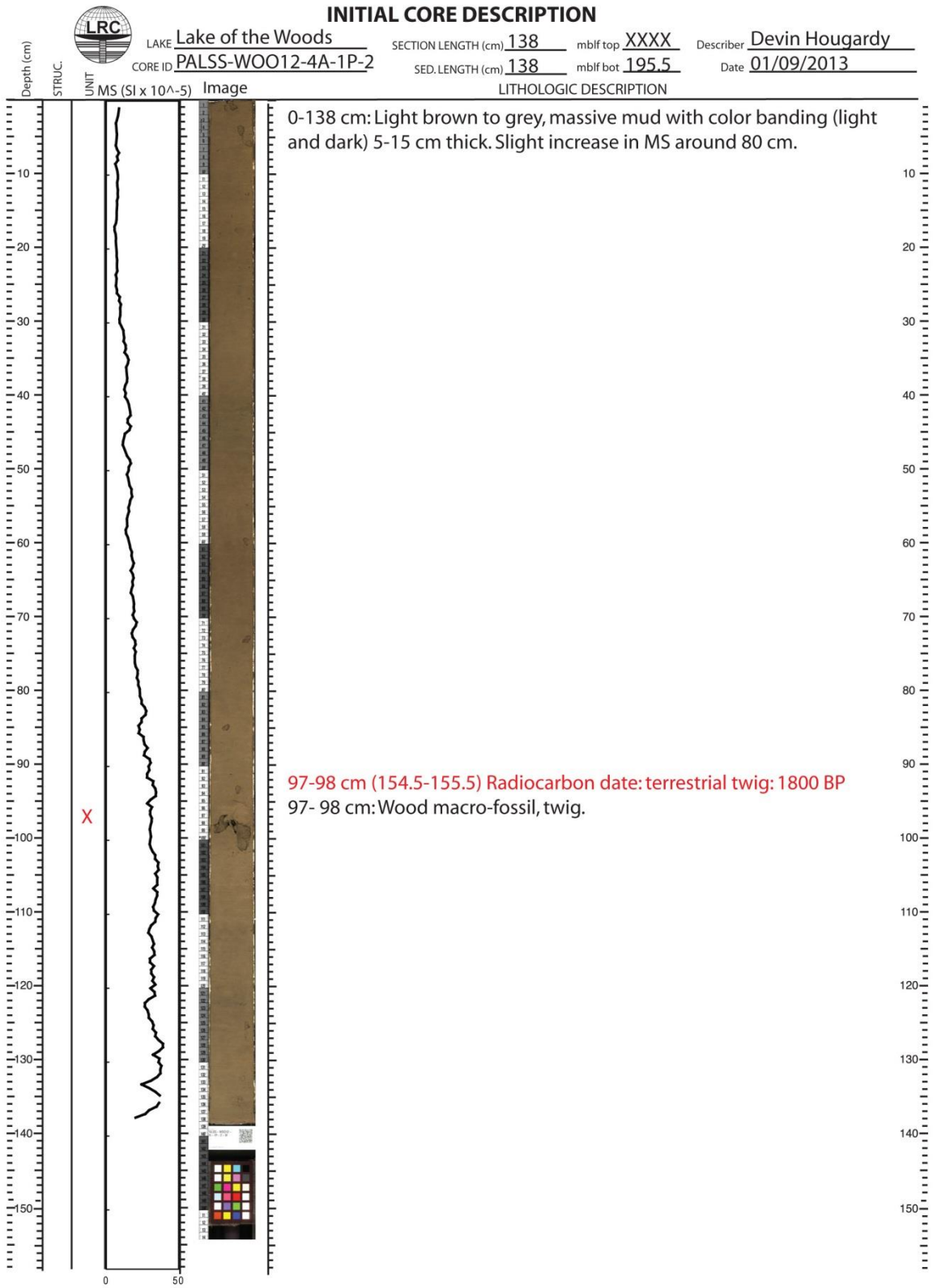

Figure 57 Core barrel sheet for PALSS-WOO12-4A-1P-2.

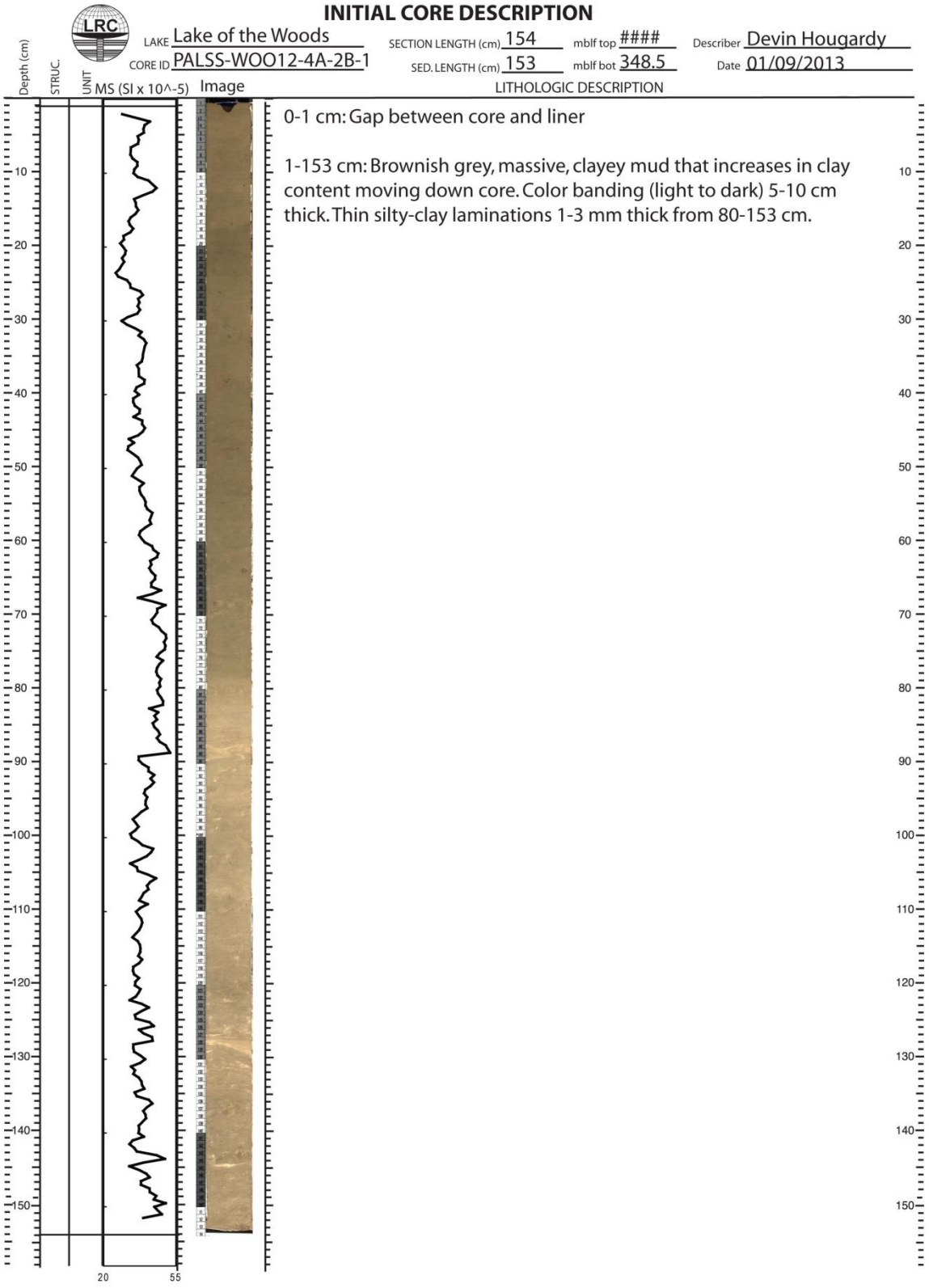

Figure 58 Core barrel sheet for PALSS-WOO12-4A-2B-1.

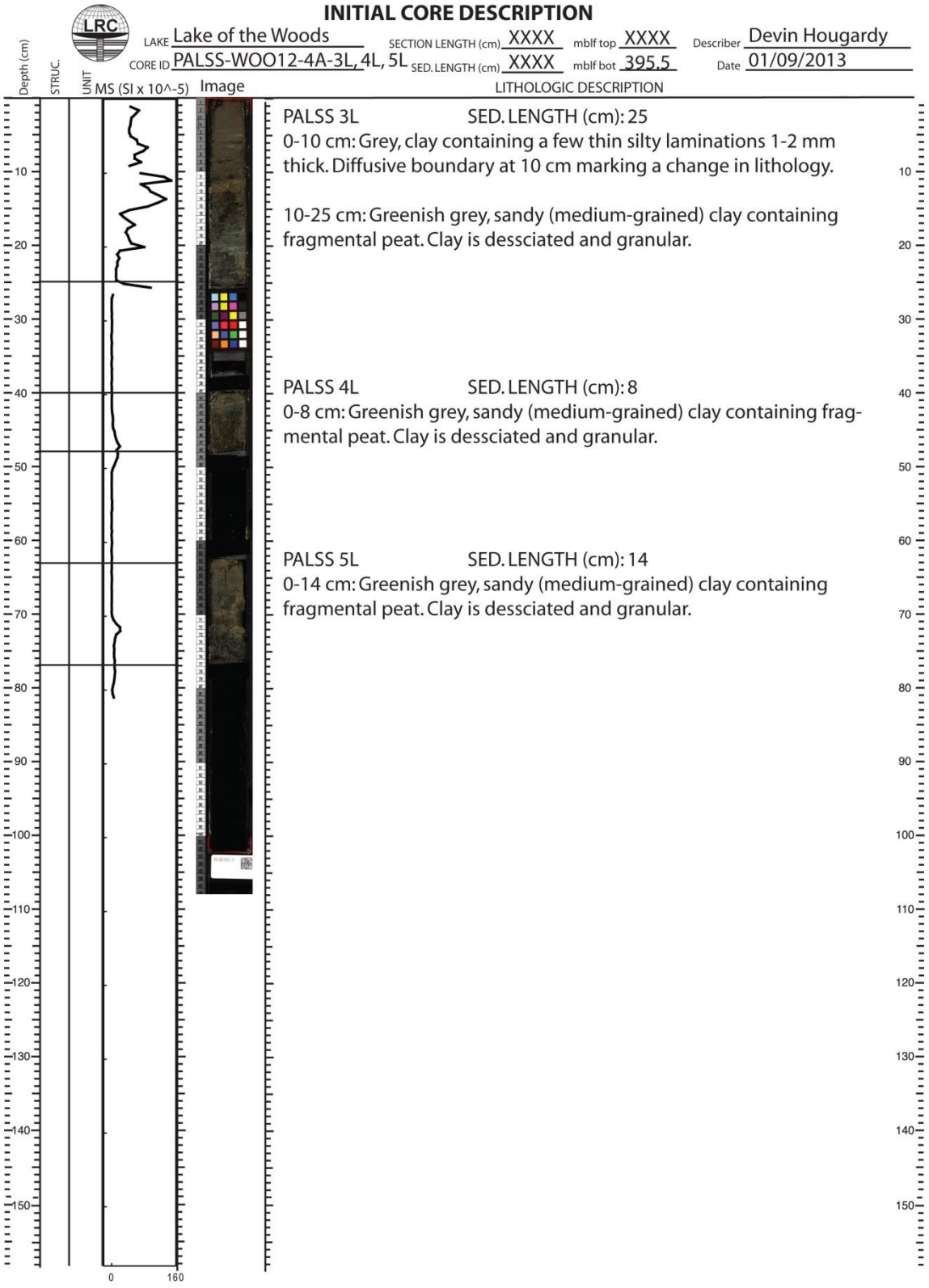

Figure 59 Core barrel sheet for PALSS-WOO12-4A-3L, 4L-and 5L.

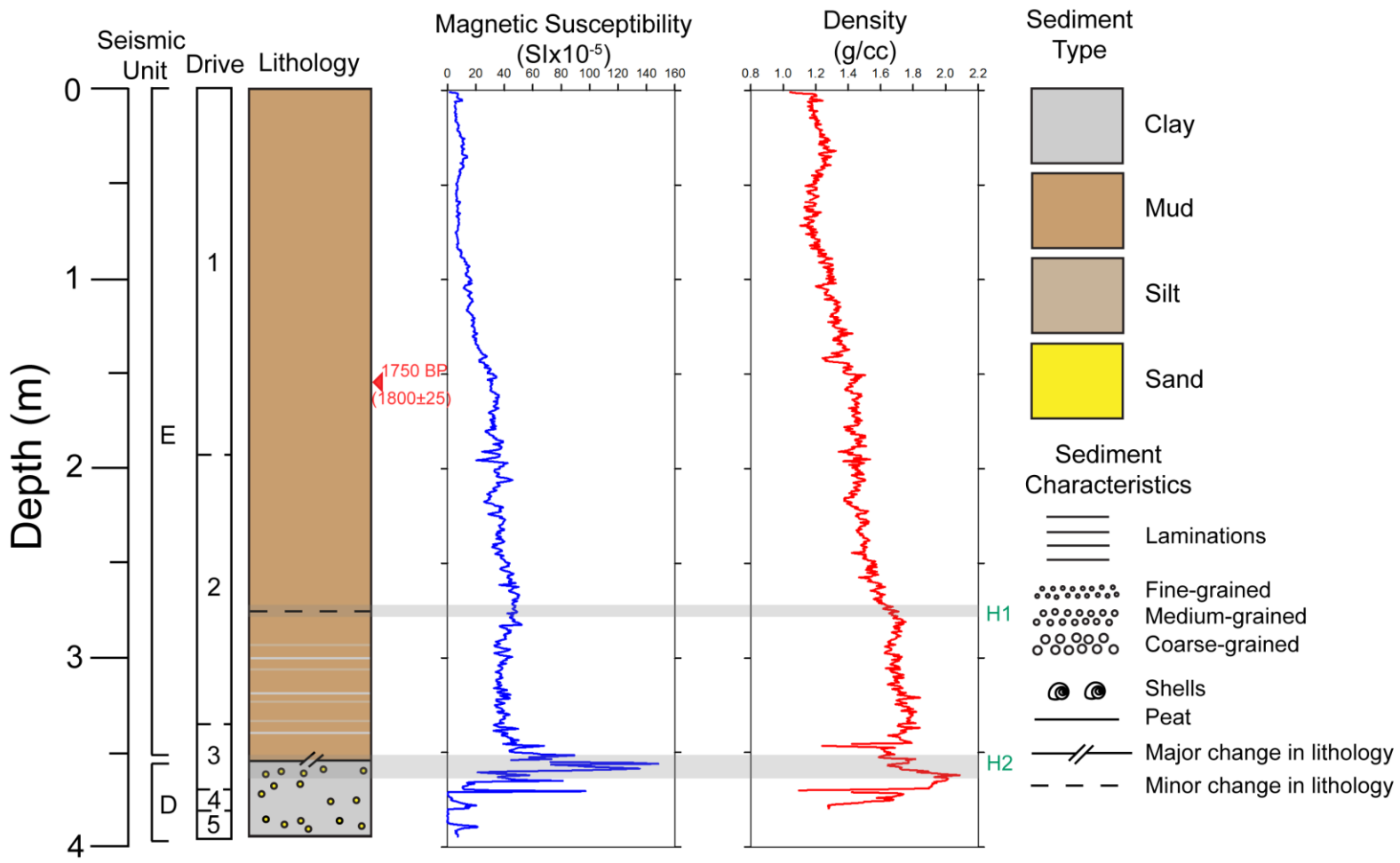

Figure 60 Stratigraphy of PALSS-4A. Drive length, stratigraphic column, magnetic susceptibility, and density data for PALSS-4A. Gray shaded bars and green labels represent prominent contrasts in acoustic impedance identified from seismic-reflection images over the core site (Figure 61). A major change in lithology form mud dominated sediment to clay containing medium-grained sand occurs at a depth of ~3.5 m and corresponds to UNCF-3 (H2). The only radiocarbon age from CU-1 was collected at a depth of 1.54-1.55 m.

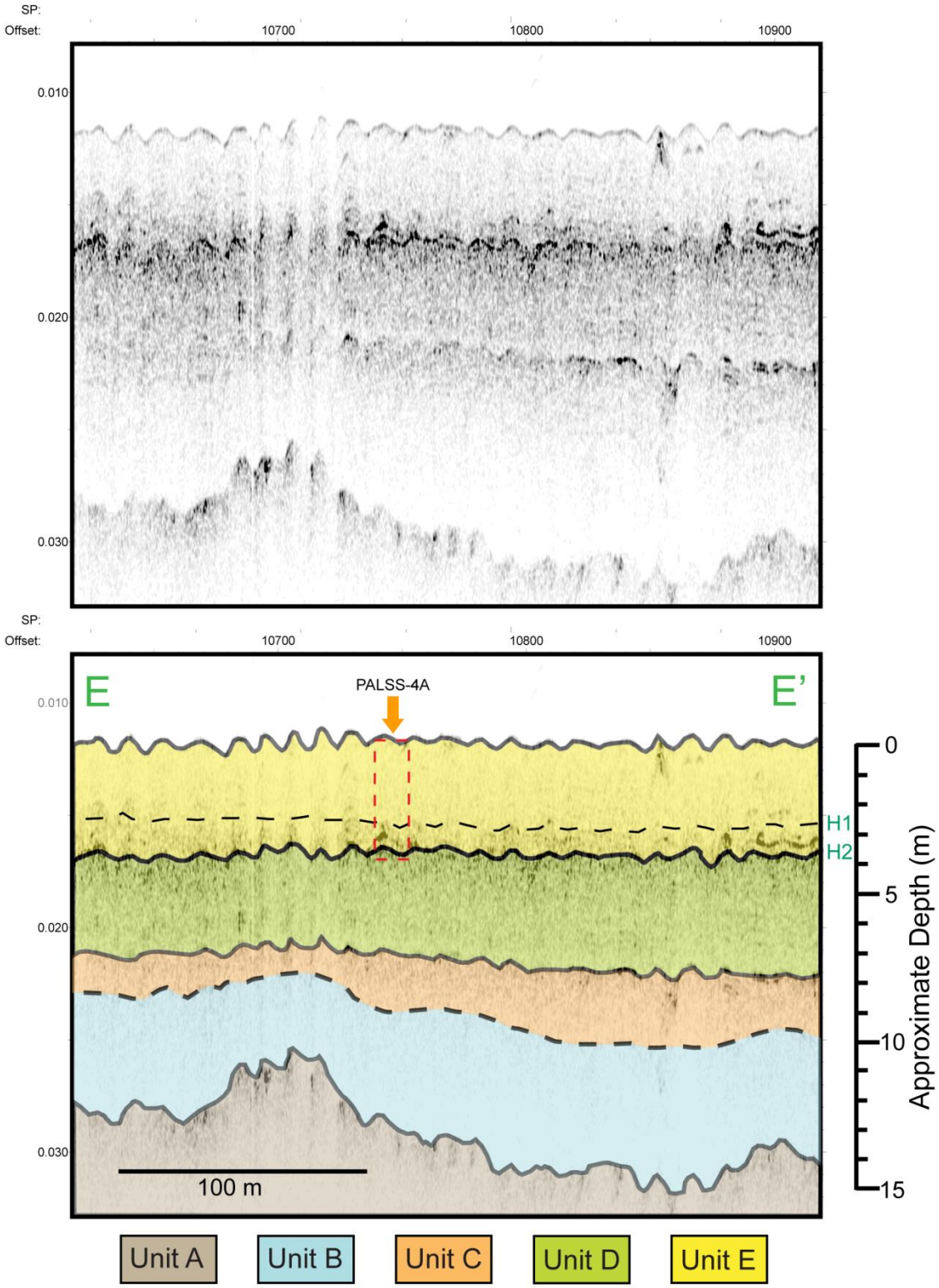

Figure 61 Seismic image of core site PALSS-4A. Interpreted seismic image (bottom) with the location and length of cores PALSS-4A (dashed red box). The bottom of the core penetrates through UNCF-3 (H2) at ~3.5 m and into SU-D. V.E.: ~16x.

Table 9. Summary of radiocarbon ages from the southern basin of Lake of the Woods

Core ID	Lab Number	Depth (cm) from top of core	Dated Material	^{14}C Age	∂^{13}C	Cal age range BP (2σ)	Probability	Cal age mean BP (1σ)	Probability	Weighted Avg. 1σ	Cal years BP
PALSS-2A	OS-103426	308-309	Peat	6930±30	-28.2	7830-7690	1	7750	1	7750	7748±40
PALSS-2A	OS-103432	652-658	Wood Macro	7040±35	-27.71	7950-7820	0.96	7910	0.57	7890	7879±41
						7810-7780	0.04	7860	0.43		
PALSS-2B	OS-103427	322-323	Peat	7500±30	-26.06	8390-8290	0.82	8350	1	8350	8340±29
						8260-8210	0.18				
PALSS-2B	OS-103428	458-459	Seeds	7940±40	-23.85	8820-8640	0.55	8740	0.45	8800	8773±108
						8980-8820	0.45	8940	0.24		
PALSS-2B	OS-103429	470	Wood Macro	9650±40	-26.85	11190-11060	0.52	11120	0.64	11040	11075±106
						10970-10790	0.45	10910	0.36		
PALSS-2B	OS-103430	587	Wood Macro	7040±40	-25.94	7950-7790	1	7910	0.55	7890	7878±46
								7860	0.45		
PALSS-2B	OS-103431	617	Wood Macro	7080±40	-24.69	7980-7830	1	7880	0.52	7900	7919±38
								7940	0.48		
PALSS-4A	OS-103125	154-155	Wood Macro	1800±25	-26.76	1820-1690	0.88	1720	0.57	1750	1724±35
						1650-1630	0.11	1770	0.28		
MOMOS-1A	48250	90-92	Clam	1460±45		1420-1290	0.97	1340	1	1340	1345±36
						1480-1460	0.02				
MOMOS-1A	61723	140-145	Seed Material	1675±20		1620-1530	1	1560	0.55	1570	1564±24
								1590	0.45		
MOMOS-1A	48217	280-282	Seed Material	7375±20		8220-8160	0.73	8190	0.89	8200	8186±20
						8310-8260	0.23	8270	0.11		
MOMOS-1A	54959	320-323	Seed Material	7140±40		8020-7930	0.92	7970	1	7970	7961±28
						7900-7870	0.08				

Radiocarbon dates were converted to calendar years before present (cal BP) using Calib v.5.0.1 (Stuiver and Reimer, 1986) and IntCal13 calibration data. MOMOS data were taken from Mellors (2010).

Chapter 5: Interpretations

5.1 Explanation of Interpretations

The purpose of this chapter is to use the observations described in Chapter 4 to develop geologically accurate interpretations of the data. I present the interpretations of the seismic images and sediment core analysis separately to develop two independent interpretations. Later, in Chapter 6, I integrate and discuss the two interpretations along with previous research outside of this thesis.

5.1.1 Seismic Unit A: Bedrock and Glacial Deposits

The high frequency seismic signal of the 3100P CHIRP profiler is unable to penetrate into highly consolidated or coarse material, such as bedrock or diamicton (poorly sorted material), making it difficult to determine the exact geology of the acoustic basement (SU-A). However, there are noticeable changes in the reflection character and configuration of the acoustic basement laterally across the basin that merits the separation between bedrock and diamicton. Near the margins, the amplitude strength of the upper boundary reflector is very high indicating a large contrast in the acoustic impedance from the overlying SU-B. The reflection configuration is smooth and the seismic signal becomes chaotic with depth suggesting that the upper boundary near the margins is highly consolidated. These regions of the acoustic basement are interpreted as bedrock (Figure 17(5)).

In the middle of the basin, the reflection configuration of the upper surface of the acoustic basement is highly irregular with abundant abrupt changes in relief. These features generally take the form of clumps that stretch laterally for tens of meters and are a few meters in height. The reflection amplitude of the acoustic basement is lower in the center than at the margins of the basin, indicating a lower contrast in acoustic impedance with the overlying sediments. This suggests that there is less contrast in lithology with the overlying material; however, it could also result from the seismic signal diminishing with depth. The latter is probably the case because similar clumped features display very high amplitude reflections closer to the margins of the basin. Stratified wavy parallel internal reflectors were observed

beneath the upper surface of the acoustic basement at a few locations (Figure 17(6)). These reflection packages are generally thin and discontinuous. The ability to distinguish internal reflections beneath the upper boundary suggests that the material near the middle of the basin is not as consolidated as that near the margins.

The acoustic basement in the middle of the basin is interpreted diamicton. No apparent evidence of deformation exists, possibly indicating that the acoustic basement here is composed of melt-out tills, though it is difficult to determine this for certain. It is possible that the stratified wavy reflections were deposited in a glacio-lacustrine environment as the ice-margin was retreating from the basin; however, the detailed origin of this unit is unclear from the seismic data.

The external geometry of the acoustic basement forms an elongated bowl shape that rises from the middle of the southern basin to become the lake floor to the north and south (Figure 22). Generally, the transition from diamicton to bedrock occurs where the acoustic basement rises to within ~2 m of the lake floor. Diamictons mask the underlying bedrock, where the acoustic basement is greater than 2 m below the lake floor, making it difficult to determine if large vertical variations in the acoustic basement are due to the structure of the bedrock or are glacial landforms such as moraines, eskers, or kames. The absence of diamictons at or near the margins of the basin suggests that the material was either removed by erosion after deposition or not deposited at all. It is difficult to speculate further from the seismic data alone, but if diamictons were eroded after deposition, material likely would have been transported by fluvial or lacustrine processes and deposited in the topographic lows of the basin.

5.1.2 Seismic Unit B: Lacustrine Deposits

Internal reflections within SU-B are relatively rare, which indicates (1) a very low variation in acoustic impedance and (2) that the lithology of this material is relatively uniform. In locations where low amplitude reflections are observed, they appear stratified wavy parallel and are draped over the underlying unit (Figure 17(7)), implying a low-energy environment of deposition. Internal reflections are discontinuous and mostly occur near the margins of the basin. Scarce internal

reflections in the middle of the basin likely result, at least in part, from attenuation of the seismic signal diminishing through the thicker sediments.

This unit is interpreted as lacustrine sediment deposited in quiescent conditions shortly after the ice-margin retreated from the basin. If deposition had occurred under more dynamic ice-proximal lacustrine conditions, the seismic data would show large contrasts in the acoustic impedance from variations in grain size and display a ponded configuration rather than sheet draped geometry. Whatever ice-proximal lacustrine deposition occurred, the deposits are probably included in the upper section of SU-A. The reflection characteristics would be similar to those of the underlying diamicton making the separation of the two difficult. As discussed in the previous section, the stratified wavy reflections in the upper section of SU-A may actually be glacio-lacustrine in origin instead of subglacial.

SU-B is very uniform in thickness throughout the survey area (Figure 23) despite being deposited on top of a clearly defined basin (Figure 22) and the unit disappears from the survey area only where truncated or obscured by shallow gas (Figures 16 and 18). The lack of depositional focusing suggests that the lake was deep enough for the entire basin to be below wave base when SU-B was deposited. Internal reflections in SU-B are truncated by all three unconformities (UNCF-1, UNCF-2, and UNCF-3) at the margins of the basin, implying multiple fluctuations in lake level occurred after SU-B was deposited.

5.1.3 Unconformity 1

UNCF-1 separates depositional SU-B and SU-C (Figures 16, 18, and 19). The reflection amplitude of UNCF-1 is high at the margins of the basin and decreases towards the middle of the basin indicating that the contrast in acoustic impedance decreases towards the middle of the basin as well. This is likely due to an overall decrease in grain size contrast from the margins towards the middle of the basin; although, it could also be related to the overall seismic signal diminishing with depth in thicker regions as described in section 5.1.2.

UNCF-1 truncates underlying internal reflections in SU-B at its margins but is concordant with the same reflections in the middle of the basin indicating that its

relation to SU-B varies laterally. The width of the zone of truncations is small (<1.5 km), with the majority of the surface lying concordant to SU-B. This suggests erosion only occurred at or near the margins of the basin and that the horizon is conformable or non-depositional at all other locations.

At or near the margins of the basin, UNCF-1 indicates a hiatus between the deposition of SU-B and SU-C and is interpreted as a relative drop in lake level. The lateral variations in both reflection character and configuration suggest that the margins of the basin were exposed to high-energy conditions while the middle and lower elevation regions were lower-energy environments. Wave action in the migrating littoral zone during the lake's regression, and subsequent transgression, would have eroded material from the top of SU-B (Figure 17(1)). Parts of the erosional zone may have also developed under subaerial conditions, however, it is not possible to discriminate between wave and wind based erosion in the seismic images. In the middle of the basin, where UNCF-1 is concordant with underlying reflections (Figure 17(2)), deposition was continuous. Increased sediment supply from the lake's inputs or from the newly eroded littoral zone during this regressive/transgressive period likely provided the material needed for a contrast in high acoustic impedance (i.e., UNCF-1).

The wave base of LOTW after the formation of UNCF-1 and immediately prior to the deposition of SU-C is estimated at where UNCF-1transitions from erosional to concordant with SU-B (Figure 27 red to light-green regions). This zone has been traced and is shown (Figure 62) in relation to the location of the wave base immediately prior to the deposition of SU-D and the modern wave base. It is clear that the surface area of the lake in the southern basin of LOTW was significantly smaller during the formation of UNCF-1 than present-day LOTW. Above UNCF-1, internal reflectors in SU-C are ponded in the topographic lows of the basin and progressively onlap onto UNCF-1 suggesting that the lake grew and coalesced outwards from the localized topographic lows as the lake level rose and deposition of SU-C began (margins of basin) or continued (center of basin).

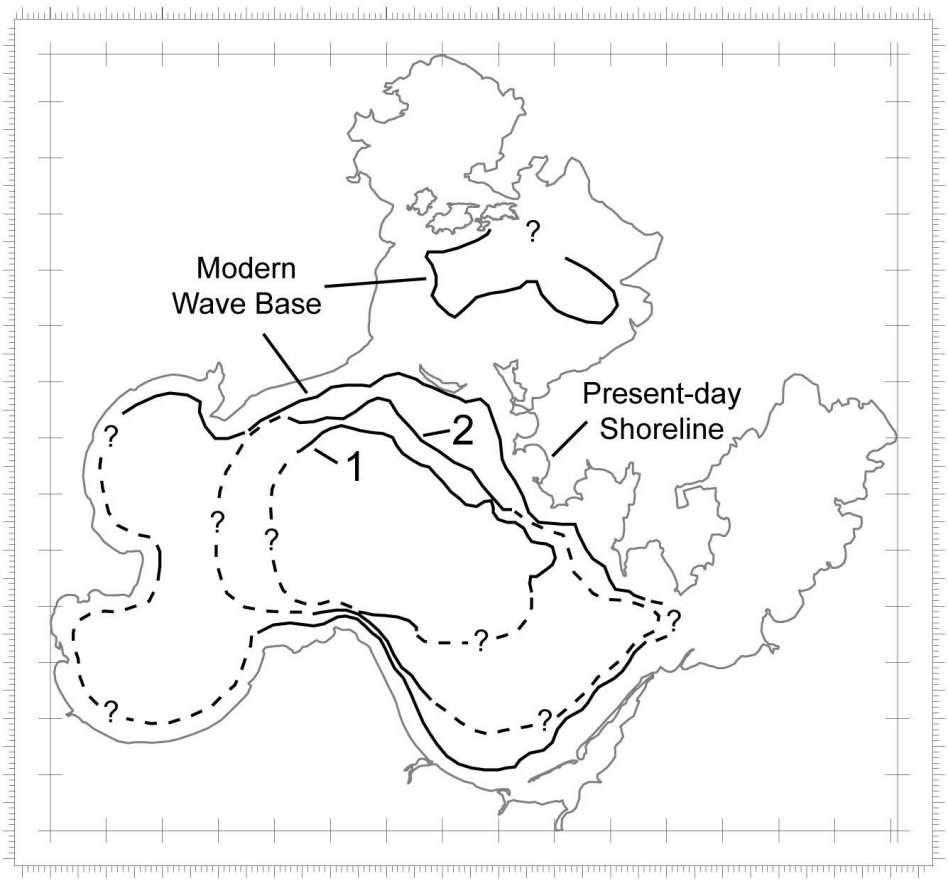

Figure 62 Wave base locations at different periods of time at LOTW. Wave base locations, indicating the transitional zone between erosion and deposition or non-deposition, following the formation of UNCF-1 (1) and UNCF-2 (2) compared to the location of the modern wave base. Regions outside of the survey area or obscured by gas are shown with a dashed line.

5.1.4 Seismic Unit C: Lacustrine Deposits

The moderate-to high-amplitude internal reflections of SU-C, together with its ponded configuration, imply a moderate- to high-energy depositional environment. The internal structure is marked by several high amplitude reflections separated by zones that are reflection-free or contain low amplitude reflections (Figure 17(8)). In seismic profiles that strike NE-SW, these zones appear to thicken progressively to the southwest above each high-amplitude reflection moving up section. They are interpreted to have formed during a combination of differential isostatic rebound on the basin and a southward transgression of Lake Agassiz (see section 2.2.1). The high-amplitude reflections likely indicate high-energy events where coarser grained material was washed in and deposited across the basin. In

between these events, deposition of uniform or slightly variable material under relatively low to moderate-energy occurred.

The reflection configuration of SU-C is complex and the data show evidence of ponded, draped, divergent, and onlapping reflectors (Figure 17(8)). Internal reflections are strongly stratified wavy parallel and generally tend to drape the underlying topography. In many cases, however, reflections pond in the topographic lows near the base of the seismic unit and onlap onto the lower boundary as the depression was progressively filled. Once the basin was partly filled, reflections became more laterally continuous and draped the underlying topography. Internal reflections also onlap onto the lower boundary at the margins of the seismic unit (Figure 19) giving the unit as a whole a ponded configuration. Because the ponded configuration occurs on both large and small spatial scales, it is interpreted that lake level was low during the deposition of the lower part of the unit but progressively rose as deposition continued up section, eventually allowing for laterally continuous deposition to occur. The amount topographic relief decreases up section as a result of the low regions filling in. Infilling does not occur uniformly across the basin, however, giving stratified reflections a divergent configuration in some regions.

The external geometry of SU-C is an elongated bowl shape that generally occupies the middle and deepest region of the basin (Figure 24). Because the upper boundary (UNCF-2) truncates internal reflections in many places and results in pinch out of SU-C, it is difficult to reconstruct the extent of region occupied by the lake at the time of deposition. It is possible that the area of deposition was once more extensive than is now represented in the survey area, and that a large amount of material was removed from the margins of the basin due to a relative drop in lake level following deposition. However, the overall thinning of the stratified reflections towards the margins suggests that the majority of deposition was constrained to the middle of the southern basin of LOTW, perhaps as a result of relatively low lake levels.

Several “wipe-out” features were observed in the upper part of SU-C (Figure 17(8)). These features, found only in the middle of the basin, typically extend tens of meters laterally and several meters vertically. Immediately below the wipe-outs,

reflections remain clear and undistorted, indicating that the wipe-outs are not related to trapped gas within the sediment. Stratified reflections adjacent to these features abruptly end at the edges of the wipe-outs, suggesting that the internal composition in the wipe-outs is relatively uniform. One interpretation is that they are channel fills that existed in the middle of the basin prior to the formation of UNCF-2. The likelihood of channel formation is discussed further in section 6.1.2.

5.1.5 Unconformity 2

UNCF-2 separates depositional SU-D from SU-C and SU-B (Figures 16, 18, and 19). Similarly to UNCF-1, the reflection of UNCF-2 is greatest at the margins and decreases towards the middle of the basin. However, this decrease is much less pronounced in UNCF-2 compared to UNCF-1, indicating that the contrast in acoustic impedance is not as laterally variable across the basin, in turn suggesting that the grain size or other lithologic character varies relatively little across the basin at the level of the unconformity.

The unconformable relationship between UNCF-2 and underlying SU-C and SU-B varies laterally over the survey area. In the majority of the survey area, the unconformity rests conformably over SU-C (Figure 17(4)). Near the margins of the basin, UNCF-2 truncates underlying internal reflections in SU-C and frequently but not always truncates UNCF-1, causing SU-C to pinch out. Shoreward of where SU-C pinches out, UNCF-2 rests unconformably over SU-B and truncates its internal reflections (Figure 19). The wave base during the formation of UNCF-2 (Figure 62) indicates that the area of deposition was more extensive than during the formation of UNCF-1.

Like UNCF-1, UNCF-2 indicates a local hiatus between the deposition of SU-D and SU-C and SU-B at or near the margins of the basin. It is interpreted to be the result of a relative drop, followed by a rise in lake level. The higher elevation margins of the basin were eroded by high-energy waves and possibly by wind if the paleoshoreline had migrated far enough inward for subaerial conditions to exist. Lakeward of the wave base, UNCF-2 lies conformable upon underlying SU-C, which suggests deposition was continuous in the middle of the basin. The reflection

amplitude of UNCF-2 generally remains high throughout the basin, suggesting a small variance in lithology and grain size distribution. This is interpreted to be the result of material from the upper part of SU-C reworked as the lake level lowered. Wind or current driven mixing may have re-suspended material from the lake-floor before it eventually settled and draped the underlying topography.

5.1.6 Seismic Unit D: Lacustrine Deposits

SU-D is strongly stratified parallel to sub-parallel. The middle of the seismic unit contains abundant low to moderate amplitude and continuous internal reflections (Figure 17(9)) suggesting a succession of laminated materials comprised of similar grain sizes such as clay and silt. At and near the basin margins, however, the reflections are often discontinuous and tend to fade in amplitude against the background noise, implying that the composition of the material is more uniform in these regions. Near the upper boundary (UNCF-3), reflections are also discontinuous and fade into the background noise, though, their reflection amplitudes are typically high, possibly suggesting that they contain coarser grained material such as a sandy sequence interbedded in mud.

Internal reflections in the lower part of the seismic unit onlap onto UNCF-2 (Figure 19) suggesting a rise in lake-level, rapid deposition, or both occurred. It is difficult to determine the extent of the lake surface during the time this unit was deposited because the upper reflections of the unit are truncated by UNCF-3 in every seismic profile. Stratified reflections fill the interior of SU-D in the central and deepest part of the basin; groups of these reflections thin radially towards the basin margins until they are truncated by UNCF-3.

5.1.7 Unconformity 3

UNCF-3 separates SU-E from all underlying lacustrine units and is observed in every survey line where not obscured by shallow gas (Figures 16, 18, and 19). Erosional truncations of underlying lacustrine and glacio-lacustrine sediments are most obvious at the margins of the basin but are also observed well into the middle of the basin. UNCF-3 appears to rest concordant with underlying reflections in the

middle of the basin. The very high reflection amplitude together with its general parallel reflection configuration in all survey lines suggests that this unconformity was formed by a similar mechanism over the entire basin. Channel scouring and subaerial conditions are ruled out because of the planar geometry of the unconformity where erosional truncations occur. Instead, the mechanism of formation is interpreted as wave-based erosion during a lake-level transgression. Low-angle reflections onlap onto UNCF-3 over a distance of several kilometers in the southern part of the basin suggests that lake was transgressing southward as deposition of the lower part SU-E began. Deposition in a differentially uplifting basin (Figure 63) resulted in onlapping reflections that occur in other lacustrine environments (Teller, 2001). Erosion was more severe in the northern part of the basin where the tops of underlying units appear to be removed (Figure 16). It is likely that prior to the formation of UNCF-3, much of the basin was exposed to subaerial conditions due to a drop in lake level that exposed much, if not all, of the entire lake floor, which was subsequently eroded as transgressing water inundated the southern basin.

5.1.8 Seismic Unit E: Lacustrine Deposits

SU-E varies both vertically and laterally in reflection character. The upper two-thirds of SU-E are generally reflection-free, suggesting uniform lithology and a low-energy depositional environment. However, some stratified parallel, low-amplitude reflections are present, but tend to be discontinuous in the middle of the basin suggesting that the lithology is more uniform in the middle of the basin than at the margins of the basin (Figures 16 and 18). Distinct hyperbolic diffractions are abundant, indicating the presence of some type of coarse material that act as well-developed point reflections. Because these hyperbolas occur independently in an otherwise reflection-free medium, their source is unlikely to be gravel-rich beds or diamictons. The hyperbolic reflections are interpreted as coming from submerged logs that were transported or inundated as LOTW transgressed southward. Shallow gas is common in the upper section of this unit in Muskeg Bay, Sabaskong Bay, and

Buffalo Bay, obscuring the seismic signal and preventing penetration at these locations.

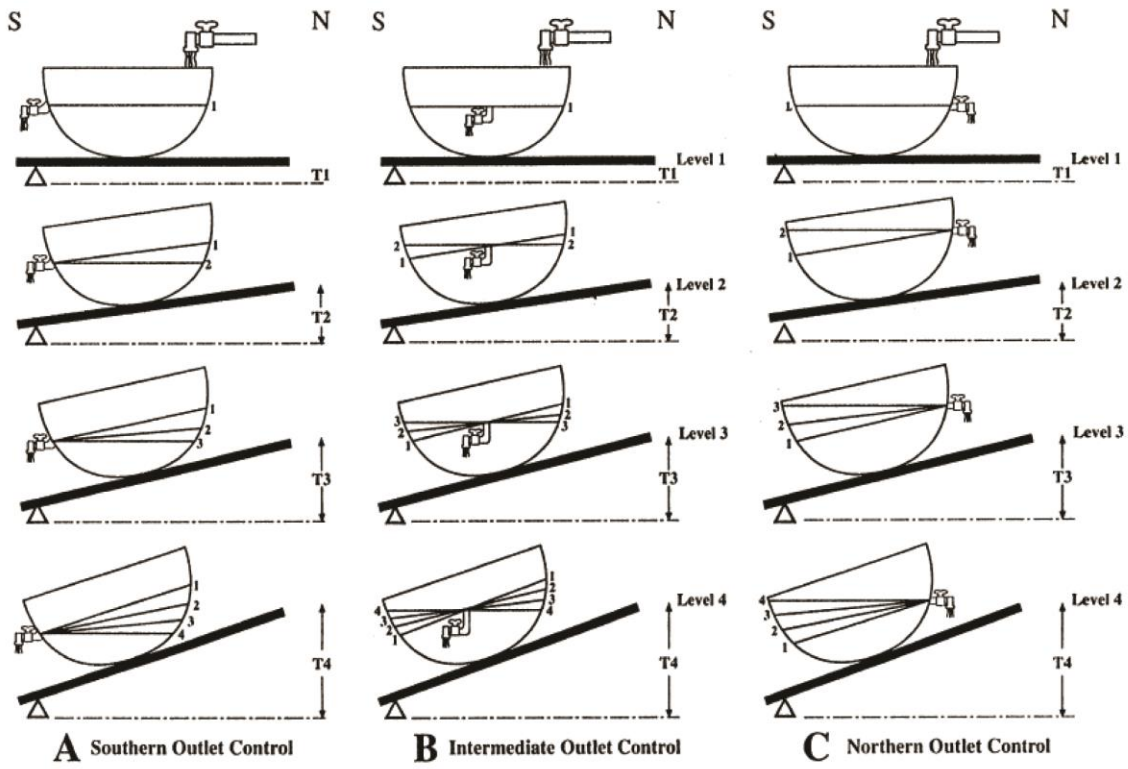

Figure 63 Outlet controlled basins experiencing uplift. Shoreline development of a basin undergoing differential isostatic rebound for three different outlet scenarios at four points in time. (A) Southern outlet: shoreline regresses everywhere across the basin at all points in time. (B) Intermediate outlet located at mid-basin isobase: transgression occurs south of the isobase but regresses north of that isobase. (C) Northern outlet: lake everywhere transgresses upslope until the spillover point is reached. If erosion occurs at spillover point, the transgressive beach in abandoned (from Teller, 2001).

The lower third of SU-E is dominated by chaotic, high-amplitude reflections in a zone that is thickest in the middle of the basin and towards its south end. This chaotic interval indicates a zone of high contrast in acoustic impedance related to a change in the physical properties of the material. Generally, the top of the chaotic interval is marked by a moderate to strong parallel reflection. A few moderate to high-amplitude reflections occur within the body of the chaotic interval, suggesting

interbedded layers of varying properties. The reflection amplitude of the lower boundary of SU-E is very high, indicating a large contrast in acoustic impedance. Large contrasts in acoustic impedance are usually produced by coarse-grained material such as sand or gravel suggesting a high-energy environment; however, they can also be produced by other acoustic impedance contrasts, such as that associated with a peat that was deposited in a low-energy environment. It is unclear from the seismic data which occurs at the surface of UNCF-3 and both (see section 5.2).

The overall thickness of SU-E clearly increases from NE to SW (Figures 16 and 24), reflecting deposition that is not focused to the deepest part of the basin. This is partly due the planar geometry of the lower boundary of the unit and the absence of localized deep regions. However, there must be another mechanism to explain why the thickest deposition occurred in the southwestern part of the basin, rather than uniformly across the basin. Tilting of the basin towards the southwest provides an explanation for this pattern and is consistent with the regional geologic history (see section 2.3.2). Internal reflections within SU-E onlap onto UNCF-3 suggesting that lake level was rising when SU-E was deposited. Onlapping reflections occur more frequently in the southern part of the survey area implying that the rising outlet was located north of the southern basin as the lake transgressed southward (Figure 63).

SU-E is the uppermost unit in the survey area and was likely deposited under similar conditions as those of modern-day LOTW. The uppermost material in the reflection-free zone presumably represents recent deposition; therefore, mapping the extent of that material would give insight into modern-day depositional patterns. Unfortunately, the low contrast in acoustic impedance within the material, due to its uniform lithology, makes mapping the upper interval challenging. It is possible, however, to extrapolate downward to the lower boundary of SU-E to provide a reasonable estimate of where the thickest modern-day-like deposition has occurred, assuming that the factors that control deposition have not changed very much. Thus, the isopach map of SU-E (Figure 26) can be used as a representation of modern-day depositional rates and patterns.

5.2 Interpretation of Sediment Cores

5.2.1 Lithological Interpretation

The sediment in the LOTW cores can be divided into two core units based on their physical properties. The uppermost core unit (CU-2) correlates very well across the southern basin (Figures 32, 43, 52, 55, and 60). Its massive lithology, fine grain size, low MS, and density all support the interpretation that this unit was deposited in a low-energy, open-water environment, similar to current conditions. All sediment cores show a gradual increase in MS and density from the top of the core to the first minor change in lithology (0.25-0.75 m above the bottom of CU-2). Because the MS and density increases occur at all core site across the basin and are not linked to any visible or compositional change in lithology, they are interpreted to be due to compaction of the sediments with increasing depth below the lake-floor.

All cores show a minor change in lithology in CU-2 from massive mud with a high water content to lower water content mud containing faint silt and clay laminae. This change correlates with the top of the zone of high-amplitude, noisy acoustic reflections zone in SU-E. The presence of silt and clay laminae indicates that the energy state of the depositional environment in this interval is slightly higher than in the overlying section. Large peaks in the MS and density at the bottom of CU-2 mark a major change in lithology from massive mud-dominated sediment to massive to laminated clay (PALSS-1A, -3A, and -4A) or laminated clayey silt (PALSS-2A and -2B). The thickness of CU-2 varies depending on the location of the core site and is thickest at core site PALSS-4A (southwest part of Big Traverse Bay) at 3.57 m thick.

The lithology in the upper part of CU-1 varies spatially across the basin. Cores closer to the margins of the modern-day lake (PALSS-1A, 3A, and 4A; Figure 15) contain gray clay with trace to moderate amounts of silt or medium-grained sand (Figures 32, 55, and 60). The thickness of CU-1 at these locations is small (< 0.5 m), though seismic imaging indicates ~8 m of lacustrine sediment lies below (Figures 56 and 61). It is interpreted that the top of CU-1 at these sites was subaerially exposed for an extended period of time, allowing for the upper 0.5 m of

sediment to partially dry and erode. Coarser-grained material (i.e., sand) was likely intermixed into the finer-grained clay and silt by eolian deposition or the reworking of material as the lake level transgressed southward forming an unconformity between CU-1 and CU-2 (i.e. UNCF-3).

The central-most cores (PALSS-2A and -2B) contain laminated clay and silt with distinct peat layers ~1-3 cm thick at the top of the CU-1 (Figures 43 and 52). Both cores extend well into CU-1 (3.5 m and 3.8 m, respectively) and show no evidence of desiccation in the top 0.50 m of CU-1, suggesting that the lake never completely dried up at this location. Instead, when other parts of the basin were subaerially exposed, this region was likely colonized by vegetation (peat at top of unit) protecting the underlying sediment from wind erosion and desiccation.

The majority of CU-1 in cores PALSS-2A and -2B is composed of parallel to sub-parallel, laminated clay and silt ~1-9 mm thick distinguished by dark and light shaded color tones. They are rhythmic and commonly occur in sets but are not interpreted as varves because (1) they are disrupted frequently by interbedded peat, sand, and layers of clay, and (2) no reliable chronology exists to support annual deposition. The depositional environment of the laminated sections is interpreted to be lacustrine, when the lake level was deep enough to allow fine-grained material to settle on the lake floor without being disturbed. Sets of laminations represent variations in energy state at the time of deposition, perhaps due to seasonal variations in the amount of ice-cover. Accordingly, the coarser, light-colored silts were deposited under higher-energy ice-free conditions, and dark-colored clays were deposited under lower-energy frozen conditions.

Multiple layers of fine-to coarse-grained sand (2-14 cm thick) occur in cores PALSS-2A and -2B, forming sharp boundaries with the laminated sediment. The sharp juxtaposition presumably indicates events where material was washed into the basin under dynamic conditions and rapidly deposited. However, these layers do not correlate well between PALSS-2A and PALSS-2B despite the cores being taken only ~1 m apart. At first, these discrepancies were thought to be artifacts related to material (mostly sand) filling in the core hole between drives. To adjust for this, if unconsolidated sand was located at the top of the drives, the sand layers were

removed from the lithology, MS, and density datasets. After removal, the remaining sand layers were located in the middle of the core (or were consolidated sand at the top of the core) but correlations between the two core sites were still not obvious. Casing was used to prevent oblique penetration of the corer, and laminations are parallel and horizontal in both cores.

When compared to the seismic image from this location (Figure 44), lithologic changes in the cores correlate poorly with the identified horizons (H5-H7) in the lower part of the section. The interpretation that UNCF-2 (H6) represents a relative drop in lake level across the basin suggests a major change in depositional environment, which would manifest itself in the lithology of the lake sediments. However, evidence of such a change in PALSS-2A and -2B is scarce (Figures 4.2.3 and 4.2.4), indicating that either (1) the depositional environment did not significantly change at this location during the formation of UNCF-2 or (2) the sediment cores did not actually reach the level of UNCF-2 (H6). The latter interpretation is preferred for the following reasons: (1) the high amplitude of the reflection associated with UNCF-2 suggests that it should be recognizable in the lithology, (2) poor correlation of sand layer thickness and depth below H5 (~4.3 m) between PALSS-2A and -2B suggests that the sand layers may be out of place in one of the cores and (3) three radiocarbon dates from *below* UNCF-2 are the same age or *younger* than all the other radiocarbon dates from CU-1 including two dates from ~2 m *above* UNCF-2 (see sections 4.2.2 and 4.2.3). Because horizons H1-H5 *do* correlate well with the lithologic changes in PALSS 2A and -2B, the sediment is interpreted as being in place from the top of the core to ~4.3 m beneath the lake floor. Below ~4.3 m, however, infill of material into one or both of the core hole appears to have resulted in the collection of younger out-of-place sediment in several lower drives.

In summary, CU-2 is composed of massive mud that becomes more compacted with depth below the lake floor. It correlates well amongst all cores, indicating that the depositional environment was similar across the basin. The bottom of CU-2 is marked by a distinct change in the lithology. The top of CU-1 shows evidence of desiccation close to the margins of the basin, and peat in the middle of the basin, indicating that the depositional environment in LOTW was

laterally variable at the time. The outer regions likely lay subaerially exposed while the middle of the basin was vegetated and may have held separate, shallow water body for an extended period of time before eventually becoming truncated by a transgressing shoreline of a larger body of water that inundated the southern basin.

The stratigraphy of CU-1 appears intact above a depth of ~4.3 m. Below that depth, inconsistencies in the core-to-core and core-to-seismic correlations suggest that the material in one or both cores PALLS-2A and -2B is out of place. The majority of the intact CU-1 sediment is composed of laminated silt and clay (1-9 mm thick) that were deposited when the lake level was relatively low. Multiple peat layers suggest that fluctuations in lake level large enough to shift the environment from aquatic to terrestrial were common. Several sand layers and intervals of desiccated clay intermixed with sand (PALSS-2B) suggest that previously deposited material was frequently washed into the basin and rapidly deposited.

5.2.2 Interpretation of Radiocarbon Ages

Eight radiocarbon dates were collected from terrestrial macro fossils (Table 9) from sediment cores PALSS-2A, -2B, and -4A. Some of the dates are difficult to interpret because they do not compare well with their stratigraphic position (e.g. Figures 43 and 52). When the core depth of the dated material is plotted against the age (Figure 64), three sections are identified, which are separated by UNCF-3 and UNCF-2. The top section (CU-2/SU-E) contains one dated wood macrofossil (1,750 cal BP) that is much younger (at least 6,000 years) than all other dates. The middle section (CU-1/SU-D) contains two dated peat layers (7,750 and 8,350 cal BP) directly below UNCF-3 and two ages (8,800 and 11,040 cal BP) about 1.5 m below UNCF-3, one from seed material and the other from a wood macrofossil. The bottom section (SU-C?) contains three dated wood macrofossils (7,890; 7,890; and 7,900 cal BP), two of which were collected in laminated sediment. All three latter dates are in distinguishable within errors, though their depths span 0.65 m.

Clearly, some of the ages do not accurately reflect the time of deposition of the sediment, apparently either too old or too young. Older carbon material can be introduced into lacustrine sediments by the erosion and reworking of previously

deposited materials. Additionally, wood macrofossils are often older than the enclosing sediment due to the elapsed time between when the plant/tree was alive onshore and when the material was deposited in the lake basin. Carbon material younger than the enclosing sediment is much harder to explain. Contamination due to geochemical processes while buried, such as methanogensis, can alter the $^{14}C/^{12}C$ ratio, and produce dates that are too young. However, this is much more common with bulk sediment samples than with macrofossils because of the resistant nature of the material of macrofossils against degradation. Older carbon may become contaminated with younger carbon during the sampling and preparation processes, lowering the mean age of the material. However, sampling contamination rarely occurs with macrofossils (especially wood) because of the abundance of material. Also very large amounts of excess radiocarbon are necessary to significantly change the age of samples in the age ranges of those in this study.

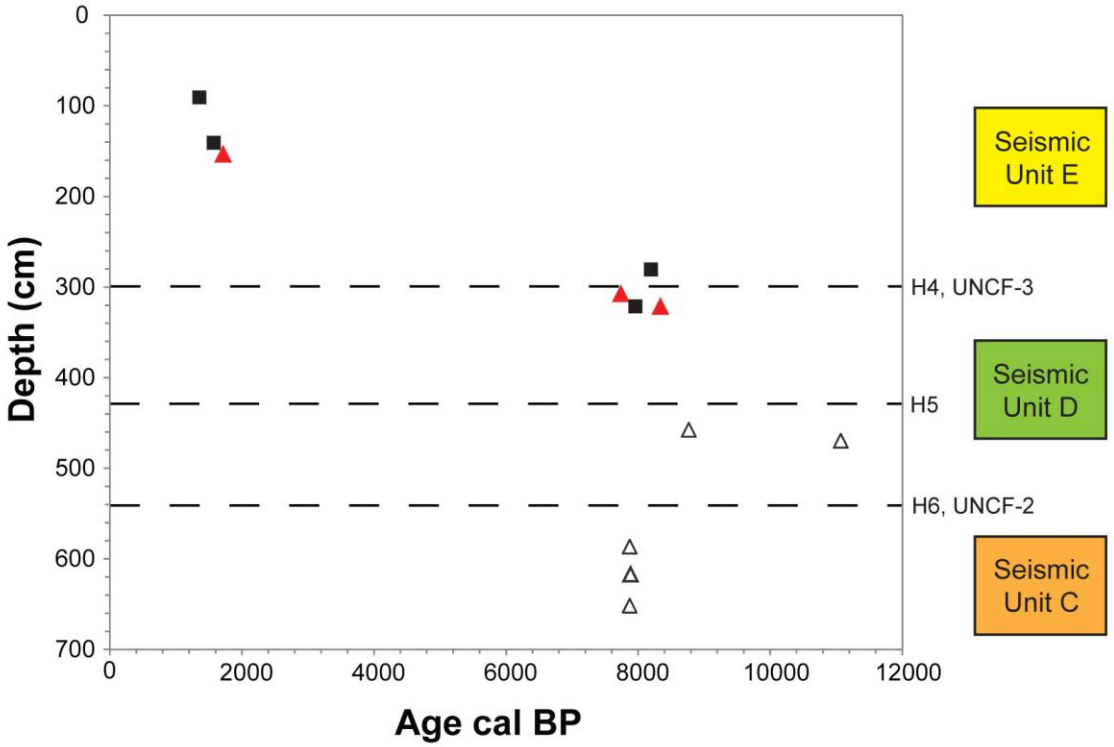

Figure 64 Radiocarbon ages from the southern basin. Eight radiocarbon ages (cal yr BP) from this thesis (triangles) and four from Mellors, 2010 (black squares) are shown in relation to the depth (cm) to prominent reflections (dashed lines) at core site PALSS-2A/2B (Note that UNCF-3 at site MOMOS-1A occurs at a depth of 280 cm). Corresponding interpreted seismic units (color coded) are labeled on the right. Selected radiocarbon ages (red triangles) agree well with ages from MOMOS-1A. Ages below 430 cm (empty triangles) are likely in out-of-place younger materials and are discounted here.

To help evaluate the radiocarbon ages in this study, analogous ages from sediment core MOMOS-1A (Mellors, 2010) located ~5 km NE of Long Point (Figure 11) were included in the depth vs age chart (Figure 64). All MOMOS-1A ages are consistent with PALSS-2A and -2B ages both above and below UNCF-3. Above UNCF-3, the ages from MOMOS-1A (1,345 and 1,564 cal BP) are in sequence with the single age from PALSS-4A and together they are interpreted to be chronologically accurate. The two ages from MOMOS-1A directly below UNCF-3 (8,186 and 7,961 cal BP) are between the age range of the dated peat layers (7,750 and 8,350 cal BP), in PALSS-2A and -2B, but produce a minor reversal.

The four ages from just below UNCF-3 yield an average age of 8,060 cal BP ((8,186+7,961+7,750+8,350)/4=8,061.75 cal BP) for the uppermost part of CU-1. The fact that the ages below 430 cm appear to be much too young is consistent with the observation (see section 5.3.1) that all material below 4.3 m is probably out of place. The remaining ages are in chronological sequence (Figure 64, red triangles), and are consistent with those from MOMOS-1A. Using the two dated peat layers below UNCF-3, the sedimentation rate for the top of CU-1 was calculated at about 0.2 mm $year^{-1}$ ((322-308) cm/(8,350-7,750)yrs=0.23 mm $year^{-1}$), although this value includes much uncertainty.

The sedimentation rate for CU-2 was calculated at about 0.9 mm $year^{-1}$ ((154-0)cm/(1750-0)yrs=0.88 mm $year^{-1}$) using zero age of the sediment surface and the wood macrofossil from PALSS-4A. This sedimentation rate compares well to rates proposed by Mellors (2010) and Molot et al. (1987) of 0.9 mm $year^{-1}$ and 0.7 mm $year^{-1}$, respectively. Extrapolating over the entire thickness of CU-2 (~3 m) yields a depositional period of about 3,300 years (300cm/0.9 mm $year^{-1}$=3,333 years). Sedimentation rates likely varied within the unit, such as in the faintly laminated silt within the mud-dominated matrix, where the lithologic variations indicate different depositional environments than those of the overlying massive mud. However, these rates likely did not vary much given the relatively uniform lithology of CU-2. Therefore, the hiatus represented by UNCF-3 is estimated to be about 4,800 years, from 8,060 to about 3,300 years ago.

Chapter 6: Discussion

6.1 Late-Quaternary History

Chapters 4 and 5 described and interpreted all seismic units, unconformities, ispopach maps, sediment core lithologies, and radiocarbon dates. The purpose of this chapter is to integrate those interpretations into the regional geologic history of LOTW.

6.1.1 Deglaciation

The upper boundary of SU-A (acoustic basement) has a smooth configuration near the margins of the basin and is interpreted as glacially eroded bedrock. LOTW's location within the Canadian Shield strongly suggests that this bedrock is Precambrian in age. In the middle of the basin, where the upper boundary of SU-A is irregular, the underlying material is interpreted as glacial diamicton deposited over Precambrian bedrock or older glacial deposits. The irregular topography and limited penetration of SU-A in the middle of the basin suggests that the material is unconsolidated and stratified in places. These are the characteristics of glacial deposits, such as a melt-out till, and, where stratified, glacio-lacustrine or glacio-fluvial deposits.

The retreat rate of the LIS across LOTW is difficult to constrain due to the lack of radiocarbon ages in the region. If deglaciation of the southern basin of LOTW occurred while Lake Agassiz stood at the Herman level, as Johnston (1946) recognized for the Rainy River basin, then deglaciation took place at about 14.1 ka cal BP. However, this requires the ice-margin to have retreated from Big Stone Moraine to LOTW in as little as 100 years. The age of the Big Stone Moraine must either be several hundred years older than the assigned age of 14.2-13.9 ka cal BP by Lepper (2007), or deglaciation of LOTW occurred several hundred years after the formation of the Herman shoreline. The level of Lake Agassiz when LOTW was deglaciated may never be known because the elevation of the LOTW basin is too low to preserve strandlines. By 12.9 ka cal BP, the southern ice-margin had retreated far enough north of the international border for lake sediment to accumulate in

northwestern Ontario (Bjorck, 1985). Therefore, the retreat of the ice-margin over LOTW took at least a few hundred years and supports the evidence for glacial material in the middle of the LOTW basin. Lake Agassiz, impounded in front of the downslope retreating ice, would have followed the southern margin of the LIS and inundated the deglaciated LOTW basin. The glacio-lacustrine environment, partly occupied by ice and partly by Lake Agassiz, offers an explanation for the localized stratified deposits at the top of SU-A. The lack of diamictons at the higher elevation margins of the basin indicates that either diamicton deposition did not occur or such deposits were later eroded. Further speculation is difficult with the resolution of 3100P CHIRP system.

6.1.2 Post-Glacial (Lake Agassiz Occupation)

The uniform thickness and draped configuration of SU-B indicates a period of high lake level followed the retreat of the ice-margin north of LOTW. The lack of depositional focusing despite being deposited in a clearly defined basin suggests that the lake level was higher than the margins of the southern basin and likely extended far beyond the boundary of present-day LOTW. According to Figures 25 and 26, the height of the lake surface would have had to be at least 30 m above the paleo lake floor to spill over the current margins of the basin, but it was probably higher. The largely reflection-free character of SU-B suggests the lithology is nearly massive, and that the ice margin had retreated far enough north of LOTW so that coarser-grained materials, typically deposited in ice-proximal environments, were absent. None of the sediment cores reached depths great enough to sample SU-B (including MOMOS cores), so the lithology and age of the sediments are unknown.

However, seismic images from Lake Winnipeg display a similar uniformly draped, predominately reflection-free unit directly above the acoustic basement (Figure 10). Sediment cores from this unit in Lake Winnipeg contain varved lacustrine sediment (Todd et al., 1998) that was deposited while Lake Agassiz occupied the Lake Winnipeg basin. Varved lacustrine clays are also observed at the bottom of sediment cores from West Hawk Lake, roughly 65 km NE of the southern basin of LOTW, (Teller et al., 2008) and from the Rainy River basin (Bajc et al.,

2000), both of which were interpreted to have been deposited during the Lockhart phase of Lake Agassiz, when lake levels were relatively high. The extensive Brenna Formation, which stretches from the Red River Valley into northwestern Ontario and southern Manitoba, indicates that relatively deep water covered much of the Agassiz basin, including LOTW, during the Lockhart phase. Such an extensive body of water could explain the uniformly draped configuration of SU-B at LOTW and the lower seismic unit at Lake Winnipeg.

At least six meters of sediment were deposited during the formation of SU-B (Figure 23) and prior to the formation of UNCF-1. Using the average thickness of Lockhart varves (~1 cm) from West Hawk Lake (Teller et al., 2008), a sedimentation rate of 1 cm/year was used to estimate the duration of deposition for SU-B. If SU-B does contain varved Lockhart phase sediment, then at least 600 years is required for the deposition of SU-B between the retreat of the LIS from the basin and the formation of UNCF-1.

The relationship between UNCF-1 and SU-B varies laterally across the basin. As much as four meters of sediment appear to have been eroded from the top of SU-B at the margins of the basin (Figures 16 and 17(3)). In the middle of the basin, however, UNCF-1 lies conformably above SU-B (Figure 17(2)). Between the deposition of SU-B and the formation of UNCF-1, the wave base migrated inward, from outside the margins of the southern basin, to the zone where UNCF-1 transitions from erosional to conformable (Figure 62). Such a large migration in shoreline position requires a relatively large drop in lake level.

A relatively large drop in lake level between the deposition of the Brenna Formation (Lockhart phase) and deposition of the Sherack Formation (Emerson phase) is indicated by subaerial deposits in the Red River Valley, Lake Manitoba (Teller and Thorleifson, 1983; Thorleifson, 1996), and Rainy River basin (Bajc et al., 2000). This same drop in lake level, which initiated the Moorhead phase of Lake Agassiz, is likely represented by UNCF-1 at LOTW. The seismic reflection identified as UNCF-1 is laterally continuous and can be identified by its relatively high-amplitude reflection strength across the entire basin (Figures 16 and 18). The amplitude strength and continuity of UNCF-1 reflects a basin-wide change in the

physical properties of the sediment that is consistent with a relatively large fluctuation in lake level. Regions where UNCF-1 lies conformably above SU-B (the horizon at these locations is not clearly unconformable but is still referred to as UNCF-1 in the text and figures) indicate that subaerial conditions did not exist across parts of the southern basin of LOTW during the Moorhead low phase, as they did in the nearby higher-elevation Rainy River basin. Continuous deposition in the middle of the basin may indicate that a connection between Lake Agassiz and the southern basin remained during the Moorhead phase, perhaps through a channel in the NW Angle as suggested by Mellors (2010), although no obvious channels were observed in the seismic images.

The duration of the low-stand Moorhead phase is still unknown. Thorleifson (1996) and others have suggested ~1,000 years, whereas Lepper et al., (2013) proposed a period of over 2,000 years (Figure 5). However long the Moorhead phase lasted, it ended when Lake Agassiz transgressed southward, driven by isostatic rebound of the outlet, and re-flooded the southern Agassiz basin. Lake Agassiz eventually reached and reoccupied the southern outlet, marking the beginning of the Emerson phase and the development of the extensive Campbell shoreline.

The sequence stratigraphy of SU-C documents a similar series of Moorhead events occurred at LOTW. The lower part of SU-C contains ponded reflections that onlap onto UNCF-1 upward from the topographic lows of the basin, indicating that sediment deposition occurred at these locations first (Figures 17(8) and 19). Above the ponded reflections, the horizons are laterally continuous, indicating that, after the localized topographic lows were filled, deposition occurred regionally across the basin. The ponded reflections represent sediment focusing that occurred in a shallow lacustrine environment. The lake likely remained shallow for some time, allowing the topographic lows to fill (mid to late-Moorhead phase) before a rise in lake level resulted in a broader deep-water zone, and laterally continuous deposition began (late-Moorhead to early-Emerson). As the wave base migrated outwards from position 1 in Figure 62, the high-energy wave base once again

eroded underlying sediments (SU-B) leaving behind an unconformity (UNCF-1) buried beneath lacustrine sediment (onlapping reflections).

There are three notable high-amplitude reflections that separate a sequence of reflection-free zones in the middle part of SU-C (Figure 17(8)). In seismic lines that strike NE-SW the reflection-free zones become progressively thicker to the southwest above each high-amplitude reflection, moving up section (Figure 17(8)). Differential isostatic rebound between the NE and SW sides of the LOTW basin may partially account for the southward thickening sediments, although the diameter of the basin is only a few tens of kilometers and the amount of differential uplift between the two margins of the basin would have been only a few meters (Figure 6 and Table 1). Alternatively, sediment deposition may have progressively increased to the south as Lake Agassiz transgressed southward and lake level rose.

The "wipe-out" features observed in the upper part of SU-C near the middle of the basin (Figure 17(8)) are unusual. They are not related to gas because they do not obscure underlying reflections. They have the appearance of relatively uniform channel-fill deposits, yet they do not extend outwards from the middle of the basin as fluvial networks typically do. Furthermore, if they were related to channels, their existence would imply that the basin was subaerially exposed prior to the formation of UNCF-2. Although SU-C contains three prominent high-amplitude internal reflections, it is unlikely that any of them formed under subaerial conditions. They do not truncate underlying reflections nor do they act as sequence boundaries between seismic units. Instead their high amplitude indicate changes in the material deposited that are either related to fluctuations in the lake-level or sediment input into the lake. Without additional information from sediment cores, it is difficult to determine the genesis of the wipe-outs features.

The complex arrangement of reflections within SU-C suggests a dynamic environment existed at the time of deposition. The lithology of Lake Agassiz sediments deposited outside the LOTW basin during the late Moorhead and the Emerson phase record a similar environment. Lacustrine sediments composed of laminated silts and clays and comparable in age to the Sherack Formation lie above lacustrine and fluvial sands and organic-rich sediment in northwestern Ontario

(Johnston, 1946). The presence of SU-C suggests Lake Agassiz also occupied LOTW at this time, and its internal reflections may be equivalent to the Sherack Formation.

SU-C is separated from overlying SU-D by UNCF-2. Internal reflections within SU-C and SU-B are truncated by UNCF-2 near the higher elevation margins of the basin, often causing SU-C to pinch out (Figures 16, 17(3), 18, and 19). The eroded reflections indicate that the high-energy littoral zone of the lake shifted towards the middle of the basin as the result of a drop in lake level. UNCF-2 lies conformably upon SU-C in the middle of the basin, indicating deposition remained continuous in this area. The estimated wave base position (Figure 62) suggests that the surface area of the lake was larger after this drop in lake level compared to that of the previous lowstand that led to the formation of UNCF-1.

Although the exact timing of the formation of UNCF-2 is unknown, it can be constrained by dated events within the broader Agassiz basin. Following the abandonment of the Campbell shoreline at about 10.5 ka cal BP, Lake Agassiz briefly occupied multiple lower-elevation shorelines until it eventually abandoned the southern outlet altogether shortly after 10.2 ka cal BP, ending the Emerson phase. By this time the eastern outlet was open, allowing for drainage through the Great Lakes and into the Atlantic Ocean.

Paleotopographic reconstructions from Teller and Yang (2005) indicate that Lake Agassiz had left LOTW ~10 ka cal BP (Figure 7) leaving behind a subaerially exposed southern basin and an isolated LOTW in the northern basin. However, these images only take into consideration the amount of isostatic uplift and do not account for hydrological conditions of the lake or possible channelways between the sub-basins of LOTW and Lake Agassiz. Ostracodes from sediment core MOMOS-WOO06-4A (Figure 9) in the NW Angle basin indicate that Lake Agassiz occupied the NW Angle until as late as 9.0 ka cal BP (Mellors, 2010). In the southern basin of LOTW, the conformable relationship between SU-C and SU-D indicates that continuous deposition occurred in the middle of the basin. However, the internal reflection character and configuration of the two seismic units are markedly different (Figures 16 and 18) indicating a shift in the depositional environment occurred between the deposition of the two seismic units.

The oldest ages from the southern basin of LOTW are 8.2 and 8.35 ka cal BP from sediment cores MOMOS-WOO06-1A and PALSS-WOO12-2B, respectively. Both ages are from material collected below an unconformity at depths that correspond to the top of SU-D (Figures 43, 44, and 52). These ages correspond well to the final drainage of Lake Agassiz into Hudson Bay, more than 900 km to the north of LOTW. The lower core unit (CU-1) from cores described in this thesis occurs at depths that correlate nicely to SU-D across the southern basin of LOTW (Figures 32, 33, 43, 44, 52, 60, and 61). The lithology of CU-1 varies at each core site from gray clay containing silts and sands to laminated silt and clay (see section 5.2.1). The two cores that penetrated deepest into CU-1 (PALSS-WOO12-2A and -2B) are composed of laminated silts and clays interbedded with layers of sand and peat (Figures 43 and 52). Both cores contain high amounts of organic material either in the form of distinct peat layers or as fragmented woody peat scattered within the laminations. Twenty kilometers to the west of core site PALSS-WOO12-2A/2B, Mellors (2010) observed unusually large amounts of charcoal within a sequence of laminated silty clay, also at depths that correspond to SU-D, compared to Lake Agassiz sequences in other cores from the NW Angle and northern basins of LOTW. Abundant organic material is typically not found in Lake Agassiz sediments because of the lack of colonized vegetation on the recently deglaciated landscape and because the dominant input into the lake was glacial meltwater.

Together these independent data strongly suggest that Lake Agassiz did not occupy, nor was it connected to, the southern basin of LOTW, from sometime prior to 8.2-8.35 ka cal BP onwards. Instead, Lake Agassiz left the southern basin earlier, before the deposition of SU-D, following a relative drop in lake level which resulted in the erosional truncations observed as UNCF-2. This may have been an abrupt event such as the abandonment of the Campbell shoreline or other shoreline, or it may have been gradual as Lake Agassiz regressed northward following the abandonment of the southern outlet. Lake Agassiz may have also remained connected to the southern basin via the NW Angle until as late as 9.0 ka cal BP, though as mentioned above, no evidence of relic channels were observed in our seismic images.

6.1.3 Transition

After Lake Agassiz withdrew from the southern basin of LOTW, the depositional environment would have changed significantly. Sediment and water supply into the basin was no longer controlled by regional events across the Agassiz basin. Instead, the water body that occupied the LOTW basin would have become much more sensitive to localized events within the LOTW basin and surrounding watershed as well as to changes in climate. Outside of the LOTW basin, the landscape was also rapidly changing. As Lake Agassiz regressed further north, thousands of remnant lakes remained in the topographic lowlands and newly exposed lacustrine sediments were primed for erosion.

At the bottom of SU-D, low-angle reflections onlap onto UNCF-2 near the margins of the southern basin (Figure 19) suggesting a rise in lake-level or rapid deposition. Assuming that isolation from Lake Agassiz did not occur before the abandonment of the Campbell shoreline at 10.5 ka cal BP, the amount of differential isostatic rebound experienced on the LOTW basin between the southern basin and the Winnipeg River was about 50 m (Figure 6 and Table 1). By 9.0 ka cal BP, when Lake Agassiz left the NW Angle basin, the differential with the present would have decayed to about 30 m. By 8.0 ka cal BP, well after Lake Agassiz drained into Hudson Bay, the differential was still about 20 m. Reorganization of the surrounding watershed, driven by the differentially rebounding landscape, probably allowed for remnant water bodies to become interconnected and drain into LOTW. The result was a relative rise in lake level that caused the wave base in the southern basin of LOTW to transgress outwards from position 2 in Figure 62. It is this transgression that is largely responsible for the erosional truncations observed as UNCF-2.

Reflections within SU-D are strongly stratified parallel and are generally similar in amplitude, suggesting a succession of laminated sediments composed of similar properties. This interpretation matches the lithology of CU-1 from sediment cores PALSS-WOO12-2A and -2B located in the middle of the basin (sections 4.2.2 and 4.2.3). The lithology of these cores suggests that lake levels were relatively low during this depositional period with occasional fluctuations large enough to briefly shift the depositional environment from lacustrine to wetland. Medium to coarse-

grained sand layers within CU-1 can be explained by short high-energy events in which material was washed in and deposited in the basin. These layers are not always apparent in the seismic images and their composition, thickness, and correlation between cores indicate they vary on a meter scale (Figures 43, 44, 52), if CU-1 in cores 2A and 2B are intact. They may be related to stream capture events in the watershed that accelerated erosion and allowed for rapid, variable deposition within the southern basin of LOTW.

All cores taken from the southern basin of LOTW contain a major change in lithology that occurs at the same depths as UNCF-3 in the seismic images (Figures 33, 34, 43, 44, 52, 55 60, and 61). Beneath the unconformity, the lithologies of the sediments are spatially variable across the basin. At core sites PALSS-WOO12-2A, -2B, and MOMOS-WOO06-1A, layers of peat 1-3 cm thick were deposited at the unconformity above laminations of silt and clay. The peat is an indicator that vegetation had colonized these locations and that the depositional environment shifted from lacustrine to wetland prior to the formation of the unconformity at around 7.75 ka cal BP. Core sites PALSS-WOO12-1A, -3A, and -4A, however, contain gray clay with interbedded silt and sand up to 0.5 m in thickness in CU-1. There is no evidence of any organic material within the unit in these cores. The sediment depths for CU-1 correspond to the upper part of SU-D, which is interpreted to have been deposited after Lake Agassiz withdrew from the basin.

Sediments from numerous lakes in the Upper Midwest indicate a prolonged dry climate around this time. These lakes and the timing of this dry interval include West Hawk Lake between 7.1-4.5 ka cal BP (Teller et al., 2008); Wampum, Manitoba between 7.1-4.5 ka cal BP (Teller et al., 2000); Lake Winnipeg between 8.2-4.3 ka cal BP (Lewis et al., 2001); ELA Lake 239 between 8.9-4.4 ka cal BP (Laird and Cumming, 2008); and Elk Lake, Minnesota between 8.0-4.0 ka cal BP (Bradbury et al., 1993). A major unconformity, identified from CHIRP seismic data formed in Elk Lake at this time (Colman et al., 2012). The majority of the southern basin of LOTW probably dried completely, with the exception of a few isolated lower elevation locations, shortly after 7.75 ka cal BP. UNCF-3, the youngest major unconformity in

the section, is correlated with low lake levels that are inferred to have occurred during this dry climate interval.

6.1.4 Lake of the Woods Occupation

No radiocarbon ages were collected directly above UNCF-3 so it is difficult to determine when deposition resumed in the southern basin. In the NW Angle basin, the age of sediment overlying paleosols (from cores WOO06-5A and WOO06-6A) is estimated to be between 4.9 and 5.5 ka cal BP (Figure 9). Mellors (2010) proposed that deposition resumed as LOTW transgressed southward from the northern basin due to differential isostatic rebound. One radiocarbon age was collected ~2 m above UNCF-3 in the southern basin from within CU-2 (Figure 60). This age of 1.75 ka cal BP agrees well with the two ages (1.34 and 1.57 ka cal BP) collected at similar depths from WOO06-1A (Figure 64). Using the sedimentation rate of 0.9 mm $year^{-1}$ (section 5.2.2), deposition is estimated to have resumed at about 3.3 ka cal BP in the southern basin.

The depositional hiatus of ~4,800 years ended when LOTW transgressed southward from the northern basin, through the NW Angle basin, and across the southern basin due to differential isostatic rebound. Low-angle reflections onlap onto UNCF-3 over several tens of kilometers towards the southern part of the basin (Figure 16), indicating a rise in lake level as transgression occurred to the south. SU-E shows distinct lateral thickening to the south of the basin (Figures 16 and 24) despite the lower boundary being virtually planar. This is consistent with a differentially uplifting basin with a northern outlet (Figure 63C).

UNCF-3 represents a hiatus in deposition between a climate-driven drop in lake level during the mid-Holocene and the rebound-driven inundation of the southern basin as LOTW transgressed southward several thousand years later. The planar surface of UNCF-3 is largely attributed to the erosional wave base of the transgressing shoreline. Similar erosional surfaces are observed in Lake Winnipeg as the result of Lake Winnipeg transgressing southward due to differential isotatic rebound (Figure 10). All underlying lacustrine sediments are truncated to some

degree by UNCF-3, but they are more severely truncated in the northern part of the basin where the rate of rebound was greater.

The lithology of CU-2 (equivalent to SU-D) is similar at all core sites in the southern basin and reflects the modern depositional environment of LOTW, in which all sub-basins were apparently hydrologically connected and the main outlet was through the Winnipeg River. The lower third of CU-2 consists of faintly laminated silt and clay that corresponds to a chaotic interval in the seismic profiles and suggests a moderately high-energy depositional environment as the lake level was rising. The upper two-thirds of CU-2 consists of homogenous mud with a high water content, which likely was deposited as the lake level neared its modern-day position 9-10 m above the lake floor (Figure 27).

6.2 Modern Depositional Basins of Lake of the Woods

The thickness of SU-E (Figure 26) and its lithological equivalent CU-2 were used to delineate the modern depositional basins of LOTW. Sediment accumulation was greatest (~4 m) in a band that wraps around Long Point in the southern part of Big Traverse Bay. This pattern is different from that of the underlying seismic units, where sediment accumulation is typically greatest in the center of Big Traverse Bay, and it is the result of differential isostatic rebound experienced on the basin with the primary outlet located to the north. Average sedimentation rates in the southern basin (0.9 mm $year^{-1}$ for the last ~1,800 years) are roughly twice as high as those in the NW Angle basin (0.1-0.5 mm $year^{-1}$) and nine times greater than those in the northern basin (Mellors, 2010). This likely reflects a greater sediment supply from shoreline erosion along the southern shore of LOTW. Sediment was eroded by the encroaching shoreline and transported offshore where it was deposited in the deeper, lower-energy environment.

Chapter 7: Conclusions

The first high-resolution seismic-reflection (CHIRP) data collected from LOTW, a remnant of glacial Lake Agassiz, display a complex arrangement of glacial and lacustrine sediments. Five unique seismic units (SU A-E) were identified and interpreted based on their reflection character, reflection configuration, and external geometry. Three erosional unconformities (UNCF 1-3) underlie the upper three seismic units and indicate that relatively large fluctuations in lake level occurred at LOTW. Sediment cores from the southern basin sample the uppermost of these unconformities, at the depth of UNCF-3, which separates modern lake sediments from mid to late-Holocene sediments. Together seismic and core data were used to reconstruct the late-Quaternary geologic history of LOTW.

Glacial diamicton was deposited on top of Precambrian bedrock as the LIS retreated north of LOTW. The deposits lie in clumps in the middle of the southern basin but are absent between the southern and NW Angle basins and at the margins of the southern basin where the acoustic basement is interpreted as bedrock. Above the acoustic basement, as much as 28 m of lacustrine sediment were observed in the southern basin in areas not obscured by biogenic gas.

Following deglaciation, Lake Agassiz occupied the southern basin of LOTW during the deposition of SU-B and SU-C. The lowermost lacustrine unit (SU-B) lies uniformly draped above the acoustic basement, indicating that the lake level was relatively high when it was deposited. At least six meters of sediment were deposited before a drop in lake level shifted wave base inwards, from outside the LOTW basin, and eroded as much as four meters of sediment at the margins of the basin, forming UNCF-1. The drop in lake level is likely contemporaneous with the onset of the Moorhead phase of Lake Agassiz, which has been identified from subaerial deposits in the Red River Valley, Lake Manitoba, and Rainy River basin. Deposition was apparently continuous in the middle of the basin, although no conclusive channels were observed between the southern basin and the NW Angle basin that would indicate Lake Agassiz was still connected. Additional seismic

surveying of this region is necessary to determine if there was a Lake Agassiz-LOTW connection through the NW Angle.

A subsequent rise in lake level at LOTW is indicated by onlapping internal reflections within SU-C onto UNCF-1. Reflections are ponded in the topographic lows of the basin and onlap outwards from the middle of the basin. The diverse nature of internal reflections within SU-C indicates that the depositional environment was relatively dynamic. SU-C is correlated with Lake Agassiz sediments deposited during the late-Moorhead and Emerson phase, which also record a dynamic environment and are likely comparable in age to the sediments imaged in SU-C.

Sometime after the abandonment of the Campbell shoreline, at about 10.5 ka cal BP (Mann et al., 1997; Lepper et al., 2013), Lake Agassiz withdrew from the LOTW basin. As Lake Agassiz regressed north, the lake level at LOTW lowered, and the wave base consequently shifted towards the middle of the southern basin. Internal reflections at the top of SU-C are truncated by a second unconformity (UNCF-2) near the margins of the basin, but the horizon is concordant with the same reflections in the middle of the basin, indicating that a water body remained in the southern basin following lake level drawdown. Reflections in the lower part of SU-D onlap onto UNCF-2 only near the margins of the basin, suggesting that the water body occupied much of the middle of the southern basin before the lake began to rise again or that rapid deposition occurred during transgression. It is difficult to distinguish between the two mechanisms from the seismic images alone and deeper sediment cores are needed to better understand the paleo-environment at the time.

The reflection character and configuration of SU-D is genetically different from underlying SU-C, indicating that the depositional environment had changed. Sediments collected from depths corresponding to the center of deposition of SU-D (PALSS-2A, 2B, and MOMOS-1A) contain high amounts of organic material and are probably not related to Lake Agassiz. Instead, these sediments (and SU-D) are thought to have been deposited during a transitional phase between isolation of the area from Lake Agassiz and its inundation by LOTW from the northern basin due to differential isostatic rebound.

The lithology of CU-1 (upper part of SU-D) is predominately composed of laminated silts and clays with interbedded peat and sand layers. The presence of several peat layers in sediment cores PALSS-2A and -2B suggest fluctuations in lake level were large and common enough to shift the depositional environment from aquatic to terrestrial or wetland at this location. Reorganization of the surrounding watershed driven by differential isostatic rebound apparently provided enough sediment and water to sustain lacustrine deposition in the southern basin of LOTW after isolation from Lake Agassiz. The uppermost radiocarbon age from a peat layer at the top of CU-1 indicates that deposition of this unit ended shortly after 7.75 ka cal BP.

The lithology at the top of CU-1 varies among the cores sites from gray clay containing silt and medium-grained sand to distinct layers of peat, indicating subaerial conditions existed across the much of the southern basin shortly after 7.75 ka cal BP. The timing correlates well with a prolonged interval of relatively dry climate during the mid-Holocene, which is recorded in other lakes in the upper Midwest.

CU-1 is separated from CU-2 in all cores by an unconformity that correlates with UNCF-3 observed in the seismic images. The unconformity is planar and erosional across the entire survey area, but erosion is greatest in the northern part of the basin. Similar erosional surfaces are observed in Lake Winnipeg as the result of a transgressing wave base driven by differential isostatic rebound. Following a climate-induced drawdown in lake level that left the southern and NW Angle basins of LOTW almost entirely subaerially exposed, differential isostatic rebound caused LOTW to transgress south, from the northern basin, and inundate the NW Angle basin and the southern basin. Deposition in the central southern basin probably resumed around 3.3 ka cal BP, although this age is estimated from sedimentation rates because no radiocarbon ages were obtained directly above UNCF-3.

The lithology of CU-2 is highly uniform across the basin and represents modern sedimentation. Sedimentation rates for CU-2 were calculated at about 0.9 mm $year^{-1}$ and are roughly double the sedimentation rates in the NW Angle basin,

suggesting that erosion of the southern shoreline contributed significantly to deposition in the southern basin.

References

Abbott, M.B., Finney, B.P., Edwards, M.E., and Kelts, K.R., 2000, Lake-level reconstructions and paleohydrology of Birch Lake, Central Alaska, based on seismic reflection profiles and core transects: Quaternary Research, v. 53, p. 154-166.

Aharon, P., 2003, Meltwater flooding events in the Gulf of Mexico revisited: Implications for rapid climate changes during the last deglaciation: Palaeoceanography, v. 18, p. 1079-1093.

Bajc, A.F., Schwert, D.P., Warner, B.G., Williams, N.E., 2000, A reconstruction of Moorhead and Emerson Phase environments along the eastern margin of glacial Lake Agassiz, Rainy River basin, northwestern Ontario: Canadian Journal of Earth Sciences, v. 37, p. 1335-1353.

Barber, D.C., Dyke, A., HillaireuMarcel, C., Jennings, A. E., Andrews, J. T., Kerwin, M. W., Bilodeau, G., McNeely, R., Southon, J., Morehead, M. D., and Gagnon, J. M., 1999, Forcing of the cold event of 8,200 years ago by catastrophic drainage of Laurentide lakes: Nature, v. 400, p. 344-348.

Bradbury, J.P., Dean, W.E., and Anderson, R.Y., 1993, Holocene climatic and limnologic history of the north-central United States as recorded in the varved sediments of Elk Lake, Minnesota: A synthesis. In: Bradbury, J.P. and Dean, W.E. (eds) Elk Lake, Minnesota: Evidence for Rapid Climate Change in the North-Central United States. Geological Society of America Special Paper 276, p. 309-328.

Broecker, W.S., Kennett, J.P., Flower, B.P., Teller, J.T., Trumbore, S., Bonani, G., and Wolf, W., 1989, Routing of meltwater from the Laurentide Ice Sheet during the Younger Dryas cold episode: Nature, v. 341, p. 318-321.

Carlson, A. E., Clark, P. U., Haley, B. A., Klinkhammer, G. P., Simmons, K., Brook, E. J., and Meissner, K. J., 2007, Geochemical proxies of North American freshwater routing during the Younger Dryas: Proceedings of the National Academy of Sciences, v. 104, p. 6556-6561.

Carlson, A. E., and Clark, P. U., 2012, Ice sheet sources of sea level rise and freshwater discharge during the last deglaciation: Reviews of Geophysics, v. 50, no. 4.

Clark, J.A., Hendriks, M., Timmermans, T.J., Struck, C., and Hilverda, K.J., 1994, Glacial isostatic deformation of the Great Lakes region: Geol. Soc. Am. Bull., v. 106, p. 19-20.

Clark, P.U., 1994, Unstable behavior of the Laurentide Ice Sheet over deforming sediment and its implications for climate change: Quaternary Research, v. 41, p. 19-25.

Clark, P.U., Marshall, S.J., Clarke, G.K.C., Hostetler, S.W., Licciardi, J.M., Teller, J.T., 2001, Freshwater Forcing of Abrupt Climate Change during the Last Glaciation: Science, v. 293, no. 5528, p. 283-287.

Clayton, L. and Moran, S.R., 1982, Chronology of late Wisconsinan glaciation in middle North America: Quaternary Science Reviews, v.1, p. 55-82.

Colman, S.M., Forester, R.M., Reynolds, R.L., Sweetkind, D.S. King, J.W., Gangemi, P., Jones, G.A., Keigwin, L.D., and Foster, D.S., 1994, Lake-level history of Lake Michigan for the past 12,000 years—The record from deep lacustrine sediments: Journal of Great Lakes Research, v. 20, p. 73-92.

Colman, S.M., Brown, E.T., and Rush, R.A., 2012, Mid-Holocene drought and lake-level change at Elk Lake, Clearwater County, Minnesota: Evidence from CHIRP seismic-reflection data, The Holocene, v. 23, p. 460-465.

Davies, T.A., Bell, T., Cooper, A.K., Josenhans, H., Polyak, L., Solheim, A., Stoker, M.S., and Stravers, J.A., 1997, Glaciated Continental Margins: An Atlas of Acoustic Images: Chapman and Hall.

Dyke, A.S. and Prest, V.K., 1987, Late Wisconsinan and Holocene history of the Laurentide Ice Sheet: Géographie physique et Quaternaire, v. XLI, n.2, p. 237-263.

Fisher, T.G., 2003, Chronology of glacial Lake Agassiz meltwater routed to the Gulf of Mexico: Quaternary Research, v. 59, p. 271-276.

Fisher, T.G., 2005, Strandline analysis in the southern basin of glacial Lake Agassiz, Minnesota and North and South Dakota, USA: GSA Bulletin, v. 117, 11/12, p. 1481-1496.

Fisher, T.G., 2007, Abandonment chronology of glacial Lake Agassiz's northwestern outlet: Palaeoceanography, Palaeoclimatology, Palaeoecology, v. 246, p. 31-44.

Fisher, T.G., Smith, D.G., and Andrews, J.T., 2002, Preboreal oscillations caused by a glacial Lake Agassiz flood: Quaternary Science Reviews, v.21, p. 873-878.

Fenton, M.M., Moran, S.R., Teller, J.T., and Clayton, L., 1983, Quaternary stratigraphy and history in the southern part of the Lake Agassiz basin: In: Teller, J.T., and Clayton, L., eds., Glacial Lake Agassiz: Geological Association of Canada Special Paper 26, p. 49-74.

Forester, R.M., Delorme, D.D., and Bradbury, J.P., 1987, Mid-Holocene climate in Northern Minnesota: Quaternary Research, v. 28, p. 263-273.

Fulton, R.J. and Prest, V.K., 1987, The Laurentide Ice Sheet and its significance: Géographie physique et Quaternaire, v. XLI, n. 2, p. 181-186.

Gary, J.L., Colman, S.M., Wattrus, N.J., Lewis, C.F.M., 2012, Post-Marquette discharge from Glacial Lake Agassiz into the Superior basin: Journal of Paleolimnology, v. 47, p. 299-311.

Hays, J.D., Imbrie, J., and Shackleton, N.J., 1976, Variations in earth's orbit: Pacemaker of the ice ages: Science, v. 194, p. 1121-1132.

Hughes, T.J., Denton, G.H., and Fastook, J.L., 1985, The Antarctic Ice Sheet: An analogue for Northern Hemisphere paleo-ice sheet?: Models in Geomorphology, p. 25-72.

Johnston, W.A., 1915, Rainy River District, Ontario: Surficial geology and soils: Geological Survey of Canada Memoir, p. 82-95.

Johnston, W.A., 1946, Glacial Lake Agassiz, with special reference to the mode of deformation of the beaches: Geological Survey of Canada Bulletin, v. 7, p. 20.

Laird, K.R. and Cumming, B.F., 2008, Reconstruction of Holocene lake level from diatoms, chrysophytes and organic matter in a drainage lake from the Experimental Lakes Area (northwestern Ontario, Canada): Quaternary Research, v. 69, p. 292-305.

Lepper, K., Fisher, T.G., Hajdas, I., and Lowell, T.V., 2007, Ages for the Big Stone Moraine and the oldest beaches of glacial Lake Agassiz: Implications for deglaciation chronology: Geology, v. 35, no. 7, p. 667-670.

Lepper, K., Gorz, K.L., Fisher, T.G., and Lowell, T.V., 2011, Age determinations for Lake Agassiz shorelines west of Fargo, North Dakota, U.S.A.: Canadian Journal of Earth Sciences, v. 48, p. 1199-1207.

Lepper, K., Buell, A.W., Fisher, T.G., and Lowell, T.V., 2013, A chronology for glacial Lake Agassiz shorelines along Upham's namesake transect: Quaternary Research, v. 80, p. 88-98.

Leverington, D.W. and Teller, J.T., 2003, Paleotopographic reconstructions of the eastern outlets of glacial Lake Agassiz: Canadian Journal of Earth Sciences, V. 40, p. 1259-1278.

Leverington, D.W., Teller, J.T., and Mann, J.D., 2002, A GIS method for reconstruction of late Quaternary landscapes from isobase data and modern topography: Computers and Geoscience, v. 28, p. 631-639.

Lewis, C.F.M., Forbes, D.L., Todd, B.J., Nielsen, E., Thorleifson, L.H., Henderson, P.J., McMartin, I., Anderson, T.W., Betcher, R.N., Buhay, W.M., Burbidge, S.M., Schröder-Adams, C.J., King, J.W., Moran, K., Gibson, C., Jarrett, C.A., Kling, H.J., Lockhart, W.L., Last, W.M., Matile, G.L.D., Risberg, J., Rodrigues, C.G., Telka, A.M., and Vance, R.E., 2001, Uplift-driven expansion delayed by middle Holocene desiccation in Lake Winnipeg, Manitoba, Canada: Geology, v. 29, no. 8, p. 743-746.

Lewis, C., Blasco, S., and Gareau, P., 2005, Glacial Isostatic Adjustment of the Laurentian Great Lakes Basin: Using the Empirical Record of Strandline Deformation for Reconstruction of Early Holocene Paleo-Lakes and Discovery of a Hydrologically Closed Phase: Géographie physique et Quaternaire, v. 59, p. 187–210).

Lowell, T.V., Fisher, T.G., Hajdas, I., Glover, K., Loope, H., and Henry, T., 2009, Radiocarbon deglaciation chronology of the Thunder Bay, Ontario area and implications for ice sheet retreat patterns: Quaternary Science Reviews, v. 28, p. 1597-1607.

LWCB (Lake of the Woods Control Board), 2002, Managing the Water Resources of the Winnipeg River Drainage Basin: LWCB Brochure, p. 7-20.

Manabe, S. and Broccoli, A.J., 1985, The influence of continental ice sheets on the climate of an ice age: Journal of Geophysical Research, v. 90, p. 2167-2190.

Mann, J.D., Rayburn, J.A., and Teller, J.T., 1997, Broken Pipe Lake, Manitoba: A remnant of an Emerson Phase Lake Agassiz lagoon: Geological Society of America, North Central Section Annual Meeting, v. 29, no. 4, p. 57-58.

Mann, M.E. and Jones, P.D., 2003, Global surface temperatures over the past two millennia: Geophysical Research Letters, v. 30, no. 15, p.CLM5-1-5-4.

Mann, M.E., Bradley, R.S., and Hughes, M.K., 1999, Northern Hemisphere Temperatures During the Past Millennium: Inferences, Uncertainties, and Limitations: Geophysical Research Letters, v. 26, no. 6, p. 759-762.

Marcott, S.A., Shakun, J.D., Clark, P.U., and Mix, A.C., 2013, A Reconstruction of Regional and Global Temperature for the Past 11,300 Years: Science, v. 339, p. 1198-1201.

Mellors, T., 2010, Holocene paleohydrology from Lake of the Woods and Shoal Lake cores using ostracodes, thecamoebians and sediment properties (master's thesis submitted, University of Manitoba).

Mickelson, D.M. and Colgan, P.M., 2003, The southern Laurentide Ice Sheet: Development in Quaternary Science, v. 1, p. 1- 16.

Miller G.H.., Alley, R.B., Brigham-Grette, J., Fitzpatrick, J.J., Polyak, L., Serreze, M.C., White, J.W.C., 2010, Arctic Amplification: can the past constrain the future?: Quaternary Science Reviews, v. 29, p. 1779-1790.

Mitchum, R.M., Vail, P.R., and Thompson, S., 1977, Seismic Stratigraphy and Global Changes in Sea Level, Part 2: The Depositional Sequence as a Basic Unit for Stratigraphic Analysis: In: Seismic stratigraphy-applications to hydrocarbon exploration, American Association of Petroleum Geologists, Memoir 26, p. 53-62.

Molot, L.A., Trick, C.G., and Zimmerman, A.P., 1987, A paleolimnological investigation of algal pigments in Lake-of-the-Woods: recent changes in trophic status near Donald Duck and Smith Islands: Report for Ontario Ministry of Environment and Energy, p. 1-40.

Myrbo, A., and Wright, H.E., 2008, The Livingstone/Bolivia SOP: Limnological Research Center Core Facility SOP Series, v. 3.1, p. 1-12.

Risberg, J., Matile, G., and Teller, J.T., 1995, Lake Agassiz water level changes as recorded by sediments and their diatoms in a core from southeastern Manitoba, Canada: Journal of European Network of Scientific and Technical Cooperation for Cultural heritage: PACT, v. 50, p. 85-96.

Ruddiman, W.F. and McIntyre, A., 1981, Oceanic mechanisms for the amplification of the 23,000-year ice-volume cycle: Science, v. 212, p. 617-627.

Sandgren, P. and Snowball, I., 2001, Applications of Mineral Magnetic Techniques to Paleolimnology. In: Last, W.M. and Smol, J.P., 2001, Tracking Environmental Change Using Lake Sediments: Volume 2: Physical and Geochemical Methods: Kluwer Academics Publishers.

Schnurrenberger, D., Russell, J., and Kelts, K., 2003, Classification of lacustrine sediments based on sedimentary components: Journal of Paleolimnology, v. 29, p. 141-154.

Sheriff, R.E., 1977, Limitation on Resolution of Seismic Reflections and Geologic Detail Derivable from Them: In: Seismic Stratigraphy-applications to hydrocarbon exploration, American Association of Petroleum Geologists, Memoir 26, p. 3-14.

Smith, D.G., and Fisher, T.G., 1993, Glacial Lake Agassiz: The northwestern outlet and paleoflood: Geology, v. 21, p. 9-12.

Stoker, M.S., Pheasant, J.B., and Josenhans, H., 1997, Seismic methods and interpretation. In: Davies, T.A., Bell, T., Cooper, A.K., Josenhans, H., Polyak, L.,

Solheim, A., Stoker, M.S., and Stravers, J.A., 1997, Glaciated Continental Margins: An Atlas of Acoustic Images: Chapman and Hall.

Teller, J.T. and Thorleifson, L.H., 1983, The Lake Agassiz—Lake Superior connection: In: Glacial Lake Agassiz, Geol. Ass. Can., v. 26, p. 261-290.

Teller, J.T., 1987, Proglacial lakes and the southern margin of the Laurentide Ice Sheet: Geol. Soc. Am., v. K-3, p. 39-69.

Teller, J.T., 1995, History and drainage of large ice-dammed lakes along the Laurentide Ice Sheet: Quaternary International, v. 28, p. 83-92.

Teller, J.T., Risberg, J., Matile, G., Zoltai, S., 2000, Postglacial history and paleoecology of Wampum, Manitoba, a former lagoon in the Lake Agassiz basin: GSA Bulletin, v. 112, no. 6, p. 943-958.

Teller, J.T., 2001, Formation of large beaches in an area of rapid differential isostatic rebound: the three-outlet control of Lake Agassiz: Quaternary Science Reviews, v. 20, p. 1649-1659.

Teller, J.T., Leverington, D.W., and Mann, J.D., 2002, Freshwater outbursts to the oceans from glacial Lake Agassiz and their role in climate change during the last deglaciation: Quaternary Science Reviews, v. 21, p. 879-887.

Teller, J.T., 2004, Controls, history, outbursts, and impacts of large late-Quaternary proglacial lakes in North America: In: The Quaternary Period in the United States, p. 45-61.

Teller, J.T. and Leverington, D.W., 2004, Glacial Lake Agassiz: A 5000 yr history of change and its relationship to the $\delta^{18}O$ record of Greenland: Geological Society of Am. Bull., v. 116, no. 5, p. 729-742.

Teller, J.T., Boyd, M., Yang, Z., Kor, P.S.G, and Fard, A.M., 2005, Alternative routing of Lake Agassiz overflow during the Younger Dryas : new dates, paleotopography, and a re-evaluation: Quaternary Science Reviews, v. 24, p. 1890-1905.

Teller, J.T., Yang, Z., Boyd, M., Buhay, W.M., McMillan, K., Kling, H.J., and Telka, A.M., 2008, Postglacial sedimentary record and history of West Hawk Lake crater, Manitoba: Journal of Paleolimnology, v. 40, p. 661-688.

Thorleifson, L.H., 1996, Review of Lake Agassiz History: In: Sediment, geomorphology, and history of the central Lake Agassiz Basin, Geol. Ass. Can. Field Trip Guidebook, p. 55-84.

Todd, B.J., Lewis, C.F.M., Nielsen, E., Thorleifson, L.H., Bezys, R.K., and Weber, W., 1997, Lake Winnipeg: geological setting and sediment seismostratigraphy: Journal of Paleolimnology, v. 19, p. 215-244.

Upham, W., 1895, The Glacial Lake Agassiz: U.S. Geological Survey Monograph, v. 25, p. 685.

Valero-Garcés, B.L., Laird, K.R., Fritz, S.C., Kelts, K., Ito, E., and Grimm, E.C., 1997, Holocen climate in the Northern Great Plains inferred from sediment stratigraphy, stable isotopes, carbonate geochemistry, diatoms, and pollen at Moon Lake, North Dakota: Quaternary Research, v. 48, p. 359-369.

Voytek, E.B., Colman, S.M., Wattrus, N.J., Gary, J.L., and Lewis, C.F.M., 2012, Thunder Bay, Ontario was not a pathway for catastrophic floods from glacial Lake Agassiz: Quaternary International, v. 260, p. 98-105.

Walcott, R.I., 1972, Late Quaternary vertical movements in eastern North America: quantitative evidence of glacio-isostatic rebound: Reviews of Geophysics and Space Physics, v. 10, p. 849-884.

Wright, H.E., 1971, Retreat of the Laurentide Ice Sheet from 14,000 to 9,000 years ago: Quaternary Research, v. 1, p. 316-330.

Yang, Z. and Teller, J.T., 2005, Modeling the history of Lake of the Woods since 11,000 cal yr B.P. using GIS: Journal of Paleolimnology, v. 33, p. 483-498.

Yansa, C.H., and Ashworth, A.C., 2005, Late Pleistocene palaeoenvironment of the southern Lake Agassiz basin, USA: Journal of Quaternary Science, v. 20, p. 255-267.

Yansa, C.H., Ashworth, A.C., and Fisher, T.G., 2002, Early Holocene plant and animal colonization of the southern basin of glacial Lake Agassiz: Winnipeg, Manitoba, 45th Conference of the International Association of Great Lakes Research, p. 46.

Zhang, R. and Delworth, T.L., 2005, Simulated Tropical Response to a Substantial Weakening of the Atlantic Thermohaline Circulation: Journal of Climate, v. 18, p. 1853-1860.